Dissertation
submitted to the
Combined Faculty of Natural Sciences and Mathematics
of the Ruperto Carola University Heidelberg, Germany
for the degree of
Doctor of Natural Sciences

Presented by

M. Sc. Muad Yusuf Abd El Hay

Born in: Kfar Sava, Israel

Oral examination: 17th of June 2021

The role of TRPV1 and TRPM2 in warm temperature detection

Referees: Jun. Prof. Dr. Daniela Mauceri

Prof. Dr. Jan Siemens

Summary

Ambient temperature is detected via specialized sensory nerve ending in the skin. The transduction of thermal stimuli into action potentials relies on the activity of temperature sensitive ion channels located in the membranes of sensory nerve endings. The molecular mechanism of cold and heat transduction is well characterized. However, the ion channels responsible for the detection of innocuous warmth are still a matter of debate.

TRPV1 and TRPM2 are temperature sensitive cation channels belonging to the family of transient receptor potential (TRP) channels. Recent findings implicate a role for both TRPV1 and TRPM2 in warm-temperature detection. Cellular data from animals lacking TRPV1 and TRPM2 or pharmacological inhibition support this idea. However, *in vivo* assessment of TRPV1- and TRPM2-involvement in temperature detection yields seemingly contradictory results.

In this study, the role of TRPV1 and TRPM2 in warmth detection was evaluated *in vitro* and *in vivo* under comparable conditions.

First, I established a three-day culturing protocol for primary DRG neurons and showed that these cultures resemble the *in vivo* conditions more-closely than overnight cultures, which are the standard in the field. Calcium imaging of DRG neurons cultured for three days showed that temperature-sensitive neurons require a combination of a minimum absolute temperature and temperature change rate for a response. Additionally, my analysis of the threshold temperatures showed that many cells that would be considered heat-sensitive (HSN), are in fact warm-sensitive neurons (WSN) that require a higher temperature change rate to respond.

Applying this analysis to cultures from animals lacking TRPV1 or TRPM2 showed a significant reduction in the proportion of WSN compared to wildtype cultures. Furthermore, the combined loss of TRPV1 and TRPM2 lead to an additive reduction in the proportion of WSN and HSN. Additionally, overexpression of TRPV1 in TRPV1-positive sensory neurons lead to an increase in the proportion of WSN, suggesting that the absolute amount of TRPV1 is capable of tuning the response threshold of sensory neurons.

In this thesis I also introduced a novel behavioral paradigm that assesses the thermal preference of animals to ambient and floor temperature, termed the thermal chamber preference (TCP) test. Using this assay, I showed that animals lacking only TRPM2 or both TRPV1 and TRPM2 have deficits in warm-temperature detection, thereby confirming the cellular data from *ex vivo* cultures. Interestingly, TRPV1-deficient animals did not show a marked difference in preference development compared to wildtype animals. However, animals overexpressing TRPV1 had a faster development of preference than wildtype animals, supporting the involvement of TRPV1 in warmth detection.

In summary, I showed that both TRPV1 and TRPM2 participate in the detection of warmth *in vitro* and *in vivo*, albeit with different contributions. Furthermore, this is the first study to investigate the combined dependence on TRPV1 and TRPM2 for warmth-detection in mice.

Zusammenfassung

Die Umgebungstemperatur wird über spezialisierte sensorische Nervenenden in der Haut erfasst. Die Umwandlung von thermischen Reizen in Aktionspotenziale beruht auf der Aktivität von temperaturempfindlichen Ionenkanälen, die sich in den Membranen der sensorischen Nervenenden befinden. Die molekularen Mechanismen der Kälte- und Hitzeempfindung sind gut charakterisiert. Hingegen sind die Ionenkanäle, die für die Erkennung von nicht-schmerzhafter Wärme verantwortlich sind, umstritten.

TRPV1 und TRPM2 sind temperatursensitive Kationenkanäle, die zur Familie der Transient Receptor Potential (TRP)-Kanäle gehören. Neuere Erkenntnisse implizieren eine Rolle sowohl für TRPV1 als auch für TRPM2 bei der Erkennung von Wärme. Zelluläre Daten von Tieren, denen TRPV1 und TRPM2 fehlen oder pharmakologisch gehemmt wurden, unterstützen diese Hypothese. Die *in vivo* Untersuchung der TRPV1- und TRPM2-Beteiligung an der Temperaturerkennung liefert jedoch scheinbar widersprüchliche Ergebnisse.

In dieser Studie wurde die Rolle von TRPV1 und TRPM2 bei der Wärmedetektion *in vitro* und *in vivo* unter vergleichbaren Bedingungen untersucht.

Zunächst etablierte ich ein dreitägiges Kultivierungsprotokoll für primäre DRG-Neuronen und zeigte, dass diese Kulturen den *in vivo*-Bedingungen näher kommen als Übernacht-Kulturen, die der Standard in diesem Bereich sind. Calcium-Imaging von DRG-Neuronen, die drei Tage lang kultiviert wurden, zeigte, dass temperaturempfindliche Neuronen eine Kombination aus einer minimalen absoluten Temperatur und einer Temperaturänderungsrate für eine Reaktion benötigen. Zusätzlich zeigte meine Analyse der Schwellentemperaturen, dass viele Zellen, die als hitzeempfindlich (HSN) gelten würden, in Wirklichkeit wärmeempfindliche Neuronen (WSN) sind, die eine höhere Temperaturänderungsrate benötigen, um zu reagieren.

Die Anwendung dieser Analyse auf Kulturen von Tieren, denen TRPV1 oder TRPM2 fehlt, zeigte eine signifikante Reduktion des Anteils der WSN im Vergleich zu Wildtyp-Kulturen. Außerdem führte der kombinierte Verlust von TRPV1 und TRPM2 zu einer additiven Reduktion des An-

teils von WSN und HSN. Zusätzlich führte die Überexpression von TRPV1 in TRPV1-positiven sensorischen Neuronen zu einer Erhöhung des Anteils von WSN, was darauf hindeutet, dass die absolute Menge von TRPV1 in der Lage ist, die Reaktionsschwelle von sensorischen Neuronen zu beeinflussen.

In dieser Arbeit habe ich auch ein neuartiges Verhaltensparadigma etabliert, das die thermische Präferenz der Tiere gegenüber der Umgebungs- und Bodentemperatur bewertet, den sogenannten Thermokammer-Präferenztest. Mit diesem Assay konnte ich zeigen, dass Tiere, denen nur TRPM2 oder sowohl TRPV1 als auch TRPM2 fehlt, Defizite bei der Erkennung von warmen Temperaturen haben, was die zellulären Daten aus *ex vivo* Kulturen bestätigt. Interessanterweise zeigten TRPV1-defiziente Tiere keinen deutlichen Unterschied in der Präferenzentwicklung im Vergleich zu Wildtyp-Tieren. Allerdings hatten Tiere, die TRPV1 überexprimierten, eine schnellere Entwicklung der Präferenz als Wildtyp-Tiere, was die Beteiligung von TRPV1 an der Wärmeerkennung unterstützt.

Zusammenfassend konnte ich zeigen, dass sowohl TRPV1 als auch TRPM2 an der Erkennung von Wärme *in vitro* und *in vivo* beteiligt sind, wenn auch mit unterschiedlichen Beiträgen. Außerdem ist dies die erste Studie, die die kombinierte Abhängigkeit von TRPV1 und TRPM2 für die Wärmeerkennung bei Mäusen untersucht.

Acknowledgments

First and foremost, I would like to thank my supervisor, Prof. Dr. Jan Siemens for giving me the chance to join his lab and the freedom to pursue a project that I care about. Additionally, I thank him for his support, supervision, and for giving me space to experiment and develop. I would like to thank Jun. Prof. Dr. Daniela Mauceri, Prof. Dr. Rohini Kuner, and Dr. Hagen Wende for being part of my advisory committee over the past years, helping me navigate through the often murky waters of a PhD.

Furthermore I am grateful to Prof. Dr. Frauke Gräter and Prof. Dr. Stephan Frings for being part of my thesis defense committee.

I am thankful to all the people that read, criticized, and corrected this thesis.

Over the years, I had the pleasure to work and discuss my research with wonderful people, that no words will do them justice. I am grateful to Dr. Gretel Kamm for her support in developing the behavioral paradigm presented in this study, her constructive critical input to this study and others, and for her support in dark times. To Dr. Juan Boffi I owe thanks for his insight into data analysis, his infectious love for science (and music), and a helping hand when needed. To Dr. Hagen Wende for his attention to detail and the pool of tremendous knowledge whenever I (and others) were stuck at the bench. I want to thank Dr. Katrin Schrenk-Siemens for the endless runs we shared, and reminding me to take a step back when things get too much. I am grateful to Julian Urban and Dr. Jörg Pohle for being my go-to math and physics brains to tap into.

I am thankful to have shared the past years with lovely colleagues that cushioned the often bumpy road we walked onto. Namely, I am grateful to Kristina Zuza, Carolina Araujo-Sousa, Sebastian Marty-Lombardo, Charlotte Rostock, Hong Wang, and Sara Nencini for the fun times in and outside the lab. Additionally, I thank Ulrike Baur-Fink, Annika von Seggern, Daniela Pimonov, Lisa Vierbaum, Christina Steinmeyer-Stannek, and Miriam Lohnert for their technical assistance and the lovely atmosphere in the lab.

I am grateful to my friends and companions in the past years. Saed Mansour, Rawan Mansour, Maren Pein, Neta Nissan, Ole Rauer, Julia Wolanski, Clara Diekmann, Regina Hocke, Marc Krüger, Henrik Jungaberle, Andrea Jungaberle, and Maximilian von Heyden. Thank you for giving me the feeling that I belong, whenever I forgot how it felt like.

Finally, I would like to thank my family for their support and sacrifice that paved the way for me to come this far. Specifically, I am grateful to my parents Zaher Abd El Hay and Bettina Kochanek, for supporting and believing in me, even in times of hardship. I am grateful to my sisters, grandmother, and my extended family for the bonds that kept me and others standing.

Thank you, Danke

Contents

1 Introduction

In 1926, Edgar Adrian recorded action potentials from the sciatic nerves of frogs in response to muscle stretching, characterizing for the first time the transduction of mechanical stimuli into nerve impulses. In 1932, he received the Nobel Prize of physiology for his work. This discovery was promptly followed by the description of temperature-evoked activity in the lingual nerve of the cat [1]. This laid the groundwork for the investigation of the somatosensory system and the way thermal stimuli are conveyed, an endeavor which goes on to this day.

1.1 Somatosensory system

The somatosensory system is the part of the peripheral nervous system (PNS) that communicates sensory modalities such as touch, posture of the body and extremities, temperature, and pain to higher order centers in the central nervous system (CNS) [2]. Specialized terminal extensions of sensory nerve fibers are responsible for the translation of the varying sensory modalities into neural signals. In physiology literature these terminals are referred to as sensory receptors (unrelated to the pharmacological definition of the word). Mechanoreceptors, such as Merkel cell complexes, Meissner corpuscles, and Pacinian corpuscles are responsible for the detection of pressure, vibration, and light touch. Muscle spindles embedded in the muscle contain stretch receptors that convey the length of the muscle, and thereby the position of the limbs (proprioception). In contrast, pain receptors (nociceptors) as well as chemical and thermal receptors do not form specialized end organs but instead terminate in the skin as unsheathed (free) nerve endings with multiple branches [3]. Recent data, however, questions the concept of bare, free nerve endings as nociceptive terminals are surrounded by specialized glial cells that aid thermal and mechanical transduction [4].

The diverse sensory receptors convert incoming stimuli into action potentials that are transmitted from the periphery to the CNS via specialized nerve fibers that convey the information of the incoming stimulus type and intensity [5].

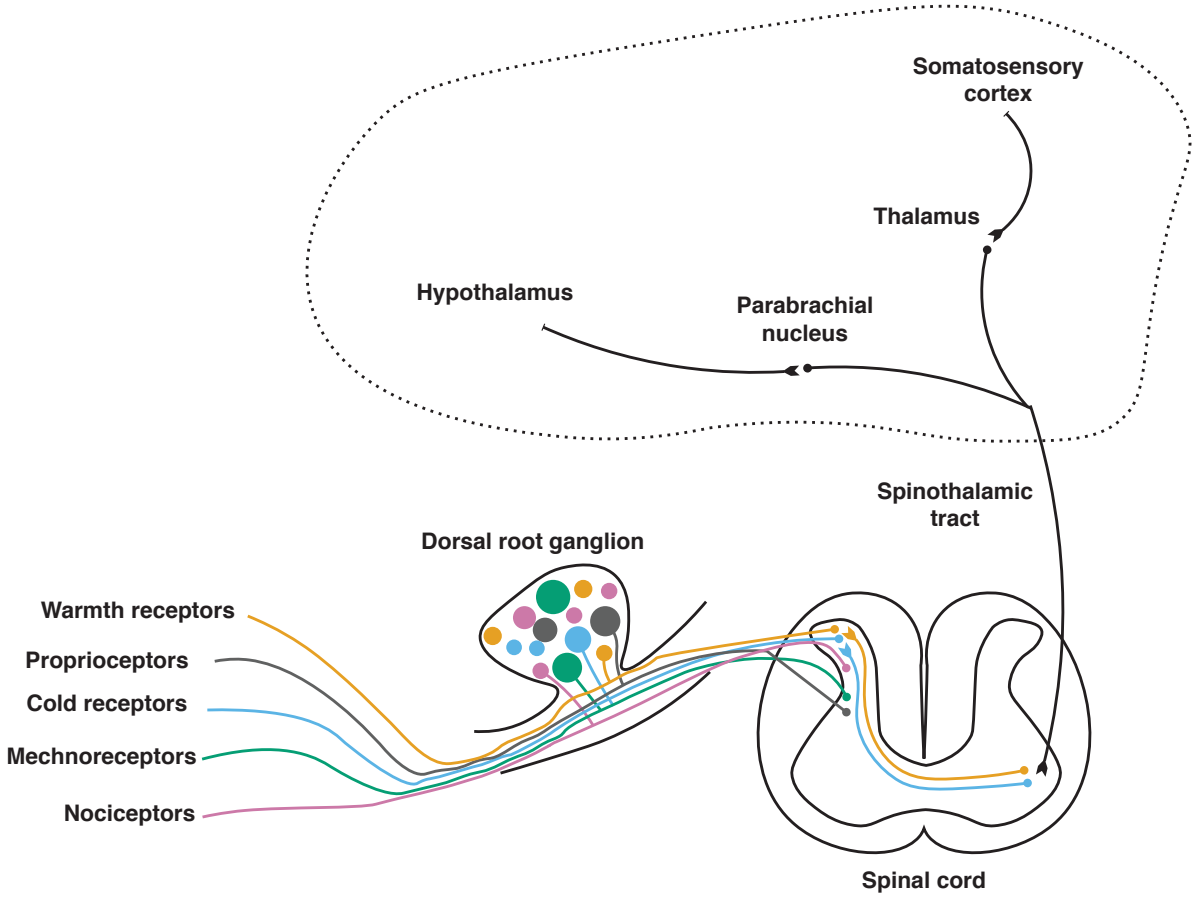

Figure 1 | Scheme depicting the anatomical and neuronal relays of sensory inputs, with focus on innocuous temperatures [6, 7].

1.1.1 Sensory fibers

Different sensory modalities recruit a wide range of fiber types for their signal transduction. Tactile stimuli as well as proprioceptive information are transduced by the fastest conducting cutaneous fibers, Aα- and Aβ-fibers. These are thickly myelinated fibers with maximum conduction velocities of around 120 m/s. Painful heat and mechanical stimuli, as well as innocuous cooling are conducted by Aδ-fibers, thinly myelinted fibers with conduction velocities of up to 36 m/s. Innocuous heat (warmth) and painful cold on the other hand are transduced by the thinnest sensory fibers, the C-fibers. Which are non-myelinated fibers with low conduction velocities of 0.4 – 2 m/s [8]. These differences in conduction velocities allow tactile, proprioceptive, and certain noxious information, which control body movement and reflexes, to reach the CNS faster than thermal or chemical stimuli [2].

1.1.2 Sensory neurons

Sensory nerve fibers are comprised of bundled axons of the primary sensory neurons, whose cell bodies reside in either the ganglia of spinal nerves (termed dorsal root ganglion, DRG) or the ganglia of cranial nerves (trigeminal ganglia, TG). DRGs and TGs present in pairs, each innervating the left or right side of the body. While there is only a single pair of TGs, in general, there are as many DRGs as spinal vertebrae, categorized according to the broad location along the spinal column (C: cervical, T: thoracic, L: lumbar, and S: sacral). DRG and TG neurons are a special type of bipolar neuron with a single axon that bifurcates into two branches. One branch projects into the periphery and one to the CNS, hence their categorization as pseudo-unipolar cells. Sensory neurons can be differentiated morphologically. Cell bodies of the heavily myelinated fibers also show a large cell size when compared to the cell bodies of C- and Aδ-fiber neurons which have predominantly smaller cell diameters (Figure 1) [9].

1.1.3 Central relays

The central branch of DRG neurons relays the peripheral signal into the CNS. Depending on the modality of the stimulus, the fibers project to different layers of the gray matter of the spinal cord. The spinal cord is divided into anatomically distinct layers, preserving the functional segregation of the sensory modalities transmitted to the CNS. The thickest fibers (Aα and Aδ) that carry tactile and proprioceptive information, terminate predominantly in the ventral and intermediate layers of the dorsal horn. From there, they are relayed ipsilaterally through the dorsal column-medial lemniscal system, passing the medulla and to the somatosensory cortex. Fibers with thermal, chemical, and noxious information (Aδ and C), on the other hand, project to the superficial layers of the spinal cord. From there, the information is carried contra-laterally through the spinothalamic tract and further relayed into the cortex and the hypothalamus passing through the thalamus and parabrachial nucleus, respectively (Figure 1) [7, 10].

1.2 Warmth detection

1.2.1 Psycho-physical sensation of warmth

Even though the systematic evaluation of temperature sensation started in the 19th century, the exact parameters that convey a conscious detection of warm stimuli are still a topic of contemporary research. Ample studies in humans and other primates converged on a set of factors that influence the subjective response to innocuous temperature stimuli. Namely, the absolute temperature of the stimuli, the magnitude of temperature change, the rate of the temperature change, the size of the area of the applied stimulus, and the body part/location of the stimulus [11]. Stable application of stimuli between 31 °C and 36 °C give a neutral sensation of temperature. Increasing or decreasing the temperature leads to a persistent sensation of either warmth or cooling, respectively. The sensation of incremental changes of temperature after adaptation to a baseline temperature depends on the magnitude, rate of change, and the area of the applied stimulus. Larger increments of temperature, faster changes in temperature, and larger stimulation areas lead to a shorter latency and increased ability of detecting the applied stimulus. Additionally, some parts of the body like the palms of the hand are more sensitive to incremental changes in temperature than other, such as the upper back. These described psycho-physical parameters are also reflected in the anatomy and physiology of the somatosensory system.

1.2.2 Innocuous temperature fibers

The discovery of temperature sensitive fibers in mammals dates back to the early 1930s when Zotterman (1935) first recorded temperature sensitive fibers in the glossopharyngeal nerve of the cat. Later works also established their presence in human and non-human primates [12–14]. Extensive studies in the 1950s described the main characteristics known to us about innocuous temperature sensitive fibers. They are unmyelinated C-fibers (except in humans, where cold fibers are of the Aδ type) that are active in a temperature range considered as non-painful (10 – 42 °C). They fire action potentials at a constant frequency, when subjected to a stimulus of a given temperature. And, their firing rate is modulated as a function of temperature and type (warm or cool).

Warm sensitive fibers increase their firing frequency with increased temperature, covering a range from 30 °C to 48 °C, inactivating at higher temperatures. Inversely, cooling down from 42 °C activates cold-sensitive fibers. Contrary to warm fibers, that respond to absolute temperatures, cold fibers react to fixed changes (deltas) in temperatures with a wide activation range from 10 °C to

42 °C. Additionally, innocuous temperature fibers show increased firing frequencies in response to faster temperature changes and larger increments of temperature [15].

1.2.3 Molecular mechanisms of warmth detection

The conversion of an external stimulus into an electrical signal by a sensory receptor is called sensory transduction. In general, external stimuli induce the opening of sodium- and calcium-permeable channels, thereby leading to an inflow of sodium and calcium, and a consecutive increase in the membrane potential, known as the receptor potential. The magnitude and length of this potential depends on the intensity of the stimulus. Upon reaching a specific threshold, the receptor potential leads to the opening of voltage-gated sodium channels and the generation of action potentials. The number and frequency of the generated action potentials depend on the magnitude and length of the receptor potential, and thereby represent the stimulus and its properties [5].

The transduction of temperature stimuli in the nerve endings of fibers has been a topic of research since the discovery of modality-specific nerve fibers. The first steps in uncovering this mystery came from the observation that specific naturally occurring compounds are able to elicit a sensation of temperature without applying a temperature stimulus. Particularly, capsaicin, an alkaloid found in the *capsicum* pepper family is capable of eliciting a feeling of burning pain upon application [16]. Another example is menthol, which conveys a feeling of cold upon ingestion. While the first observation that capsaicin is capable of activating thermosensitive nerve fibers dates back to the 1960s, it was only until the 1990s that a capsaicin-sensitive ion channel was described [17]. Through the use of a molecular cloning screen, TRPV1, a member of the transient receptor potential (TRP) family, was identified as the *de-facto* receptor for capsaicin. A later study showed that TRPV1 is activated by heat, thereby confirming the connection between the sensation of heat induced by capsaicin application and TRPV1 [18]. Analogously, another member of the TRP-family, TPRM8, is activated by menthol and plays a crucial role in cold sensation [19–21].

1.3 TRP-channels

TRP-channels are a large group of calcium- and sodium-permeable channels that span multiple families, with varying physiological roles across the body [22]. The discoveries of TRPV1 and TRPM8 were the founding stones for the family of thermo-sensitive TRP channels. The van-

niloid (TRPV1, TRPV2, TRPV3, TRPV4), the melastatin (TRPM2, TRPM3, TRPM4, TRPM5, and TRPM8) as well as the ankyrin (TRPA1) TRP-subfamilies all contain temperature-sensitive channels that respond to various temperatures across the physiological temperature range (Figure 2). In addition to the TRP-family, other channels are known which show temperature-dependent channel opening. Some members of the two-pore potassium channel family such as TREK1, TREK2, and TRAAK, as well as the chloride channel anoctamin 1 ANO1 also show temperature-dependent activity [23].

Among the ion channels known to participate in temperature detection, TRPV1, TRPM2, and TRPM8 are postulated to play major roles in the detection of warmth. In the next sections, I will introduce these channels more thoroughly and place them in context with current knowledge about warmth detection.

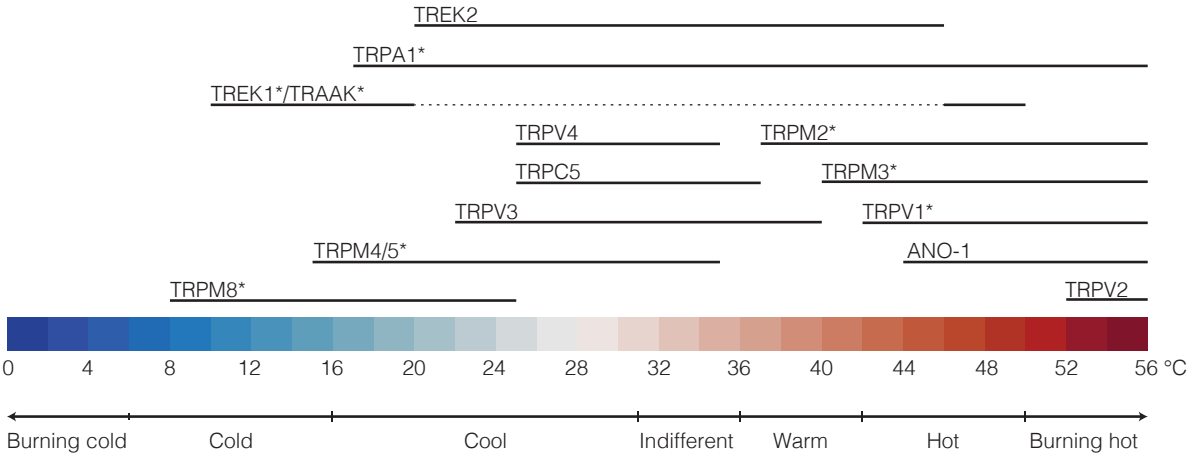

Figure 2 | Temperature-sensitive channels implicated in the detection and sensation of warmth. Top: Represantion of the postulated range of temperature activity. Bottom: psycho-physical representation of temperature sensation in humans. Channels shown to affect *in vivo* temperature detection denoted with $*$. [11, 23–25].

1.3.1 TRPV1

TRPV1 belongs to the subfamily of TRP channels which bear a binding site for vanilloid compounds (hence TRPV). It has six trans-membrane domains forming a homotetrametic, non-selective, cationic trans-membrane channel with an activation threshold of >42 °C [17]. Due to the high activation threshold, TRPV1 was speculated to be the main sensor for hot, painful temperatures. Experiments using the hot plate assay first tested the *in vivo* relevance of TRPV1. In this assay, the animal is placed in a chamber with a heated plate (>50 °C) and the latency until a painful response (jumping, flinching) is quantified [26]. Using TRPV1-KO animals, one study showed no

significant prolongation of the response latency at 50 °C and 52 °C, compared to wildtype animals [27]. However, at temperatures above 52 °C, another study did observe a significantly slower response latency of TRPV1-KO animals [18]. While the loss of TRPV1 lead to a slow response latency in the hot plat assay, it did not completely abolish the responses to heat. This suggests a possible compensation and/or involvement of other temperature sensors in the heat range. Indeed, a recent study establishes that a trio of TRP-channels, namely TRPV1, TRPM3, and TRPA1 are responsible for the sensation of painful heat. Only the combined genetic deletion of all three channels lead to a complete loss of sensitivity to painful heat [28].

While TRPV1 is only partially responsible for the sensation of painful heat, its involvement in inflammation-induced heat hypersensitivity (thermal hyperalgesia) is essential. The application of a radiant heat source to the hind paws of animals allows the assessment of the painful heat threshold by quantifying the withdrawal latency of the paw (Hargreaves assay) [29]. Injecting inflammatory agents such as Carrageenan or Complete Freund's Adjuvant (CFA) into the paw of wildtype animals leads to a sensitization of the paw, observed as a shorter withdrawal latency. This sensitization effect, however, is largely abolished in TRPV1-KO animals, when compared to wildtypes [18, 27]. These results and others using physiological inflammatory agents such as bradykinin, serotonin, nerve growth factor (NGF), and prostaglandin E2 (PGE2) confirmed the importance of TRPV1 in thermal hyperalgesia [30].

The above mentioned studies showed that TRPV1 is mainly involved in the processing of painful thermal signals. However, it came with a surprise when a recent study presented compelling evidence for a role of TRPV1 in sensing non-painful warm temperatures [31].

The application of temperature stimuli through the oral cavity of mice, combined with calcium imaging of the trigeminal ganglion *in vivo* allows the monitoring of hundreds of individual sensory neurons in response to temperature. Using warm and hot temperature steps (36 – 53 °C), two distinct populations of responsive neurons are observed. First, a larger population consisting of heat sensitive cells with a threshold temperature of 42 – 43 °C. These cells act as a binary switch between warmth and heat. Secondly, a smaller population comprising only about 2% of all analyzed neurons (or 5% of all heat responders) which are activated by temperatures as low as 36 °C. Furthermore, their calcium amplitude increases with increasing temperature, mirroring classical warm-sensitive fibers [31].

Interestingly, virtually all warmth sensitive neurons found in this study also respond to the TRPV1-agonist capsaicin, while only 70% of the heat responders do. Additionally, pharmacological blockade of TRPV1 leads to a complete silencing of the warmth sensitive cells while only affecting 10-25% of the heat sensitive neurons. Repeating the temperature ramps in animals lacking TRPV1 re-

veals a complete absence of warm-sensitive neurons. These cellular observations were supported *in vivo* through operand conditioning behavioral testing in which mice had to discriminate between 32° and 40° to receive a water reward. Injection with the same TRPV1-inhibitor as used above lead to a 20% drop in performance, confirming an involvement of TRPV1 in the detection of warm temperatures [31].

1.3.2 TRPM2

TRPM2 is a widely expressed member of the melastatin subfamily of TRP-channels. Similar to TRPV1, it is a non-selective cationic channel with a maximum opening probability at around 37 °C [32, 33]. The first report showing a temperature-dependent effect for TRPM2 described its ability to modulate the secretion of insulin in pancreatic islet cells [33]. However, it was not until 2016 that a role for TRPM2 in somatosensation was described. Calcium imaging of cultured DRG neurons revealed a discrete subpopulation of heat-sensitive cells (stimulated with 46 °C) that did not respond to agonists of known heat-activated TRP-channels such as TRPV1, TRPM3, and TRPA1. This population, which consists of around 9% of all analyzed cells, did however respond to H_2O_2 and 2-Aminoethoxydiphenyl borate (2-APB), both drugs that activate TRPM2 [34]. Additionally, the proportion of these novel heat-sensitive neurons was reduced to around 3% in TRPM2-KO animals, strongly suggesting TRPM2 as a novel heat-sensitive TRP channel.

The role of TRPM2 in temperature detection *in vivo* was tested using the temperature place-preference (TPP) test. Briefly, the test involves placing the animal into an arena that is split into two areas with differentially heated plates. One of the plates is kept at a thermoneutral, comfortable temperature (30 – 33 °C) while the other is set to a testing temperature [35]. Wildtype animals presented with 33 °C and 38 – 43 °C develop a preference over time for the cooler side set to 33 °C. Contrary to expectations, TRPM2-KO animals showed a normal preference for 33 °C when confronted with heat (43 °C). However, in contrast to wildtype animals, TRPM2-KO animals were not able to differentiate between 33 °C and 38 °C (warmth). This striking result makes TRPM2 the main candidate responsible for warmth detection.

1.3.3 TRPM8

TRPM8 is the native receptor for menthol, a naturally occurring compound found in the common mint. It is, like TRPV1 and TRPM2, a non-selective cation channel, with the difference that it is

activated by cold temperatures (<26 °C) [20, 21]. Sensory neurons and nerve fibers recorded from TRPM8-deficient mice show a near-absence of response to cool and cold stimuli. Additionally, when using the TPP test, TRPM8-KO animals show a lack of preference in a wide range of temperatures (10 – 25 °C) that produce aversion in wildtype animals [20, 21, 36]. In addition to the TPP test, the thermal gradient test is also used to assess temperature detection. In this test, the floor temperature is held at a constant gradient that covers a range of temperatures and the time spent on each temperature is quantified. Presented with a gradient from 15 °C to 53.5 °C, wildtype animals predominantly occupy a range between 30.5 °C and 38.5 °C. Animals lacking TRPM8, however, show a wider range of preference (21.5 – 38.5 °C)[20]. These results suggest a crucial role of TRPM8 in cold temperature detection.

Interestingly, a closer investigation of the thermal gradient tests also showed a deficiency of TRPM8-KO animals to locate the warm temperature range [20]. This goes in line with recent data demonstrating TRPM8 involvement in the detection of warmth. In an assay similar to the operand behavior test used to assess oral temperature detection (see section 1.3.1), animals were trained to report a warming temperature step from 32 °C to 42 °C applied to their paws [37]. From all tested genotypes, which included TRPV1-KO, TRPM2-KO, TRPV1/M3/A1-KO, and TRPM8-KO, only TRPM8-deficient mice failed to learn the behavioral task. Supported by fiber recordings in the same study, the data suggests that warmth-sensation *in vivo* results from the concerted activity of warmth-sensitive fibers and inactivity of cold-sensitive fibers [37].

The ability of TRPV1-KO and TRPM2-KO animals to reliably report the warming of the paw from 32 °C to 42 °C (albeit with a decrease in sensitivity) is surprising, as both TRPV1 and TRPM2 are necessary for warmth-detection in other behavioral paradigms [31, 34]. Incidentally, the roles of TRPV1 and TRPM2 as warmth-sensors are still a matter of debate, the reasons of which are further elaborated in the following chapter.

1.3.4 Conflicting roles of TRPV1 and TRPM2

TRPV1

While the role of TRPV1 in heat detection (especially under inflammatory conditions) is well established, its involvement in the detection of warmth is controversial. As described in section 1.3.1, both the absence and pharmacological inhibition of TRPV1 abolishes warmth responses in recorded trigeminal ganglion neurons [31]. Analogously, blockade of TRPV1 activity leads to a

significant drop in the discrimination performance of mice trained to report 32 °C versus 40 °C [31]. Using a similar operant behavioral assay, mice lacking TRPV1 reliably learn to report a warming stimulus (32 – 42 °C) applied to the paw, albeit with a lower sensitivity compared to wildtypes [37]. Both reports argue for, at least, a partial relevance of TRPV1 in warmth detection. The picture differs, however, when using non-evoked, voluntary behavioral assays. TRPV1-KO animals tested using the thermal gradient test (explained in section 1.3.3) or the TPP test (section 1.3.2), show no significant difference in their warm temperature discrimination when compared to wildtype animals [36, 38, 39]. Combining this evidence suggests a context-dependent role of TRPV1 and leaves the question unanswered whether TRPV1 can be considered a warmth-sensor.

TRPM2

The postulated role of TRPM2 in warm temperature detection was also challenged using a trained operant behavioral task. Similar to TRPV1-KO animals, TRPM2-KO animals were probed for their ability to detect a warming temperature stimulus from 32 °C to 42 °C [37]. Intriguingly, and in a similar fashion to TRPV1-KO animals, TRPM2-deficient animals are also able to stably report the stimulus, despite a reduced sensitivity [37]. This stood in contrast to the inability of TRPM2-KO animals to distinguish between 33 °C and 38 °C in the TPP test [34]. Additionally, criticism towards TRPM2 as a relevant temperature detector in sensory neurons arose from cellular data. The study describing TRPM2 as a novel warmth-sensitive channel found TRPM2-dependent responses only upon application of a heat stimulus (46 °C) in primary DRG cultures. Furthermore, the TRPM2-positive population is shown to exclusively express TRPM2, but no other thermosensitive channel [34]. However, in another study, using the same temperature stimulus and culturing system with cells lacking TRPV1, TRPM3, and TRPA1 combined, completely abolished any temperature response, arguing that TRPM2 does not play a role in temperature detection [28]. Additionally, *in vivo* calcium imaging in trigeminal ganglion neurons shows that all warmth-sensitive neurons are TRPV1-positive [31]. In summary, these reports question the existence of an exclusively TRPM2-positive sensory neuron population that responds to either warmth or heat. Recently, two brief reports show the existence of an exclusively TRPM2-positive heat-sensitive population [40, 41]. This population is, however, only detected when the stimulus temperature passes 48 °C, further questioning TRPM2 as a warm-temperature sensor.

The *in vivo* experiments related to TRPM2 suggest a role of the channel in warmth detection, without defects in heat detection. The cellular data summarized above, however, argue that TRPM2 is only necessary for temperature detection above 48 °C. In contrast, the involvement of TRPV1 in warmth detection is supported by cellular data. However, the use of different behavioral assays

yields contradictory results. The current evidence on the roles of TRPV1 and TRPM2 as warmth-sensors remains inconclusive. A thorough review of the literature did not reveal any study that compared the response of TRPV1-KO and TRPM2-KO sensory neurons to warmth. Additionally, the partial phenotypes of TRPV1-deficient and TRPM2-deficient animals in both discussed operant behavior assays poses the question whether warmth is detected through the combined activity of both TRPV1 and TRPM2.

1.4 Aim of the study

The sensation of warm temperatures is conveyed by the activity of specialized temperature-sensitive cells of the somatosensory system and their nerve endings. The thermal information is carried through sensory fibers and ganglia to the central nervous system.

Advances in molecular cloning identified a family of temperature-sensitive ion channels (TRP-channels) capable of translating a thermal stimulus into action potentials. While the channels responsible for the detection of cold and painful heat were identified, the molecular mechanism of warmth transduction remained elusive.

Two recent studies proposed that TRPV1 and TRPM2 constitute the central channels in warmth detection [31, 34]. These results, however, stand in contrast to previous and more recent data, challenging the current views on the role both channels play in warmth detection 1.3.4.

Therefore, the aim of this study was to elucidate the roles of TRPV1 and TRPM2, under identical experimental conditions, in warmth detection *in vitro* and *in vivo*. Additionally, this study aimed to answer whether a combined activity of both channels, TRPV1 and TRPM2, is necessary for warmth detection, a scenario that was not investigated before.

2 Materials and Methods

2.1 Materials

Reagents

Reagent name	Cat. No.	Source
4-(2-hydroxyethyl)-1-piperazineethanesulfonic acid (HEPES)	9105.4	Carl Roth
Agarose Biozym LE	840000	Biozym
Ammonium sulfate ($(NH_4)2SO_4$)	A4418	Sigma Aldrich
Antibioic-Antimitotic (100X)	15240062	Thermo Fischer Scientific
Betaine	B2629	Sigma Aldrich
Bovine serum albumin (BSA) fraction V	T844.1	Carl Roth
Cal-520 AM	21130	AAT Bioquest
Calcium chloride dihydrate ($CaCl2 \cdot 2H2O$)	1023821000	Merck Millipore
Capsaicin	0462	Tocris
Collagenase	C0130	Sigma
Cresole red	KK15.1	Carl Roth
D(+)-Glucose	108337	Merck Millipore
D(+)-Saccharose	4621.1	Carl Roth
Dulbecc's' modified eagle media (DMEM)/F12 without Glutamine	21331046	Thermo Fischer Scientific
Dimethyl sulfoxide (DMSO)	D2438-50ml	Sigma
Ethidium bromide	2218.2	Carl Roth
Ethylene diamine tetraacetic acid (EDTA)	8043.2	Carl Roth
FastGene Taq DNA Polymerase	LS22	Nippon Genetics
Fetal calf serum (FCS) - EU Approved (South American)	10270	Invitrogen

Continued on next page

Continued from previous page

Reagent name	Cat. No.	Source
Isoflurane	HDG9623	Baxter
L-alanyl-L-glutamine dipeptide (Glutamax Supplement 100X)	35050	Invitrogen
Laminin	L2020	Sigma
Magnesium chloride ($MgCl_2$)	M8266-1KG	Sigma Aldrich
Plastic glue	UH46650	UHU
Pluoronic F127 tenside	P6866	Invitrogen
Poly-D-Lysine (PDL)	P7886	Sigma
Potassium chloride (KCl)	LC-5916.1	Labochem international
Proteinase K	7528.1	Carl Roth
Sodium dodecyl sulfate (SDS)	2326.2	Carl Roth
Silicone for universal use		MEM Dichten
Sodium chloride ($NaCl$)	31434-1KG-R	Sigma Aldrich
Tris-HCl	5429.3	Carl Roth
Trypsin-EDTA 0.05 %	25300054	Thermo Fischer
β-mercaptoethanol	M6250	Sigma Aldrich
dNTP mix	N0447L	New England Biolabs
Dulbecco's PBS	14040141	Thermo Fischer Scientific

Solutions and media

Ringers solution	**High potassium ringers solution**
140 mM $NaCl$	140 mM $NaCl$
5 mM KCl	100 mM KCl
2 mM $MgCl_2$	2 mM $MgCl_2$
2 mM $CaCl_2$	2 mM $CaCl_2$
10 mM Glucose	10 mM Glucose
10 mM HEPES	10 mM HEPES
adjusted to pH 7.4	adjusted to pH 7.4
Low-EDTA buffer solution	**Biopsy buffer**
10 mM $Tris-HCl$	100 mM Tris
0.1 mM $EDTA$	5 mM EDTA
	0.2 % SDS

2x PCR Mix	200 mM $NaCl$
45 mM Tris pH 8.8	
3.5 mM $MgCl_2$	**Primary sensory neuron medium**
11 mM $(NH_4)_2SO_4$	DMEM/F12 w/o Glutamin
13 % D-Saccarose	10 % heat-inactivated FCS
0.005 % Cresole red	2 mM L-glutamine (Glutamax)
1:1000 β-Mercapto ethanol	1X Antibioic-Antimitotic

Consumables

Component	Cat. No.	Source
CS-22/40 rectangular coverglass for perfusion chamber	64-0707	Warner instruments
Cell culture dish (sterile) 10cm Greiner CELLSTAR	P7612	Merck Millipore
Cell culure plates (sterile) 6/12-well		Sarstedt
Cellulose filter paper (Whatman)		
Falcon tube 15/50ml	11507411	Fischer Scientific
Glass coverslip (5 mm) Menzel (0.13 – 0.16 mm	11888372	Fischer Scientific
Kartell™ Colorimetric 8 Cell Tray	10441551	Fischer Scientific
Luer-Lock plastic syringes (20/50ml)	BD 309654	Fischer Scientific
MP-8 perfusion manifold	64-0211	Warner instruments
Microlance 3 injection needles 27G	305771	Becton Dickinson
Millex-GS membrane filter 0.22 µm	SLGS033SB	Millipore
PCR tube strips (8)	BR781320	Millipore
PCR tupe strip caps (8)	BR781340	Millipore
PE-160/10 polyethylene tubing for perfusion manifold	64-0755	Warner instruments
Parafilm M parrafine film	CNP8.1	Carl Roth
Reaction tubes 1.5/2ml		Sarstedt
Silicone pinch valve tubing	05-14	AutoMate Scientific
Syrologic syringes 10/25/50ml		Sarstedt
Teflon PTFE tubing (TT-25)	64-0168	Warner Instruments

Surgical tools

Tool	Cat. No.	Source
Dumont Tweezers #5	501985	World Precision Instruments (W.P.I.) Gmbh
Iris Scissors, 11 cm, Tungsten Carbide	500216-G	World Precision Instruments (W.P.I.) Gmbh
Mini Dissecting Scissors, 9.5 cm	503241	World Precision Instruments (W.P.I.) Gmbh
Surgical Scissors - Sharp-Blunt	14001-16	Fine Science Tools (F.S.T.) Germany
Vannas Spring Scissors 3 mm	15000-10	Fine Science Tools (F.S.T.) Germany

Hardware

Tool	Source
ARCTIC A10 Refrigerated Circulator	Fischer Scientific
AxioObserver D1 microscope	Zeiss Microscopy
BAT-12 microprobe thermometer	Physitemp
BJ 410C scale	Precisa
Biometra TRIO thermal cycler	Biometra
Cell incubator	Binder Gmbh
CoolSnap HQ2 camera	Photometrics
EHEIM air200 aquarium pump	Eheim
ET470/40x excitation filter	Chroma
ET525/50m emission filter	Chroma
EcoVac safety vacuum pump (Schuett Biotech)	Fischer scientific
Electrophoresis Power Supply 250V	VWR
FL EC P&C reflector module cube	Zeiss Microscopy
FT 495 dichroic mirror	Zeiss Microscopy
Fluar 10x/0,5 M27 objective	Zeiss Microscopy
Intellimixer rotation mixer	neoLab
Lambda DG-4 lightsource	Sutter instruments
Megafuge 1.0 R swinging bucket centrifugre	Heraeus
Owl Easycast electrophoresis chamber	Thermo Fischer
RC-22 perfusion chamber	Warner instruments
Safe 2020 biological safety cabinet type II	Thermo Fischer
USB-1608G DAQ	Measurment Computing
ValveBank II perfusion system	AutoMate Scientific
Zyla 4.2 Plus camera	Andor Technology
sympHony pH meter	VWR
Thermes USB	Physitemp
X48 B6015L12F NF1 computer fan	ASUS
Multitemp III citculating waterbath	Pharmacia Biotech
LOGO! TD controller	Siemens
USB webcam 1080P	Spedal

Software

Name	Source
Adobe Illustrator 2020	Adobe
Daisylab 12	National Instruments
Emacs org-mode	Schulte et al. 2012 [42]
GNU Emacs	Stallman 1981 [43]
LOGO! Soft Comfort	Siemens
Metafluor	Molecular devices
Miniscope DAQ acquisition software	Cai et al. 2016 [44]
Python	van Rossum et al. 1995 [45]
R 4.0.3	R core team [46]
LaTeX and mimosis class	https://github.com/Pseudomanifold/latex-mimosis
ffmpeg 4.2	Tomar et al. 2006 [47]
scimax for Emacs	https://github.com/jkitchin/scimax
R packages	
ComplexHeatmap	Gu et al. 2016 [48]
EBImage	Pau et al. 2010 [49]
Spectrum	John et al. 2020 [50]
cmocean	Thyng et al. 2016 [51]
cowplot	Wilke et al. 2020 [52]
eulerr	Larsson et al. 2021 [53]
ggforce	Pedersen et al 2021 [54]
ggplot2	Wickham et al. 2016 [55]
ggpubr	Kassambara et al. 2020 [56]
ggridges	Wilke et al. 2021 [57]
imputeTS	Moritz et. al. 2017 [58]
matrixStats	Bengtsson et al. 2021 [59]
multcomp	Liland et al. 2010 [60]
patchwork	Pedersen et al. 2020 [61]
rstatix	Kassambara et al. 2021 [62]
survival	Therneau et al. 2020 [63]
survminer	Kassambara et al. 2020 [64]
tidyverse	Wickham et al. 2019 [65]
twosamples	Dowd et al. 2020 [66]

Continued on next page

Continued from previous page

Name	Source
R packages used for neuroimgr	
MultiAssayExperiment	Ramos et al. 2017 [67]
SummarizedExperiment	Morgan et al. 2020 [68]
baseline	Liland et al. 2010 [60]
reticulate	Ushey et al. 2020 [69]
upbm	Kimes et al. 2020 [70]
Python packages	
Cellpose 0.6.1	Stringer et al. 2021 [71]
DeepLabCut 2.2b8	Mathis et al. 2018 [72]
Suite2p 0.9.3	Pachitariu et al. 2016 [73]
Icons	
Air	Alvida Biersack from the Noun Project
Fan	hanthagawri from the Noun Project
Thermometer	Vectorstall from the Noun Project

Experimental animals

1. Lines

Name	Official nomenclature	Source
TRPM2-KO	$Trpm2^{tm1Yamo}$	[74]
TRPV1-KO	B6.129X1-Trpv1tm1Jul/J	[18]
TRPV1-OX	C57BL/6N-Tg(Trpv1)5917Jsmn/J	[30]
Wildtype	C57BL/6NRj	Janvier Labs

2. Animals

Summary of all animals used by experiment type seen in Table 8. Detailed list of all animals used for DRG cultures and behavioral testing can be found in the appendix (Table 4.3.3).

Table 8 | Summary statistics of all animal used in this study, split by experiment type.

DRG cultures				**TCP test**			
Genotype	Age (weeks)	Sex		Genotype	Age (weeks)	Sex	
Wildtype	11.8 ± 2.5	17 M	1 F	Wildtype	14.0 ± 11.0	30 M	0 F
TRPM2-KO	12.6 ± 2.8	1 M	2 F	TRPM2-KO	11.8 ± 6.1	18 M	0 F
TRPV1-KO	10.1 ± 2.4	5 M	0 F	TRPV1-KO	11.8 ± 7.5	17 M	0 F
TRPV1M2-KO	11.9 ± 0.6	3 M	0 F	TRPV1M2-DKO	11.4 ± 6.4	11 M	0 F
TRPV1-OX	11.4 ± 1.7	4 M	0 F	TRPV1-OX	9.4 ± 0.7	9 M	0 F

3. Genotyping primers

Internal name	Animal line	Sequence (5' to 3')	Annealing Temp. (°C)
M2-10R-HW-new	TRPM2-KO	CCT CAC CAT CCG CTT CAC GAT	58
$M2_{Kun}$-Fw-new		AAG CCC TGC CTC CTG GTG TGC	58
Pneo5a-new		GCC ACA CGC GTC ACC TTA ATA TG	58
Tag TrpV1 F6	TRPV1-OX	TGA CAA GAA GAG CGT GGA GGG G	63
Tag TrpV1 R6		AGC TGA CGG TGA TGA TAG GGC AGG	63
TrpV1 for (TrpV1 5911 ko)		CCT GCT CAA CAT GCT CAT TG	55
TrpV1 rev (TrpV1 5911 ko)	TRPV1-KO	TCC TCA TGC ACT TCA GGA AA	55

2.2 Methods

2.2.1 Animal housing and genotyping

Housing and protocol

Animals were housed under specific-pathogen-free (SPF) conditions in the interfacultary biomedical animal housing facility at the Neuenheimer Feld campus. A 12 hour day-night cycle was kept. Housing temperature and humidity were kept at 22 ± 2 °C and 50 − 60 %, respectively. Animals were fed *ad libitum* with Altromin Rod 16 or Rod 18 animal food. Housing environment was enriched using Crincklets Nest-Pads and ABBEDD LT-E-001 bedding. All animals used for behavior ran under protocol G201/16. Animals sacrificed for cell culture preparations according to protocol T05-19.

For tissue preparation, animals were removed from the SPF barrier and sacrificed on the same day with an overdose of Isoflurane followed by decapitation. For behavioral experiments, the animals were transferred into the experimental room which also acted as a housing room where temperature, day-night cycles, and humidity were kept similar to the animal facility.

Biopsy digestion

Animal biopsies (tail or ear) were collected by the animal facility staff. Additionally, tail biopsies were collected from all mutant genotypes after every experiment was finished to verify the genotype. Biopsies were incubated in 50 µL biopsy buffer (section 2.1) containing 0.3 mg proteinase K overnight at 56 °C. On the following day, the samples were incubated at 96 °C for 10 minutes to inactivate the proteinase, and topped up with 350 µL of $ddH2O$. The resulting samples were kept at 4 °C until processing.

Genotyping

The digested animal biopsy was spun at 7000 rpm for 10 seconds to sediment the undigested tissue. A mastermix according to the recipe in Table 10 was prepared, dispersed (19 µl) into 8-strip PCR tubes, and 1 µl of the digested animal biopsy added to the master-mix. Then, the tubes were placed

into a PCR machine and cycled according to the protocol in table 11. After PCR, the samples were ran on a 1 % agarose gel containing ethidium bromide for 1 hour at 130 V before imaging.

Table 10 | PCR pipetting mix for genotyping. ∗ indicates exta reagents for TRPM2-KO PCR.

Reagent	1x (µl)
2x PCR Mix	10
dNTP mix	1
Primer 1	1
Primer 2	1
Primer 3 ∗	1
Betaine ∗	2.5
FastTaq polymerase	0.125
$ddH2O$	fill up to 19 µl
DNA from biopsy	1

Table 11 | Thermal cycler protocol for DNA amplification. ∗ indicates steps to be repeated.

Step	Temperature (°C)	Time (s)	
Initial denaturation	95	180	
Denaturation	95	30	*
Annealing	see section 3	30	*
Extension	72	60	* repeat 34 times
Final extension	72	300	
End	16	∞	

2.2.2 Primary sensory neuron culture

Coating coverslips with PDL and Laminin

Glass coverslips (5 mm diameter) were washed overnight in 1 M HCl followed by a wash in 70% ethanol. Then, coverslips were spread onto filter paper and left to dry under UV-light (inside cell culture hood) for one hour. Coverslips were then stored in a sterile container until used.

Before an experiment, coverslips were coated with poly-D-lysine (PDL), followed by laminin. Washed and sterile coverslips were coated with 50 µl of PDL solution and incubated for at least 30 min at 37 °C. Then, the coverslips were washed with 50 µl of sterile PBS and coated with 30 µl of laminin solution in $H2O$ and incubated for at least 30 min at 37 °C. Afterwards, the coated coverslips were transferred onto 6- or 12-well plates (2 or 1 coverslip per well, respectively), the

remaining solution aspirated, and the coverslips left to dry for at least 45 min before cells were seeded.

Procedure

Adult primary DRG cultures were prepared using 6-15 week old animals. First, animals were culled by an overdose of isoflurane, the fur sprayed with 70 % ethanol and the head decapitated as close as possible to the skull, to retain the largest number of intact DRGs in the spinal column. Then, a central cut through the skin from rostral to caudal, reaching the tail, was done and the skin removed to both sides to expose the spinal column. Using medium sized scissors and holding the tail of the animal, two lateral cuts to the sides of the tail were done to free the caudal part of the spinal column. Repeated cuts on both sides of the column from caudal to rostral coupled with occasional separation of the ventral connection allowed the clean excision of the whole spinal column from the sacral to the cervical area. Using the same scissors, excessive tissue attached to the spinal column was removed to the point that a clear mid-line of the spinal column was visible on the dorsal/posterior side (created by the spinous process of the vertebrae) and the ventral/anterior side of the column.

Once the mid-line was clearly visible on both sides of the entire excised spinal column, small bone-scissors were used to cut along the mid-line, starting from the rostral side, with one shaft of the scissor inside the spinal canal. This process was repeated, alternating between cutting through the mid-line on both the posterior and anterior side until the spinal canal was too narrow for further cutting. Then, the remaining sacral part of the spinal column was severed resulting into two lateral parts of the spinal column that were covered in filter paper and placed on ice.

Then, one lateral part of the spinal column was moved from the ice onto an agar plate and fixed into the agar using two fine injection needles with the medial part of the spinal column facing upwards. If done well, the spinal cord would cover the whole spinal column and the DRGs underneath. Under a binocular microscope, starting from the caudal side, the spinal cord was removed piece-wise, uncovering 3-4 DRGs at once. Using the fine forceps, the DRGs were held at their central nerve branches and excised using fine, curved forceps and then moved into a shallow well containing ice-cold Ringer's solution. This process was repeated until all DRGs were collected. DRGs collected from one half of the spinal column yield 3-4 coverslips of DRG culture at a density that is suitable for calcium imaging. For larger experiments, both sides of the spinal column were used (8-9 coverslips).

After all needed DRGs are collected, the shallow well plate with the DRGs was moved under the binocular. Then, the DRGs were freed from their peripheral and central nerve branches and cut in half before transferring them into a tube containing 1 ml of 1.25 mg/ml collagenase solution in Ringer's. Then, the DRGs in collagenase solution were incubated in a water-bath for 60 min at 37 °C, flipping the tube every 15 min as the DRGs sediment to the bottom of the tube. After incubation, the collagnase solution above the sedimented DRGs was carefully aspirated and replaced with a 2.5 mg/ml trypsin solution in Ringer's and incubated at 37 °C for 15 min.

After successive incubation with collagenase and trypsin, the solution above the sedimented DRGs was carefully aspirated and replaced with 800 µl of complete culturing media, to block the activity of trypsin. Then, using a 1 ml pipette, the DRGs were titruated by pipetting the solution up and down 10 times. Then 500 µl of the cell-suspension was transferred into a 2 ml tube for collection. This process was repeated until 2 ml of cell suspension was collected. The remaining liquid including the non-digested debris was discarded.

Then, 2 ml of a 150 mg/ml solution of bovine serum albumin (BSA) in complete medium was pipetted into a 15 ml sterile reagent tube followed by the careful layering (by tilting the tube) of the collected cell suspension onto the BSA solution. Next, the tube was centrifuged at 900 rpm for 10 min, forming a barely-visible pellet of cells. After centrifugation, the supernatant was removed until approximately 20 µl of solution was left. Then, an appropriate amount of complete culturing medium was added in a fashion that one coverslip is seeded with 10 µl of cell suspension and all DRGs collected from one animal produce 8-9 coverslips. Then, using the produced cell suspension, 10 µl are spotted onto the center of the double-coated and dried coverslip, forming a liquid dome. The seeded coverslips inside the well plates were then carefully transferred into the incubator and kept there for 60 min so that cells can securely attach to the coated surface. After incubation, the wells of the 6-/12-well plate were flooded with 2 ml or 1 ml of complete culturing media, covering the seeded coverslips and placed back into the incubator.

For overnight cultures, the coverslips were used one day after preparation. Stimulation with kinase inhibitors was achieved by adding the inhibitors to complete culturing media from the beginning of the procedure, ensuring a maximal effect. For three-day cultures, the medium was changed one day after preparation and then kept in culture for two additional days until the day of the experiment.

2.2.3 Calcium imaging

Procedure

The cells were kept in culture for either one or three days, depending on the experiment. Prior to imaging, the coverslips were moved into an incubation chamber built from a 10 cm plate-cover covered with non-streched parafilm of the same size, inside a 20 cm plate. The cells were washed once with 50 µl of Ringers solution and then loaded with 50 µl of a 10 µM Cal520-AM and 0.05 % Pluronic acid F-127 in Ringers solution. The cells were kept for 1 h at 37 °C followed by replacement of the dye-solution with Ringer's solution and a subsequent 30 min incubation period at room temperature. Exposure to light was avoided.

The perfusion system was set to a maximum of 3 ml/min with the suction so that it allowed laminar flow in the perfusion chamber. The coverslip with the loaded cells was placed in the perfusion chamber and tucked close to the outlet, to reduce movement artifacts. The thermocouple was placed as close as possible to the coverslip. When using the CoolSnapHQ2, exposure time was set to 5 ms with a gain of 3x and a binning of 3 by 3. When using the Zyla 4.2, exposure times were set to 80 ms and a binning of 2 by 2. Lamp intensity was set to 30 % for all experiments, to reduce bleaching. Images were acquired using the MetaFluor software at a frequency of 4 Hz, or 10 Hz. Example fields of view (FOV) depicted in Figure 1. In a standard experiment, stimuli were 25 s long followed by 3 – 5 min perfusion with room temperature Ringer's to allow the cells to recover from stimulation. Solutions were heated by passing through house-made glass coils connected to a heated circulating water bath. Benchmarks of applied stimuli and their stability across imaging setting depicted in Figure 2. Each coverslip was imaged for a maximum of 40 min and coverslips were not kept longer than 2 h after loading.

Analysis

Motion correction and signal extraction was performed using the Suite2p pipeline (version 0.9.3) using the parameters in Code Snippet .1 in the appendix [73]. Cell regions of interest (ROIs) were detected using the Cellpose package (integrated into Suite2p) [71]. Average fluorescence of detected cells and surrounding neuropili were calculated by Suite2p.

Output files from Suite2p were imported using a self-written R-package called "neuroimgr". The package implements a calcium imaging object based on the SummarizedExperiment object from

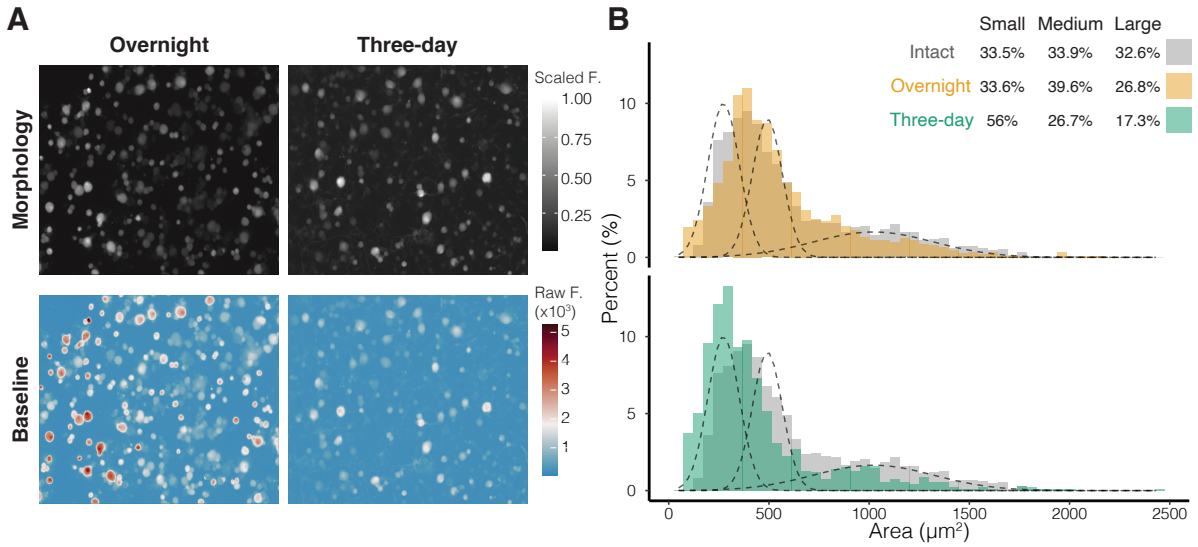

Figure 1 | Overnight and three-day culture examples and sizes. **A** Scaled gray values of DRG cultures loaded with Cal-520 AM during calcium imaging in overnight and three-day cultures. **B** Baseline raw fluorescence of FOV shown in **A**. **C** Cell area distributions of overnight and three-day cultured DRG neurons in comparison to cell areas of sectioned intact DRGs. Intact DRG cell areas were kindly provided by Dr. Hagen Wende. Plotted intact cells were pooled from 6 animals with n = 1863 cells in total. Plotted areas of overnight and three-day cultures pooled from two animals with n =7305 and n = 4660 cells, respectively. A univariate gaussian mixture model was fitted to the pooled data to split the distributions into three gaussian distributions as described previously [75]. Resulting distributions were named small (228.88 ± 80.11 µm^2), medium (451.63 ± 76.22 µm^2), and large (992.00 ± 307.22 µm^2). Plotted table depicts proportion of cells falling into either distribution.

the bioconductor R project and provides basic tools such as plotting and normalization of neuronal traces. For more information, visit https://github.com/Cumol/neuroimgr.

The extracted neuronal calcium traces form Suite2p were corrected for neuropili contamination by subtracting 70 % of the background neuropili traces from a cells' neuronal calcium trace. Normalized traces were calculated using the $^{\Delta F}/_{F_0}$ method. Briefly, baseline fluorescence (F_0) is estimated by calculating the mean of fluorescence before a given stimulus. Then, the baseline fluorescence is subtracted from the fluorescence at any given time (F) and the result (ΔF) divided again by the baseline fluorescence (F_0). $^{F-F_0}/_{F_0}$. For heatmaps, F_0 was estimated using the mean of the first 10 s of the stimulus. For stimulus-specific $^{\Delta F}/_{F_0}$ the first 10 frames of the 25 s stimulus were used as F_0.

Due to the temperature-dependence of chemical calcium dyes [76], responders were individually detected for each temperature stimulus. Specifically, calcium traces during a temperature stimulus were isolated and normalized to the first 2 s of the 25 s long stimulus. Then, the normalized traces from all the experiments during a specific temperature stimulus (first, second, etc.) were pooled,

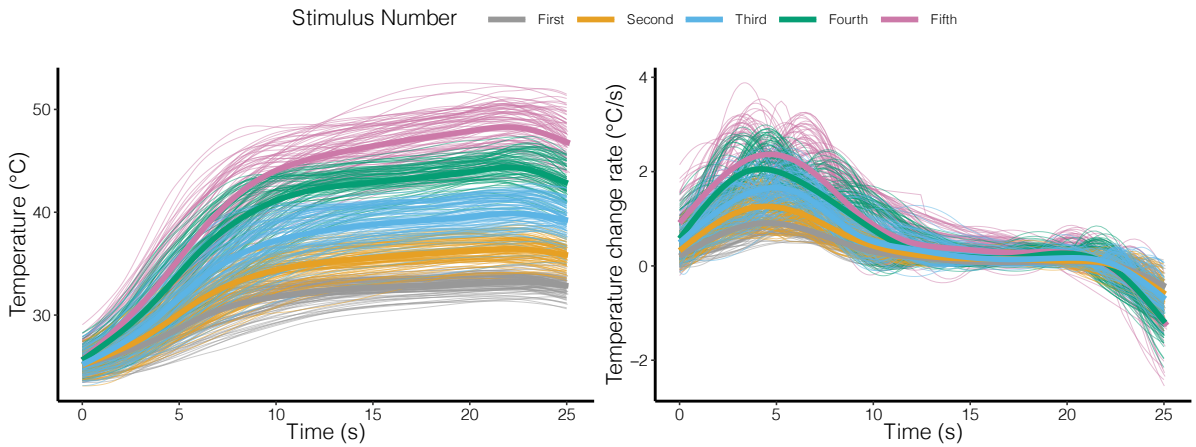

Figure 2 | Summary of applied temperature stimuli across all calcium imaging sessions. Individual imaging sessions depicted in thin lines. Thick lines depict the average of all stimuli. Left panel: absolute reached temperature (°C). Right panel: temperature change rate (°C/s).

downsampled to 4 Hz and separated via spectral clustering into a responding cluster and a non-responding cluster (using fast approximate clustering and 500 initial centroids via the Spectrum R-package [50]). Cells that did not respond to any stimulus (temperature, capsaicin, or high-potassium ringers) were removed from the analysis. Next, threshold temperature parameters for each stimulus and responding cell were calculated. Specifically, the maximum and minimum fluorescence during each stimulus were determined. Then, the closest time-point to 10 % of the range between minimum and maximum was calculated and used as threshold to estimate the temperature (T) and temperature change rate ($\delta T/\delta t$) parameters per cell during each stimulus. The same process was used to estimate the 90 % threshold. The time between the 10 % and 90 % threshold represented the rise time of the cell during the stimulus.

Heatmaps were generated using the ComplexHeatmaps package [48] and the plotted $\Delta F/F_0$ values were clipped between the 1 % and 99 % percentile. Euler schemes were generated using the eulerr package [53]. Remaining plots were rendered using the ggplot2 package. Color palettes for heatmaps and 2D-kernel density estimations were generated using the cmocean package [51]. Cumulative event analysis was done using the survival package [63]. Single and multiple pairwise Log-Rank tests were run through the survdiff and pairwise-survdiff functions provided by the survminer package [64]. Comparison of 1D-densities via reweighted wasserstein distances were done using the twosamples R package [66]. General statistical testing was don using the rstatix and multcomp packages [62, 77].

2.2.4 Thermal preference chamber

Setup

Dimensions and sizes of different setup components are discussed in section 3.2.1. The enclosure consists of two styrofoam boxes connected using plastic glue and sealed off with silicone. The steel base-plate and cage were custom built by the mechanic workshop on-site. The cover consisted of a foam/wood sandwich with a plexiglass inset. Two IT-18 flexible thermocouples attached to the wall were used as reference thermometers. Two peltier elements connected to two computer fans were used to control the chamber temperatures. The peltier elements were controlled by a custom built Siemens LOGO TD! controller and accessed using Siemens LOGO! Soft Comfort software. Two generic themocouples were used as a feedback to control the system. Animals were housed in the experimental room for at least 24 h before the experiment. The experimental room was kept dimmed and at a day-night cycle of 12 h. Recording was done using a Spedal webcam combined with a capture software from the UCLA miniscope project at 20 frames per second [44]. The output files for each animal were then concatenated using ffmpeg before further processing [47].

Markerless pose estimation and analysis

Due to the fact that the animal is recorded in a relatively dark enclosure, traditional packages of object detection did not perform well (tested via trial and error, data not shown). Therefore, the deep learning python library DeepLabCut v2.2b8 used [72]. A ResNet50 neural network was trained on representative images from multiple animals, days, and room positions to recognize the snout, right eat, left ear, body center, tail base, tail tip, and the four base-plate and cage corners. The training was repeated until manual inspection of the labelled videos did not reveal major mistakes. A total of 4 rounds with 10-70k iterations were needed to properly train the network. The library was then ran on the full-sized concatenated videos and the results populated into a comma-separated value (CSV) file.

A higher number of trained limbs increases the precision of the trained neural network [72]. For the final analysis, only the body center was used. The predicted positions were assessed for low likelihood (<0.6) of the prediction. Videos that contained more than 30 % of low-likelihood predictions were visually inspected and removed in cases the animal was predominantly climbing or escaped the cage. The low-likelihood frames were removed and interpolated using the imputeTS

R library [58]. Then, the data was downsamples from 20 Hz to 1 Hz and scaled to the 2D positions of the corners of the base-plate. The resulting X- and Y-positions of the animals' body center were used for all consecutive analysis.

Animals that did not cross from one chamber to the other for more than 6 min were removed from the analysis. Further outliers for each genotype were assessed by boxplot methods implemented in the rstatix package [62]. Briefly, animals that were outside 1.5 times the 25 % to 75 % interquartile range were removed. One-Way analysis of variance (ANOVA) was ran as implemented in the rstatix package. For pairwise multiple comparisons, Tukeys' HSD was used. For comparisons to a reference group (wildtype) either two-sample t-test (when comparing two groups) or Dunnets' *post-hoc* (implemented in the multicomp package [60]) were used.

3 Results

3.1 Representation of warmth in dorsal root ganglion cultures

3.1.1 Warmth detection in DRG cultures

To probe the responses of sensory neurons to temperature stimuli, I opted to use calcium imaging on dispersed dorsal root ganglion (DRG) cultures. This approach allows the investigation of hundreds of cells in parallel as well as easy pharmacological intervention.

Briefly, I prepared dispersed DRG neurons from adult mice according to the protocol described in Section 2.2.2, seeded the cells on glass coverslips, and cultured them overnight in DRG culturing medium. On the following day, I loaded the cells with the highly sensitive, non-ratiometric calcium dye Cal-520 [78]. I then transferred the cover slip with the DRG neurons to a constantly perfused microscopy chamber for consecutive calcium imaging. Calcium imaging was performed as described in Section 2.2.3. Figure 1 A and B show example results of a calcium imaging session with one coverslip. The stimulation protocol consisted of five short (25s) temperature steps ranging from 32 °C to 47 °C. Additionally, a supra-maximal capsaicin stimulus (1 µM) was used to probe for TRPV1 expression [79], and a final stimulus with Ringer's solution containing 100 mM KCl to depolarize the neurons and differentiate them from non-neuronal cells by evoking a large calcium response.

The short temperature stimuli applied elicited calcium responses in 46.5 ± 10.9 % of all analyzed neurons across all temperatures tested (Figure 1 B and C). Warm-sensitive neurons (WSN); neurons that respond to temperatures below 42 °C, represent 27.4 ± 8.3 % of all imaged neurons while heat-sensitive neurons (HSN); responding only to temperatures above 42 °C, represent 19.1 ± 5.5 % (Figure 1 D). Surprisingly, these observations differ from the proportion of WSN and HSN ob-

served *in vivo*. Approximately 2 % of TG and 6 % of DRG neurons respond to warmth *in vivo*, while 50 % and 60 % of all analyzed cells are heat-sensitive, respectively [31, 80].

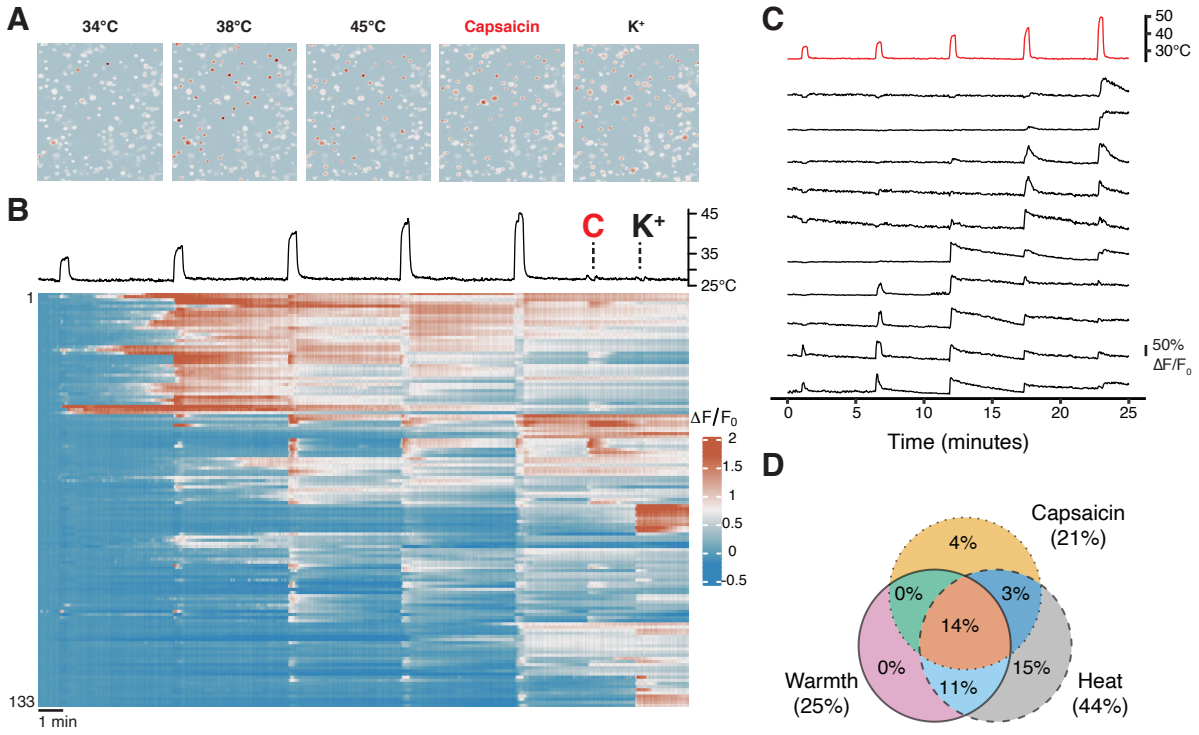

Figure 1 | Calcium imaging in overnight DRG cultures. A Representative calcium imaging field of view (FOV). Plotted are the averaged raw intensities throughout each stimulus. Temperatures represent the maximum temperature reached during the stimulus. Capsaicin (1 µM) and high potassium stimulus (K^+) were used to identify TRPV1-positive cells and neurons, respectively. **B** Top panel: Trace of the chamber temperature over time showing five sequentially increasing temperature stimuli (25 s) followed by a 1 µM capsaicin (C), and high potassium stimulus (K^+). Lower panel: Changes in relative fluorescence ($\Delta F/F_o$) of individual cells from **A**. Each row represents a single cell (n = 133). Rows were reordered by euclidean distance. **C** Bottom panel: Representative traces of individual neurons responding to the different temperature stimuli (top panel). **D** Venn diagram scheme of responder categories. Warmth (<42 °C), heat (≥42 °C). Combined data from 2 animals and 5 FOVs (n = 285 ± 85 cells per FOV).

The discrepancy in responder proportions between the *ex-vivo* preparation and the *in vivo* data could be partially explained by the bias of DRG cultures towards small and medium sized cells (6 % enrichment compared to intact tissue, see section 2.2.3), which include the thermo-sensitive population of DRG neurons (C-fibers). This bias, however, cannot account for a 4-5 times increase in the number of WSN (Figure 1 D). Furthermore, all WSN recorded from TGs *in vivo* respond to capsaicin whereas only 54.6 ± 9.4 % of WSN in the *ex vivo* DRG culture did so. One likely explanation for the discrepancy may lie in the inability of cultured cells to fully return to baseline after stimulation, an effect observed throughout all imaged *ex vivo* cultures (Figure 1 B and C). This observation, in addition to the discrepancy in the WSN proportions open the question whether DRG cultures are an appropriate model of the *in vivo* state.

Since the extraction and dissociation of DRG neurons entails cutting off the peripheral and central nerve branches, it represents an axotomy [81]. Therefore, DRG cultures might represent an injury model. In agreement with this hypothesis, injury of the oral mucosa (by treatment with a 15 s, 55 °C stimulus) results in a dramatic increase in the proportion of warm sensitive TG neurons *in vivo* [31]. Interestingly, the procedure leads to the recruitment of normally noxious heat-sensitive cells into the warm range by sensitizing them, thereby expanding the pool of warm temperature responding cells. Similarly, the DRG preparation protocol could lead to the activation of injury-related pathways, and thereby cause an inflated amount of WSN, comprising a mix of native WSN and sensitized HSN.

DRG neuron sensitization has been widely investigated in the literature. The described mechanisms of action revolve around the concerted activity of the PKA, PKC, and PI3-Kinase pathways [82]. A closer investigation of DRG-dissociation associated sensitization postulates a central role for the adenylate cyclase 2 (AC2), downstream of PKA [83, 84]. Additionally, DRG neuron cultures are a common model system for axonal regeneration studies due to their ability to robustly regenerate their lost axons over the course of a few days and grow long projections that can be studied [81].

3.1.2 Optimizing culturing conditions for assessing temperature sensitivity in primary DRG cultures

Since DRG preparation involves axotomy, I decided to address this problem by optimizing the DRG culture protocol. To do this, I cultured the cells for a longer period of time allowing them to regenerate their axons. This could potentially lead to a recovery from the injury, resulting in a culture that more closely resembles the *in vivo* condition. In an attempt to stop the injury-related mechanisms from occurring, I also cultured the cells overnight with a cocktail of inhibitors against PKA, PKC, and PI3-Kinase or an inhibitor of the AC2 alone.

The results of these experiments showed that the three-day cultures have a reduced number of overall responses compared to the overnight culture (Figure 2 A). Furthermore, the ability of neurons to return to baseline after each stimulus was enhanced (except for the highest temperature stimulus (>45 °C), Figure 2 A). The responder proportions were reduced over the whole range of temperature stimuli when compared to overnight cultures (Figure 2 B). Notably, the reduction in responders was particularly strong in the warm temperature range (<42 °C, Figure 2 B and C). The proportion of WSN reduced to 7.5 ± 1.4 % ($p < 0.05$ two-sample t-test with Holm's *post hoc*) of all cells in the three-day culture, compared to the overnight cultures (27.4 ± 8.3 % (Figure 2 C).

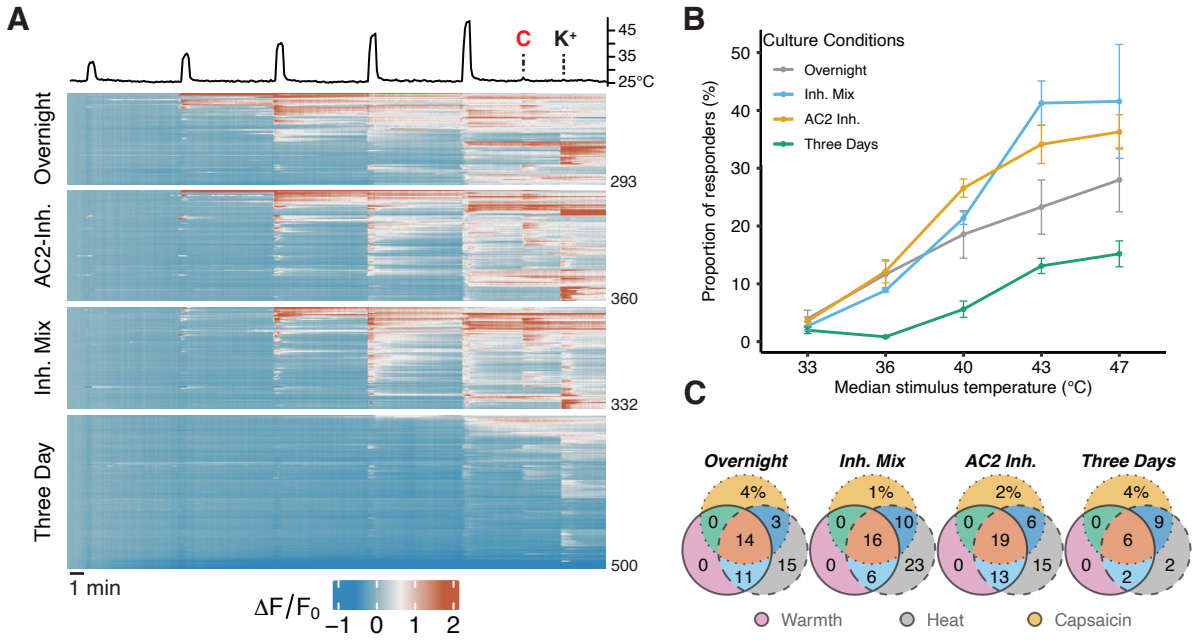

Figure 2 | Optimization of culturing conditions of DRG neurons. A Top panel: Representative temperature trace recorded from the imaging chamber containing the cultured cells. Five temperature stimuli (25s) were applied, followed by a 1 µM capsaicin (C), and high potassium stimulus (K^+). Bottom panel: Representative heatmap of a single FOV per condition. Overnight culture (n = 298), overnight culture treated with a AC2-inhibitor (SQ 22536 100 µM, AC2-Inh., n = 360), overnight culture treated with a mix of PKC (Bisindolylmaleimide I, 2 µM), PKA (H-89, 5 µM), and PI3K-inhibitor (LY294002, 20 µM) identified by 'Inh. Mix' (n = 200), and three day culture (n = 500). **B** Proportion of cells responding to a given temperature stimulus for different culturing conditions. Cells were analyzed from two individual animals and 2-4 FOVs per condition. Average of 1180 ± 348 cells per condition. Mean and S.E.M. are plotted. **C** Venn diagram schemes showing the overlap of warmth, heat, and capsaicin responders in the different culture conditions tested.

The treatment of overnight cultures with either inhibitor combinations lead to a slight improvement of the cells' ability to return to baseline after stimulation, suggesting a partial recovery from the procedure (Figure 2 A). However, neither inhibitor condition lead to a significant reduction in the proportion of WSN (21.9 ± 1.0 % Inhibitor-Mix, and 32.8 ± 6.0 % AC2-Inhibitor) (Figure 2 C).

In summary, I found that three-day cultures, in comparison to overnight cultures, lead to a reduction in the proportion of WSN and an improved ability to recover after stimulation. Inhibition of inflammatory pathways in overnight cultures, however, did not lead to an improvement, compared to three day cultures. Therefore, I decided to use three-day cultures in the following experiments as they more-closely resemble the *in vivo* condition.

3.1.3 Warm-sensitive cells require a minimum temperature and temperature change rate for their activity

Next, I used the three-day culture protocol to analyze DRG neuron responses to warm and hot temperature stimuli. As described in the introduction (sections 1.2.1 and 1.2.2), the response to a given temperature stimulus depends on the absolute temperature reached, the stimulation area size, the baseline temperature before the stimulus, and the temperature change rate [11]. Commonly, WSN are defined as cells that respond to stimuli below 42 °C, using the maximum reached temperature during the stimulus as a threshold (Figure 3 A). During the analysis, I found that some cells that would be considered HSN by the classic criterium already showed a calcium transient at temperatures below 42 °C (Figure 3 A and B). This observation is also recapitulated in published examples of *in vivo* calcium imaging in DRG neurons [80]. This suggests that these cells actually represent warm sensitive neurons, and not HSNs.

Calcium transients are a delayed reporter of action potentials. To correctly determine the conditions that trigger a temperature-dependent response, the beginning of the calcium transient should be estimated. To do this, I used 10 % of the maximum fluorescence during a stimulus as a response threshold. This method proved to be a robust approximation of the fluorescence change-point (data not shown) and allows the deduction of the threshold temperature of a given cell during a stimulus (Figure 3 B). Using this analysis I confirmed that the temperature threshold (T) for some HSN lies below 42 °C, with the only difference being that the rate of the temperature change ($^{\delta T}/_{\delta t}$) applied in the stimulus was higher than during the previous stimuli, where the cell did not respond (Figure 3 B). Furthermore, plotting the minimum response T and corresponding $^{\delta T}/_{\delta t}$ of all imaged wildtype neurons reveals that 60 % of cells classically categorized as HSNs have T thresholds below 42 °C (Figure 3 C). This suggests that in addition to a certain threshold temperature, WSNs and HSNs require a minimum $^{\delta T}/_{\delta t}$ to be activated.

If a minimum stimulus T and $^{\delta T}/_{\delta t}$ combination is applied, a response will always occur. However, it is unclear whether temperature-sensitive cells maintain their threshold T or $^{\delta T}/_{\delta t}$ over multiple stimuli at different maximum T and $^{\delta T}/_{\delta t}$. To answer this question, I deduced the threshold T and $^{\delta T}/_{\delta t}$ of each cell at multiple consecutive stimuli and calculated the corresponding standard deviations (Figure 3 D top panel). This analysis showed that the majority of analyzed cells maintain their T and $^{\delta T}/_{\delta t}$ thresholds in a narrow range with average standard deviations of ±2.01 °C and ±0.59 °C/s, respectively (Figure 3 D bottom panel).

In summary, the response threshold analysis of the recorded neurons indicates that in the range between 25 °C and 45 °C, DRG neurons require a certain combination of absolute temperature

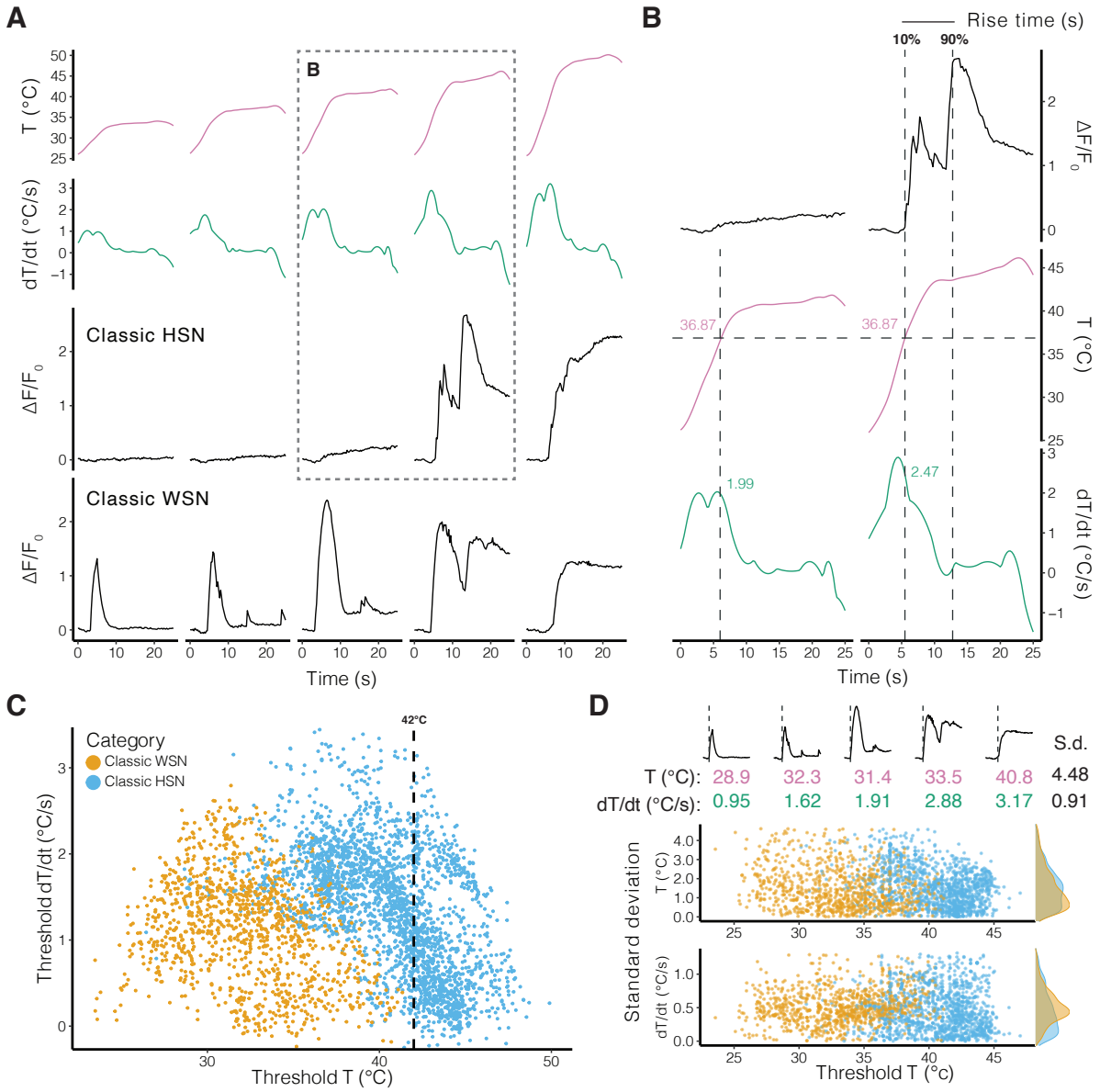

Figure 3 | Characteristics of neuronal temperature response kinetics. A Examples of cells defined by classic criteria as warm-sensitive (WSN) and heat-sensitive neurons (HSN). Top two panels: Stimulus temperature (T) and temperature change rate ($\delta T/\delta t$) during each stimulus. Bottom two panels: Normalized fluorescence ($\Delta F/F_o$) traces of representative cells in response to 5 consecutive temperature stimuli. The dashed box depicts the magnified trace shown in B. **B** Continuous vertical dashed lines represent the 10 % threshold and 90 % threshold of the cells response. The time between the 10 % and 90 % threshold is the rise time of the cells response. Horizontal dashed line represents the cells response temperature in both stimuli. The vertical line in the left panel indicates the corresponding $\delta T/\delta t$ at the threshold T. **C** Scatter plot of minimum threshold temperature (T) and corresponding temperature change rate ($\delta T/\delta t$) of wild-type cells. Different colors represent categorization of thermal responders by classical criteria. The dashed line indicates the threshold temperature (42 °C) for HSN categorization (n = 3794 pooled from 13 animals). **D** Stability of threshold temperature (T) and temperature change rate ($\delta T/\delta t$) in consecutive simulations. Top panel: Response traces of each stimulus of the example classical WSN shown in **A**. The threshold temperature (T) and temperature change rate ($\delta T/\delta t$) for each stimulus are depicted below and the standard deviation (S.d.) for both was plotted to the right. Bottom two panels: scatter plots of the standard deviations for T and $\delta T/\delta t$ against threshold T of all cells described in **C** that had at least two responses to temperature across an imaging session (n = 2290). Different colors represent same categorization as in **C**. Side plots depict density histograms of the standard deviations per condition and category.

and minimum temperature change rate for activity. Additionally, once the minimum threshold temperature and change rate are given, WSN and HSN respond to the same temperature and change rate, with a fairly low variability.

3.1.4 Genetic deletion of TRP-channels leads to shift in temperature response characteristics

In the previous section, I established the methodological foundation for the characterization of peripheral neuron responses to temperature based on recordings in wildtype cells. Next, I tested the dependence of warmth and heat responses on the temperature-sensitive ion channels TRPV1 and TRPM2, as they were both suggested to be major players in warmth detection *in vivo* (see section 1.3.1 and 1.3.2) [31, 34]. To that end, I applied the previously detailed calcium imaging methodology and data analysis to cells from animals lacking TRPV1, TRPM2, or both (Figure 4).

Cultures obtained from all TRP-channel knockouts showed a significant reduction in the proportion of responders in the range from 30 °C to 44 °C, compared to wildtype cells (4 A and B). Interestingly, in temperatures above 38 °C, TRPV1/M2 double knock-out (DKO) cells showed a stronger reduction in responses, when compared to either TRPV1 or TRPM2 single knock-out cells. This suggests an additive effect of the loss of both TRPV1 and TRPM2.

Analyzing the responders with thresholds below 42 °C, the lack of both TRPV1 and TRPM2 combined lead to a loss of cells responding to temperature changes ($\delta T/\delta t$) above 1.5 °C/s, while TRPV1-KO alone enriched said population of fast $\delta T/\delta t$ responders, suggesting a possible compensatory mechanism (Figure 4 C left). Additionally, TRPV1-KO and double knockout cells had a marked prolongation of their rise times. Interestingly, WSN from TRPM2-KO animals show a similar distribution of $\delta T/\delta t$ thresholds and rise time, compared to wildtype cells.

Taken together, the loss of either TRPV1 or TRPM2 lead to a significant reduction in the proportion of WSN and the combined loss of both channels had an additive effect. Furthermore, the lack of either TRPV1 or TRPV1/M2 combined caused a shift in the response characteristics of the remaining cells. This goes in line with previous data indicating that both channels are major contributors to warmth detection and supports the hypothesis that both channels are needed for warmth detection.

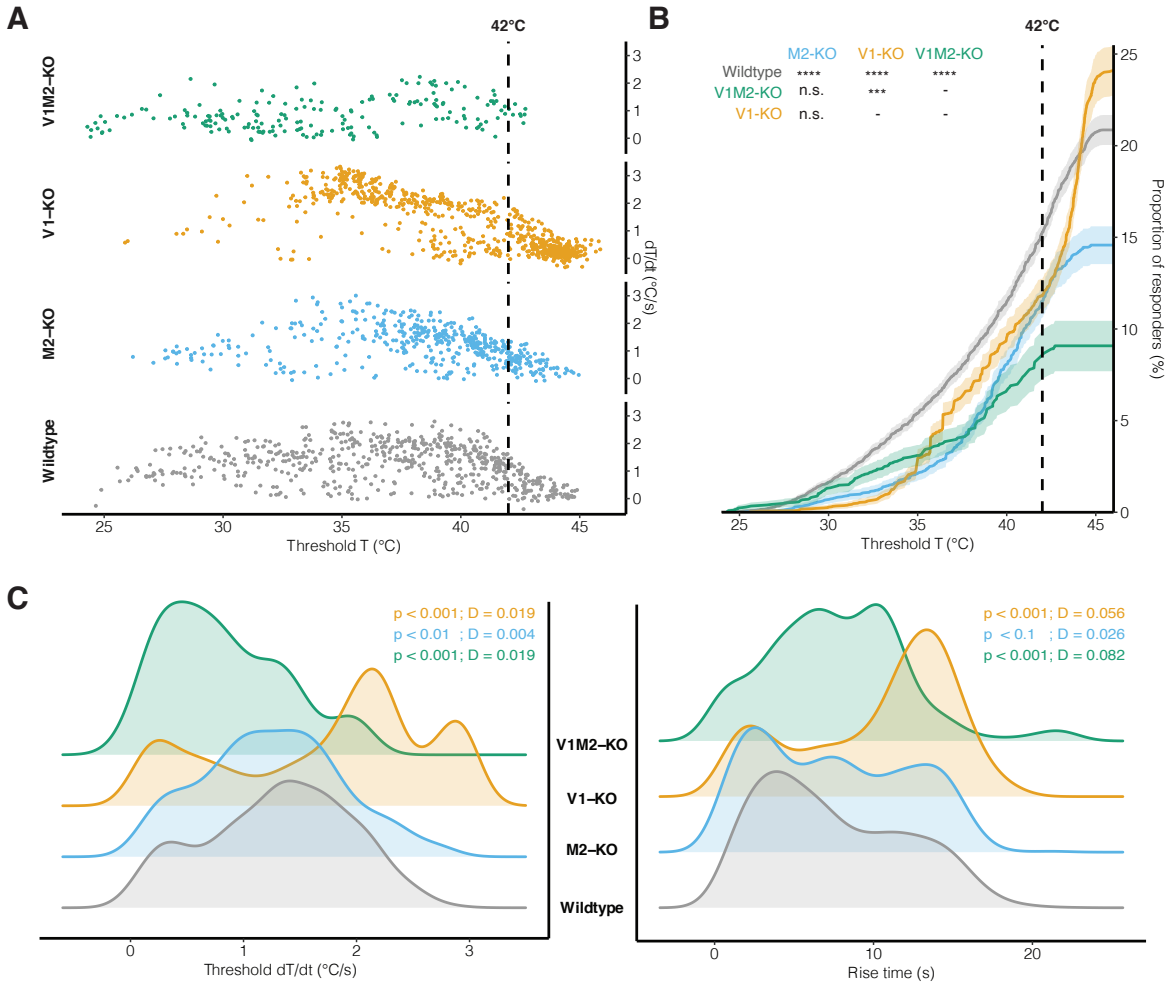

Figure 4 | Response characteristics of cells lacking TRPV1, TRPM2, or both. A Temperature (T) and temperature change rate ($\delta T/\delta t$) thresholds of cells lacking TRPV1 (V1-KO), TRPM2 (M2-KO) or both (V1M2-KO). Cells from wildtype animals serve as control. Shown are all temperature responders from an equal amount of recorded cells per genotype (n = 3500 randomly sampled cells). **B** Cumulative proportion of responders by threshold temperature. Mean and 95% CI are plotted. Statistical testing was only performed at 42 °C. Multiple pairwise Log-Rank test with Benjamini-Hochberg *post-hoc* test. Wildtpye; n = 12747 cells from 8 individual animals, TRPM2-KO; n = 4963 cells from 3 animals, TRPV1-KO; n = 4656 cells from 3 animals, TRPV1M2-KO; n = 3520 cells from 3 animals. $*$ (p <0.05), $**$ (p <0.01), $***$ (p <0.001), $****$ (p <0.0001) **C** Density plots of threshold temperature change rate ($\delta T/\delta t$) (left panel) and rise time (right panel) for all cells from **B** with a threshold temperature <42 °C. Weighted Wasserstein distances were used to compare distributions to wildtype. The D-value represents the absolute distance between the tested distributions. The closer this number is to 0 the more likely it is that the two samples were drawn from the same distribution. A p-value below 0.05 signals the inability to reject the null hypothesis (that both distributions were drawn from the same distribution).

3.1.5 Over expression of Trpv1 shifts temperature response profile

TRPV1 is traditionally known as a noxious heat sensor [85, 86]. However, the majority (75 %) of warmth sensitive cells recorded in this study respond to the TRPV1-agonist capsaicin (Figure 2

C). This is in line with previous *in vivo* data showing that all WSN in TGs are TRPV1-positive [31]. Furthermore, plotting the distribution of capsaicin responders and non-responders in wildtype animals showed that the majority of the warm temperature response is carried by TRPV1-positive cells (Figure 5 A). Taken together with the data collected from TRPV1-deficient cells, this supports a role for TRPV1 in warmth detection.

TRPV1 shows a small but significant current flow at temperatures below 42 °C, when expressed in heterologous systems [86]. While these currents are minor, they could reach considerable levels with higher amounts of TRPV1 in the cell membrane. Intriguingly, in a study in rats, a population of DRG cells expressing high amounts of TRPV1 is activated by innocuous warmth [87]. This prompted me to determine if overexpression of Trpv1 could lead to an increased sensitivity to temperature in WSN.

To test this possibility, I used a mouse line that over-expresses Trpv1 in Trpv1-positive cells (V1-OX in 5 B, described in [30]) and repeated the temperature protocol with three temperature stimuli, stepping up to 39 °C. Overexpression of Trpv1 lead to a 3-4 fold increase in the WSN population (Figure 5 D). This increase was not due to a larger proportion of Trpv1-positive cells overall (Figure 5 B) and therefore reflects an increased temperature sensitivity.

Investigation of the response characteristics of V1-OX cells compared to wildtype cells (Figure 5 E) reveals that WSN from V1-OX animals show an enrichment of cells responding to faster temperature change rates ($\delta T/\delta t$ of >1 °C/s). The stimulus rise times, however, were not markedly affected (Figure 5 F).

The increase in the proportion of WSN coupled with the enrichment of fast $\delta T/\delta t$ responders without changing the proportion of TRPV1-positive cells suggest a shift in temperature sensitivity of TRPV1-positive cells in V1-OX DRG neurons. In summary, this data implies that higher amounts of TRPV1 in Trpv1-expressing sensory neurons are able to reduce the temperature threshold of WSN by increasing their sensitivity to lower temperatures.

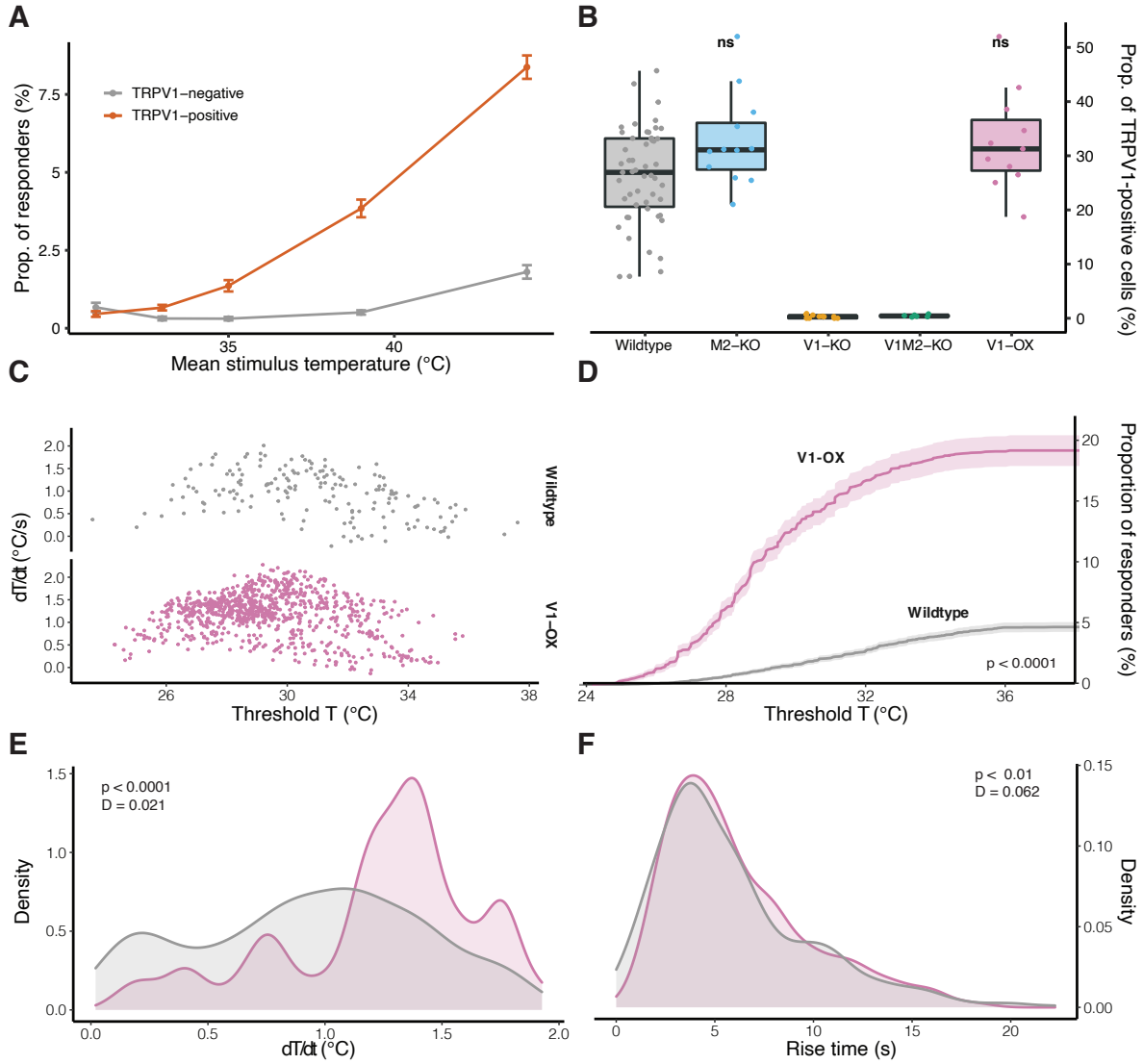

Figure 5 | **Modulation of warmth response by TRPV1. A** Proportion of wildtype DRG neurons responding to the TRPV1-agonist capsaicin (1 µM) across multiple temperature stimuli. Pooled data from 16 animals with 1375 ± 516 cells per animal. **B** Proportion of TRPV1-positive cells (response to capsaicin (1 µM)) by genotype. One-way ANOVA followed by multiple comparison testing against wildtype with Holms' *post-hoc* test. Median, interquartile range, and full range are indicated by the box plots. **C** Overview of threshold temperature (T) and change rate ($\delta T/\delta t$) of WSN overexpressing Trpv1 (V1-OX) and wildtype WSN. Responding cells from 3800 randomly sampled neurons from 2 V1-OX and 8 wildtype animals are plotted. **D** Cumulative proportion of response temperature for all temperature responders from V1-OX (n = 731 of a total of 3875 recorded cells) and wildtype animals (n = 513 from a total of 11062 cells). Cumulative events compared via Log-Rank test. **E**, and **F**; Density plots of threshold temperature rate ($\delta T/\delta t$) and rise time for WSN from **D**. Densities were compared using reweighted Wasserstein distance as described in Figure 4.

3.2 Assessment of *in vivo* temperature preference

The previous data suggests important and varying roles for TRPV1 and TRPM2 in dissociated sensory neurons. The lack of either channel lead to a significant decrease in the proportion of WSN as well as shifts in their response characteristics. Additionally, I show that TRPV1-levels are capable of tuning the response of WSN to temperature. While these *in vitro* observations are striking, it is unknown whether the observed effects will also translate into *in vivo* phenotypes.

As summarized above (section 1.3.2), TRPM2-KO animals have no preference when presented with a 38 °C heated side in the TPP test, while wildtype animals clearly avoid 38 °C [34]. TRPV1-KO animals on the other hand behaved similar to wildtypes under these conditions [31]. In the TPP test, the bottom plates of the chamber are heated. Therefore, the animals develop a preference based on the temperature sensitivity of the paws and snout, which they use to probe the temperature of surroundings objects. However, animals can integrate temperature information from the paws, snout, and the rest of the body. Therefore, the question arose whether the results of the TPP test would change if the animals are confronted with ambient and floor temperatures, affecting their entire bodies, instead of only a heated floor plate.

Therefore, in collaboration with my colleague Dr. Gretel Kamm, we designed and established a modified version of the thermal two-place preference test we call the thermal chamber preference (TCP) test.

3.2.1 Establishment of an ambient temperature preference test

Thermal preference chamber test

The experimental setup consists of two chambers with differing ambient and floor temperatures. The arena (60.3 × 26.1 cm) is isolated with a 4.3 cm thick Styrofoam wall containing two large peltier elements on each side (Figure 6). The peltier elements are equipped with a heat sink that covers the whole element and two generic computer fans on top to disperse the heat. Additionally, both peltiers are connected to a circulating water bath set to 28 °C for cooling. The enclosure contains a 13 × 31.4 cm steel cage with a steel baseplate. The two compartments are separated by a 6.3 cm wide and 6.3 cm high tunnel to separate the two chambers from each other and minimize air exchange between the chambers. The tunnel is kept illuminated via a transparent plexiglass cube to reduce the likelihood for the animal to hide in the tunnel. The setup is covered with a

foam/wood cover with a transparent plexiglass inlay to allow video recording from above. Thermometers attached to the inner walls of the chamber allow for an automatic control of the peltier elements function and temperature monitoring during the experiment.

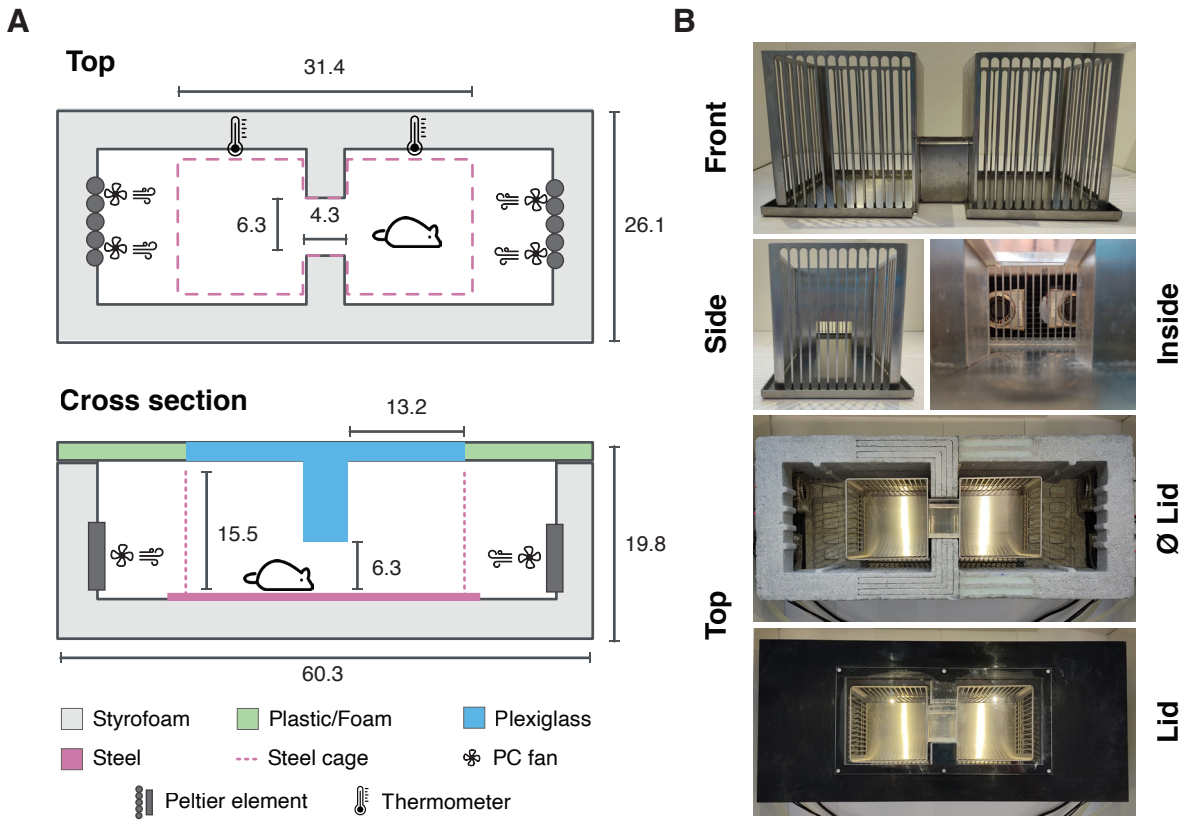

Figure 6 | **Thermal preference chamber. A** Schematic of the thermal preference chamber. Not shown is a circulating water bath supplying water at 28 °C to cool the peltier element. Dimensions in centimeters (cm). **B** Representative images of the experimental setup. Shown are the front and side view of the steel cage, as well as the view inside the setup. Inside view shows the PC fans attached to the peltier element. Top view depicted with and without (∅) lid. Cables connected to the setup are used to power and control the peltier elements. Tubing supplies water at 28 °C.

Benchmarking the performance of the TCP test

Next, we wanted to assess the ability of the setup to reach and maintain predefined temperatures in each chamber. To do this, we placed multiple thermometers in each chamber to report the floor, ambient, and wall temperatures (Figure 7 A). Temperatures developed differently depending on the measured compartment (Figure 7 B). While the temperature at the wall of the setup increased and stabilized rapidly, this was not the case for the floor and ambient temperatures. In fact, the ambient and floor temperature started stabilizing at different times, depending on the target temperature (after 50 min in the 31 °C chamber, and 80 min in the 38 °C chamber). A closer

look at the temperatures after stabilization (Figure 7 C) shows that the wall and ambient temperatures oscillate while the floor temperature is stable. The oscillation reflects the function of the peltier as the elements are toggled on and off as a function of feedback from the thermostat, surging the temperature upwards after activation and declining when inactive. Said oscillations in the ambient and wall temperatures are stable and cover a range of 0.5 – 1 °C, depending on the target temperature (Figure 7 D). The lack of oscillation in the steel baseplate is due to the higher heat capacity of steel (468 J K/kg) in comparison to air (100.35 J K/kg), which requires a 4-5 times higher amount of energy for the same temperature change [88].

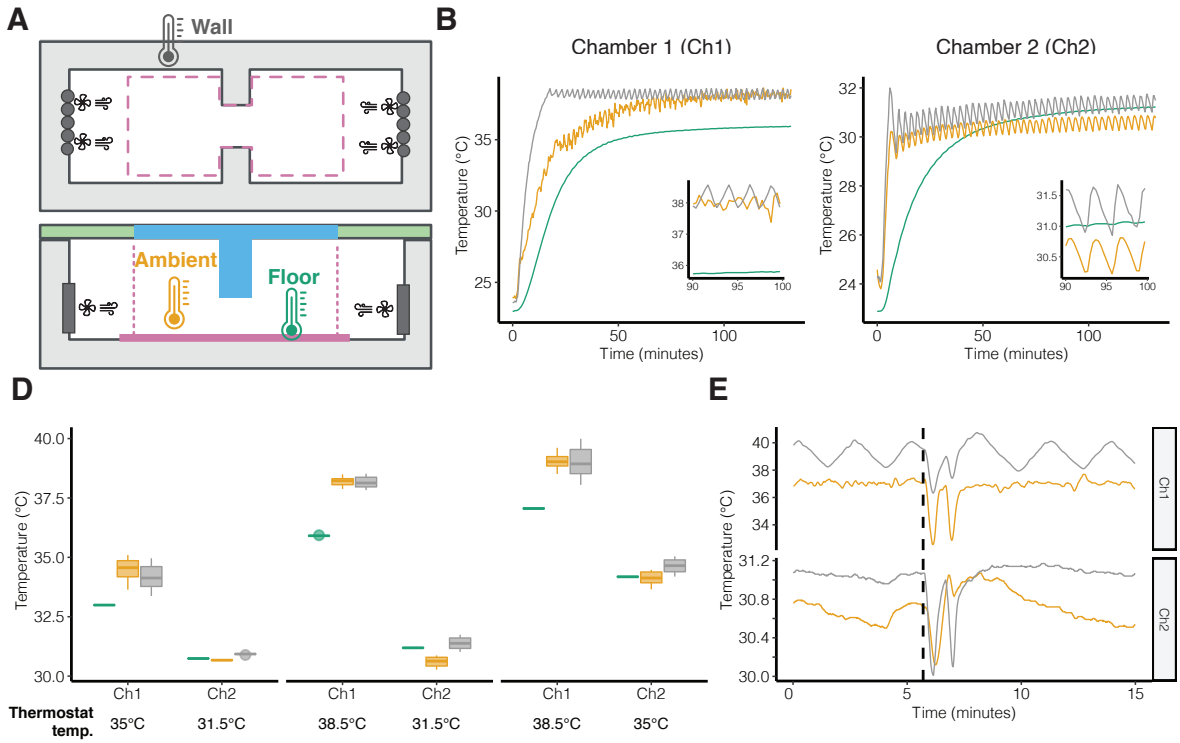

Figure 7 | Thermal preference chamber temperature benchmark. A Scheme of experimental setup depicting the position of the placed thermometers. Each chamber was equipped with all three types of thermometer-positions. All thermometers were placed at equal X-positions. Ambient and wall thermometers were placed at 2 cm, and 3 cm height, respectively. Floor thermometer was attached directly to the steel base place. **B** Development of temperature over time starting from room temperature (25 °C). Chamber 1 (Ch1, top panel) was set to 38.5 °C and chamber 2 (Ch2, bottom panel) to 31.5 °C. Insets zoom in to the last 10 min shown in **B**. **D** Median, interquartile range, and full range of temperatures reached at each measured position over a period of 10 min. **E** Simulation of temperature change when opening the chamber for 10 s after reaching stable temperatures. Dashed line indicates time of chamber opening.

Furthermore, we found that the floor temperature is 1 – 2 °C lower than the ambient temperature on the side with the higher target temperature. This can also be observed when plotting the median temperature reached at each position after stabilization (Figure 7 D). The inability of the floor temperature to equilibrate to the same temperature as the ambient temperature might be due to the baseplate acting as a heat sink between both chambers. Due to the high heat conductivity of

steel (16.3 – 24 W K/m at 25 °C), temperature from the hot side is quickly transferred to the colder side and passed onto the ambient air [88]. This effect also establishes a temperature gradient in the baseplate. This can be circumvented by using two separate baseplates per chamber, leading to a discontinuous floor, which can affect the animals' behavior. We decided to continue with the current setup since the ambient temperature in the chambers was reached and maintained reasonably well and the temperature difference of the floor was small.

We next examined the ability of the system to recover from disturbances like opening the lid to put an experimental animal (Figure 7 E). After an initial drop of 4 °C and 1 °C (38.5 °C and 31 °C side, respectively) the chamber recovered and equilibrated to its previous stable temperature in less than 5 min. This confirms the possibility of measuring multiple animals in succession without the need to wait 50-80 minutes for a cold cage to stabilize.

Experimental procedure and analysis

Animals were transported into the experimental room a day prior to the experiment. On the first day of the experiment, the setup was started and allowed to stabilize for 1.5 h before proceeding. Mice were recorded for 30 min in the setup before they were moved back to their original cage. We waited 5 min before we introduced the next animal to re-equilibrate the chamber temperatures. Different temperature combinations were performed on separate days. Videos were recorded for all experiments and used for automatic analysis.

Data analysis was performed using DeepLabCut, a markerless pose estimation library [72]. To do this, I trained a deep neural network to detect bodyparts of the animals (Figure 8 A and section 2.2.4). I only considered the center of the animal for data analysis and scaled the coordinates to the corners of the baseplate (for a more detailed walk-through of the post-processing see section 2.2.4). This method and analysis allows for the precise tracking of the animals' location in two-dimensional space (Figure 8 B) as well as the temporal occupation on the horizontal axis (Figure 8 C).

In summary, we established an assay that allows assessing temperature preference based on ambient and floor temperature. The setup is capable of keeping a stable temperature throughout the experiment, and recovers quickly after minor disturbances. Additionally, using a trained neural network allowed automatic and reproducible tracking of the animals' position in the setup.

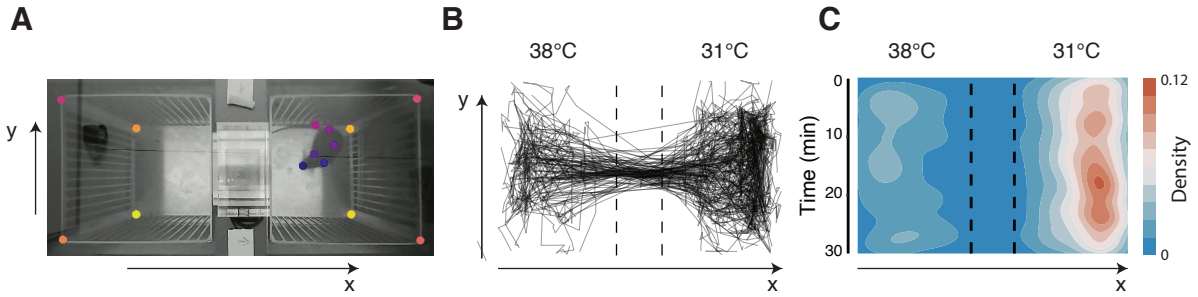

Figure 8 | Data analysis of thermal chamber preference test. A Example of markerless pose estimation using DeepLabCut [72]. Differently colored dots depict individual body parts of the animal as well as points of interest in the experiment such as lower and upper corners of the arena. **B** Path traveled by a single wildtype animal recorded for 30 min when presented with two chambers at 38 °C and 31 °C. Tracking data was downscaled temporally from 20 Hz to 1 Hz. **C** Heatmap of animal location (x-axis from **B**) over time. Plot depicts the kernel density estimation of the x-location. Red depicts a high occupation probability while blue signals a low occupation probability. In this example, the animal spent more time at 31 °C over 38 °C throughout the experiment, suggesting a preference for 31 °C.

3.2.2 TRPM2-KO and TRPV1/M2-DKO animals show deficits in temperature discrimination

After establishing the novel behavioral paradigm, I wanted to test whether the cellular data from the calcium imaging experiments with *ex vivo* DRG cultures translate into behavioral phenotypes. Thus, I recorded the behavior of TRPV1-KO, TRPM2-KO, and TPRV1/M2-DKO animals in comparison to wildtypes in the TCP test.

I found that wildtype animals develop a clear preference for the 31 °C side when having either 34 °C or 38 °C as second option (9 A and B). The preference is less pronounced when presented with cold ambient temperature (25 °C, Figure 11 A). TRPM2-KO animals showed a reduced preference for 31 °C compared to wildtype animals, when presented with either 34 °C or 38 °C. This effect was more pronounced at 34 °C, where the animals even preferred 34 °C over 31 °C. Interestingly, TRPV1-KO animals showed similar preference behavior as wildtype animals in all tested temperatures. Strikingly, the combined loss of both TRPV1 and TRPM2 only showed a significant lack of preference at 38 °C (Figure 11 A and B). At 34 °C, TRPV1/M2-DKO animals showed a reduced preference for 31 °C, albeit not significant. The observed phenotype of TRPV1/M2-DKO animals at 38 °C was stronger than for TRPM2-KO alone, suggesting an additive effect caused by the combined loss of TRPV1 and TRPM2 (Figure 11 B).

As a way to further examine the observed behavior, I also quantified the number of crosses (from one chamber to the other) as well as the length of each visit to the test side (Figure 9 B). The observed phenotypes are partially reflected in the increased average visit length at the test side but

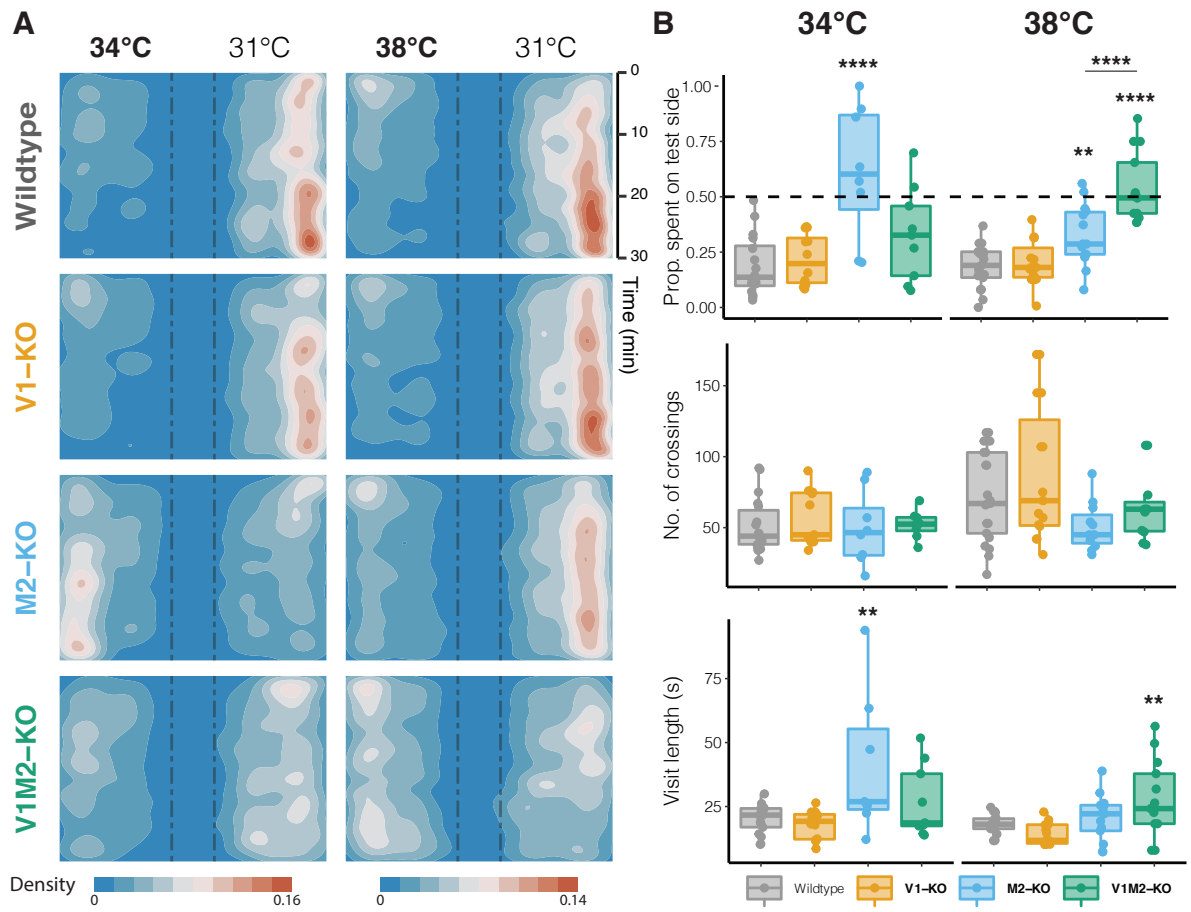

Figure 9 | Temperature preference in TRPV1-KO, TRPM2-KO, and TRPV1/M2-DKO animals. A Kernel density estimation of X-location over time. Animals pooled by genotype and temperature combination. Test temperature indicated in bold. Dashed line represents tunnel between chambers. Densities scaled to each temperature combination. Wildtype; n = 16/21 (from left to right), TRPV1-KO (V1-KO) n = 12/15, TRPM2-KO (M2-KO) n = 8/14, TRPV1M2-DKO (V1M2-KO) n = 9/13. **B** Top panel: Proportion of time spent in the test chamber quantified for the last 10 minutes of the assay. Middle panel: Total number of crosses between chambers throughout the whole experiment. Bottom panel: Average visit length to the test chamber. Plotted are median, interquartile range and range. Outliers were removed via box plot methods (section 2.2.4). One-way ANOVA with Dunnet's *post-hoc* test against wildtype. Comparison between genotypes using Tukey HSD test. ∗∗ ($p < 0.01$), ∗ ∗ ∗∗ ($p < 0.0001$).

not in the number of crossings. Interestingly, TRPM2-KO and TRPV1/M2-DKO animals showed no deficits in cold temperature detection and similar behavior to wildtypes across all quantified metrics when presented with 25 °C (Figure 11). This suggests that the deficits in preference development of TRPM2-KO and TRPV1/M2-DKO animals at warm temperatures are due to impaired detection of the test temperature. An effect that is reflected in a prolonged visit length at the test side.

Taken together, TRPM2- and TRPV1M2-DKO, but not TRPV1-KO animals show a lack of preference when presented with warm temperatures such as 34 °C and 38 °C. An observation that is reflected in a prolonged visit time in the warmer chamber.

3.2.3 Overexpression of TRPV1 reduces preference latency

In DRG cultures, TRPV1-overexpression lead to an increase in the proportion of WSN (Figure 5). To test whether this phenotype alters warm temperature detection *in vivo*, I repeated the temperature preference test with TRPV1-OX animals (Figure 10). Overexpression lead to a faster establishment of preference, compared to wildtype animals (Figure 10 A and B). This phenotype was reflected in a significantly reduced number of crosses throughout the whole experiment, but not in the average visit length to the warmer chamber (Figure 10 C). No significant differences compared to wildtype animals were observed when TRPV1-OX animals were presented with 25 °C (Figure 11). This suggests that TRPV1-OX animals require fewer visit to the test side to establish preference, and therefore show a faster preference development.

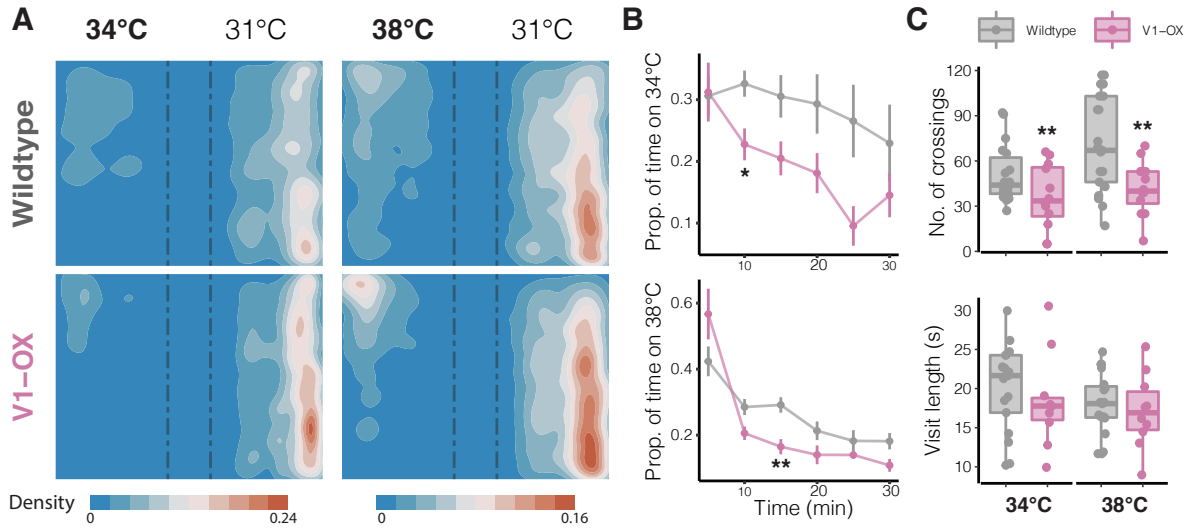

Figure 10 | Temperature preference of TRPV1-overexpressing animals. A Kernel density estimation of X-location over time. Animals pooled by genotype and temperature combination. Test temperature indicated in bold. Dashed line represents tunnel between chambers. Densities scaled to each temperature combination. Wildtype; n = 16/21 (from left to right), TRPV1-overexpression (V1-OX) n = 12/12. **B** Proportion of time spent on test side. Plotted are the mean ± S.E.M. One-way ANOVA with Sidaks' *post-hoc* test. **C** Top panel: Total number of crosses between chambers throughout the whole experiment. Bottom panel: Average visit length to the test chamber. Plotted are median, interquartile range and range. Outliers were removed via box plot methods (section 2.2.4). Pairwise t-test for each temperature combination. $*$ ($p < 0.05$), $**$ ($p < 0.01$).

Taken together, TRPM2- and TRPV1M2-DKO animals showed deficits in warm temperature detection as they failed to develop preference for 34 °C and 38 °C, respectively. Additionally, animals overexpressing TRPV1 showed a faster development of preference when presented with warm temperatures. Surprisingly, TRPV1-KO animals which had reduced proportions of WSN in *ex vivo* DRG cultures, showed no marked difference to wildtype animals in all tested temperature combinations.

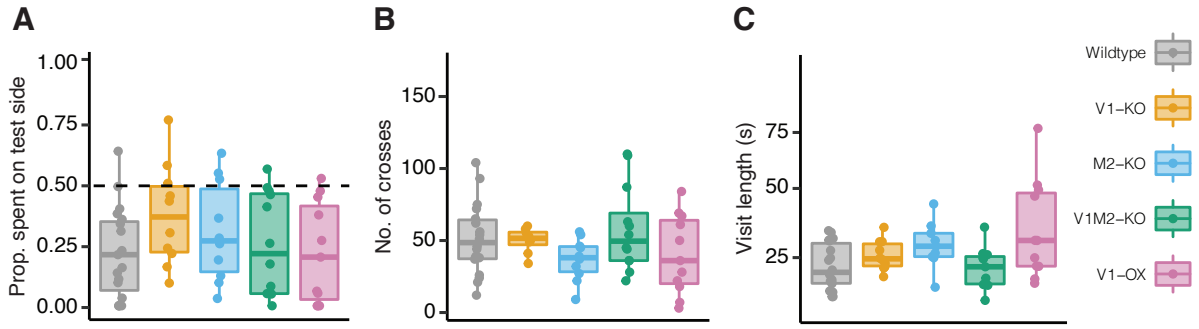

Figure 11 | Behavioral parameters of tested genotypes at 25 °C. **A** Proportion of time spent in the test chamber side quantified for the last 10 min of the assay. **B** Total number of crosses between chambers throughout the whole experiment. **C** Average visit length to the test chamber. Plotted are median, interquartile range and range. Outliers were removed via box plot methods (section 2.2.4). One-way ANOVA with Dunnet's *post-hoc* test against wildtype.

4 Discussion

The roles of the temperature-sensitive channels TRPV1 and TRPM2 in warmth-sensation are a matter of debate (section 1.3.4). Operant behavior assays suggest a role of both channels in the trained detection of warmth [31, 80], while voluntary behavioral tasks show only a defect in animals lacking TRPM2 [89], but not TRPV1 [36]. On a cellular level, TRPV1-KO animals show no response of TG neurons to warm stimuli *in vivo* [31]. Cultures from TRPM2-KO animals, on the other hand, were not probed in the warm temperature range, but show reduced proportions of responders when a heat stimulus is applied [89]. Additionally, no study investigated the combined effect of both channels on warmth detection. To address the inconsistencies between the *in vivo* and *in vitro* results, and to test the combined relevance of both TRPV1 and TRPM2, this study established optimal culturing conditions for the assessment of warmth *in vitro*. Additionally, this study introduces a novel behavioral paradigm to test the preference of mice to ambient temperatures, which was used to assess the role of TRPV1 and TRPM2 in warmth detection *in vivo*.

4.1 *In vitro* sensory neuron cultures

4.1.1 Three-day cultures as an alternative to overnight cultures

In my extensive literature review I found no previous study systematically investigating the response of cultured sensory neurons to warm temperature stimuli. Culturing DRG neurons overnight followed by the application of a series of increasing temperature steps (33 – 47 °C) revealed that approximately 27 % of the recorded neurons respond to stimuli below 42 °C (Figure 1). This stood in contrast to data showing that only 2 – 6 % of all sensory neurons are wamrth sensitive *in vivo* [31, 80]. The expansion of WSN-proportions is reminiscent of a post-injury state, in which HSN become sensitized to warm stimuli [31, 90]. Additionally, I found that the recorded neurons did not return to their pre-stimulus baseline. This suggested to me that the overnight cultures of DRG neurons represents an injury model.

Injuries to peripheral nerves such as compression or lesion lead to hyperexcitability in the respective sensory neurons [91–93]. The preparation of DRG or TG cultures entails severing the axons of the cells (axotomy) and consequent disruption of the tissue (section 2.2.2). Electrophysiological recordings of acutely cultured DRG and TG neurons show hyper-excitability in comparison to cells from intact ganglia, similar to an injury of the nerves [83, 84, 94]. Additionally, DRG and TG neuron cultures overexpress Atf3, a transcription factor only active in sensory neurons after injury [94–96]. Combined, this evidence further supports the notion that DRG and TG cultures represent an injury model.

To address the injury state of DRG neurons in culture, I prolonged the culture protocol to three days to allow the cells to recover from the procedure. This lead to the reduction in the proportion of WSN to 7.5 % (Figure 2). Additionally, the cultured cells regained the ability to return to their pre-stimulus baseline after a warm stimulus, resembling the *in vivo* state.

A recent study investigating the transcriptomes of DRG neurons cultured for 4 days shows an overexpression of inflammatory markers (including Atf3) in comparison to native DRG neurons [97]. Additionally, single-cell sequencing of TG and DRG neurons following the time course after nerve injury shows a population of Atf3-expressing neurons only present in the injured samples [98, 99]. Furthermore, the expression of Atf3 follows the course of the injury. The proportion of Atf3-expressing neurons is the highest one day after injury and only starts declining 14-21 days after the injury. This is also reflected in single-cell sequencing of cultured DRG neurons where all cells cultured overnight show high expression of Atf3 (data not shown). Taken together, these reports suggest that the three-day cultures tested in this study do not represent a fully recovered state. Longer culturing periods coupled with an assessment of Atf3-expression could help define the time point of recovery in cultures. DRG neurons cultured on multi-electrode arrays for up to 21 days show an increase in the mean recorded spontaneous activity at 37 °C over the culturing period, plateauing after 9 days in culture [100]. Since warm-senstive fibers *in vivo* show continuous activity at 37 °C [101], the recorded spontaneous activity in cultures at 9 days could therefore signal a recovery of the culture, further supporting a prolonged culturing period. However, while feasible, longer culturing periods could lead to cell culture-related artifacts, such as the formation of aberrant glutamatergic synapses, which do not occur in DRG neurons *in vivo* [97, 102, 103].

The tested three-day culture protocol showed a marked improvement in terms of temperature responsiveness compared to overnight cultures, with similar response proportions to the *in vivo* data. Cell culture systems will never fully resemble the *in vivo* state, but represent a reasonable alternative to elaborate *ex vivo* experiments. Therefore, culturing primary DRG neurons for three days might pose a good compromise between culturing length, technical feasibility, and physiological relevance.

4.1.2 Adequate stimulus for innocuous warmth sensors

Warm sensitive fibers and neurons are defined by a more or less linear increase of action potential firing in response to stimuli below 42 °C [101]. A detailed analysis of the calcium response of DRG neurons in this study showed that a combination of temperature and temperature change rate is required for a response to thermal stimuli (Figure 3). The calcium transients measured using calcium imaging are a delayed reporter of action potentials, as the used dyes have delays and rise-times of at least 200 ms while common neuronal action potentials have a duration of 1 ms. The adequate stimulus of a thermo-sensitive neuron is the stimulus that leads to a first action potential, therefore, using calcium imaging, the beginning of the calcium transient reports the closest estimation of the adequate stimulus. In this study, the beginning of the calcium transient was approximated by defining the time-point at which the cell reached 10 % of its maximum calcium signal (Figure 3). Analysis of the corresponding threshold temperature and temperature change rate revealed that 60 % of cells that are classically defined as HSN in fact respond to warm temperatures, given an adequate minimum temperature change rate.

In addition to absolute temperature, temperature change rate also affects the detection and perception of warm stimuli. In warm-sensitive fibers, applying temperature ramps with a fixed target temperature and increasing temperature change rates leads to an increase in firing frequency [101, 104–106]. Rhesus monkeys that were trained to detect warming stimuli perform better and with shorter response latencies when the same stimulus is given at increasing temperature change rates [107]. Analogously, psycho-physical studies with humans show that faster stimuli lead to a stronger perception of warmth, an improved detection of small temperature increments, and a shorter response latency to warming stimuli [106, 108, 109]. Interestingly, increasing the temperature change rate does not markedly alter the threshold temperature of warm- and heat-sensitive fibers [105, 110]. This is also reflected in this study where cells retained their temperature and change rate thresholds in a narrow range, even when the stimuli increased in intensity (Figure 3).

The observation that some classically defined HSN start their calcium transients at temperatures below 42 °C was also shown in the *in vivo* calcium imaging experiments done in TGs and DRGs [31, 80]. In these studies, the analysis of temperature responses was solely focused on the absolute temperature and the change in temperature (delta), without considering the rate of temperature change. However, the data presented in this study showed that WSN require a combination of a specific threshold temperature and minimum temperature change rate for their response, highlighting the importance of this parameter for future studies.

Since temperature change rates affect the accuracy of perceptual warmth detection, it is possible that cells and fibers that were classically deemed heat-sensitive in fact also contribute to the detection of warmth, when fast temperature changes occur. This could be tested in an operant behavior assay by the application of stimuli with a fixed target temperature (e.g. 38 °C) and increasing temperature change rates (i.e. shorter stimulus duration).

In summary, I established a suitable culturing method for the analysis of warm-sensitive peripheral sensory neurons and devised a method to detect and characterize their responses via calcium imaging. Thus, with these tools in hand, I moved on to address the role of TRPV1 and TRPM2 in warm-temperature detection.

4.1.3 TRPV1 and TRPM2 play different roles in warm-temperature detection

TRPV1 and TRPM2 are both implicated in the response to warm-temperature stimuli [31, 34]. Calcium imaging of primary cultures from animals lacking TRPV1 and TRPM2 in this study showed a significant reduction in the proportion of WSN in both genotypes (Figure 4). Furthermore, the combined deficiency of both channels leads to a stronger reduction in the proportion of WSN than in the single knockout cultures.

To the best of my knowledge, this is the first study testing the role of TRPM2 in sensory neurons using warm temperature stimuli. Previous studies using cultured DRG neurons only assessed the relevance of TRPM2 in heat detection with stimuli above 45 °C [34, 40, 41]. I found that TRPM2-KO cultures show a significant reduction in the proportion of WSN, an effect that is sustained at temperatures above 42 °C (heat). This suggests that TRPM2 is required for warmth detection in at least some WSNs. Intriguingly, these results are similar to the observations from TRPM2-KO DRG cultures stimulated with heat (>45 °C) [34, 40]. Tan et al. describe a population of HSN comprising 10 % of all recorded cells that does not respond to TRPV1/A1/M3 agonists. This population is reduced to 3 % in TRPM2-KO animals, analogous to the 5–6 % loss in WSN reported in this study (Figure 4). It is therefore possible that both described populations are identical, with the difference that the previous study was done in overnight DRG cultures, thereby masking the phenotype in the warm temperature range (as discussed above).

For TRPV1, my results show a similar tendency to the *in vivo* calcium imaging experiments in TG neurons done by Yarmolinsky and colleagues, but do not fully recapitulate the observations [31]. Specifically, loss of TRPV1 leads to a complete absence of warm-sensitive TG neurons *in*

vivo. Using the same analysis method with cultured DRG neurons in this study shows only a 75 % reduction in the proportions of WSN. In addition to the caveats of *ex vivo* cultures discussed above, a possible explanation is the difference in the studied tissue. TG neurons innervate the head and face while DRGs innervate different parts and tissues throughout the body, depending on their location along the spinal column. Single-cell sequencing results comparing TG and DRG neurons suggests that the composition of cell populations is similar, but not identical [111]. Additionally, the proportions of TRPV1-positive cells in DRG and TG is similar, however, the overall Trpv1-expression in whole TG tissue is higher than in DRGs [112, 113]. Intriguingly, contrary to TRPM2-KO cultures, the cumulative proportion of all temperature-responders in TRPV1-KO cultures was similar to wildtype cultures (Figure 4). This suggests that TRPV1-deficiency only alters the response threshold of thermo-sensitive DRG neurons towards higher temperatures, without affecting their thermosensitivity *per se*.

The analysis of TRPV1-KO neurons revealed an enrichment of cells with fast temperature change rate thresholds (>1.5 °C/s), compared to wildtype and TRPM2-KO cultures (Figure 4). This shift indicates that in some cells, TRPV1 partakes in the thermosensitivity (by reducing the temperature threshold), but is not required for a response to temperature. The residual capacity of TRPV1-KO cultures to respond to thermal stimuli hints to the involvement of other thermo-sensitive channels. In support of this hypothesis, the combined lack of both TRPV1 and TRPM2 in DRG cultures showed an additive reduction in the proportion of WSN, compared to the single knockouts (Figure 4). Specifically, TRPV1M2-DKO cultures showed a complete loss of cells with a fast temperature change rate threshold (>1.5 °C/s). This suggests that TRPM2 was responsible for a proportion of the residual thermosensitivity observed in TRPV1-KO cultures. Additionally, this data also implies that TRPV1 and TRPM2 are co-expressed in some DRG neurons. Indeed, single-cell sequencing analysis shows that Trpm2 is expressed in 10.7 % of all DRG neurons, with 58 % of Trpm2-positive cells also expressing Trpv1 (combined analysis of [114, 115], data not shown).

Interpreting the results in the light of data collected from adult DRG neurons should be handled cautiously since both Trpv1 and Trpm2 have wide expression patterns during DRG development (up to 60 %), that narrows down in adult cells [114, 116, 117]. The magnitude of this expression pattern is demonstrated when ablating the Trpv1-positive lineage, an intervention that leads to a complete loss of thermosensitivity in adult mice [36, 112]. A study of neuronal development in TRPM2-deficient mice showed an aberrant cortical maturation under hyperthermia, supporting a role TRPM2 as a temperature sensor in development [118]. While the roles of both channels during sensory neuron development are still unknown, they could affect the development of a wide range of DRG neurons, beyond the cells that express both channels in the adult animals. A way to circumvent the developmental influence of the channels is the pharmacological inhibition of TRPV1 and TRPM2. A battery of highly specific and thoroughly tested TRPV1-antagonists

exist [119]. TRPM2, however, lacks comparable pharmacological tools with the best inhibitor available, 2-APB, having an array of off-target effects, including acting as an agonist for TRPV1 [120]. Nevertheless, combining pharmacological and genetic tools could shed some light on the development-associated effects of TRPV1 and TRPM2 deficiency.

The combined deletion of TRPV1 and TRPM2 lead to a 50 % reduction in the proportion of WSN (Figure 4). The existence of residual WSN implies the presence of other thermo-sensitive channels responsible for warmth detection. Two possible candidates are TRPA1 and TRPM3. Recent reports showed that TRPV1, TRPM3, and TRPA1 are co-expressed in the same population of sensory neurons [28, 34, 40]. Additionally, a combined deletion of all three channels is required for a complete loss of painful heat sensitivity, demonstrating the overlapping functional profiles of thermo-TRP channels [28]. TRPA1 in particular is a promising candidate. TRPA1 expression in DRG and TG neurons co-localizes 30 – 100 % with TRPV1, depending on the studied tissue and methodology [121–123]. Additionally, 79 % of WSN in the TG respond to an oral stimulus of AITC, a TRPA1 agonist [90]. However, calcium imaging of TG cells marked using a Trpa1-Cre line showed predominant activity of Trpa1-positive cells in the heat range with only rare responses to warm temperature stimuli [31]. A study using TRPV1 and TRPA1 antagonists provided direct evidence for a combined role of TRPV1 and TRPA1 in warmth detection. Only the joint injection of both inhibitors leads to a loss of preference development in the TPP test, given 34 °C and 38 °C as options [124]. The role of TRPA1 as a temperature sensor and its exact range of temperature activity is controversial, with recent data suggesting an involvement in both cold and heat detection [125]. Intriguingly, a recent study in Drosophila larvae suggests that instead of activating in a certain temperature range, TRPA1 is tuned to the temperature change rate [126]. TRPV1-KO cultures showed an enrichment of cells with a fast temperature change rate. Since the loss of single TRP-channels can be genetically compensated by other TRP-channels [28], and TRPA1 and TRPV1 are commonly co-expressed, it is possible that TRPA1 functionally compensates for the loss of TRPV1. Taken together, TRPA1 is a promising additional candidate that could be involved in warmth-detection.

Interestingly, the additive effect of TRPV1- and TRPM2-KO is most prominent at threshold temperatures above 42 °C. This is reminiscent of the observation that the response threshold for TRPM2 in primary cultures is higher (>45 °C) than its postulated threshold from heterologous expression systems (35 – 37 °C), intact tissue slices (40 °C), and *in vivo* behavior (38 °C) [33, 34, 41, 127]. While the threshold assessment method used in my experiment shifts the temperature thresholds for TRPM2 to below 42 °C, the largest effect is still observed at temperatures above 38 °C (Figure 4), and therefore beyond its postulated temperature threshold from *in vivo* observations. One possible explanation is that TRPM2 relies on a co-factor that is lost upon culturing [40, 41]. Another possibility is that the cell somas of sensory neurons do not perfectly reflect the

electrochemical properties of the sensory nerve endings (SNE). SNEs have a much smaller radius and volume compared to the cell somas [128]. This could allow for smaller stimuli to induce large receptor potentials and consecutive action potentials due to the inverse relationship of volume and ion concentration. Indeed, separate stimulation of DRG somata and nerve terminals cultured in microfluidic chambers reveals a 2-4 times higher sensitivity of the terminals to protons and capsaicin, compared to the cell bodies [129]. Additionally, analysis of calcium transients from soma and neurites reveals a higher sensitivity to stimuli in the neurite compartment [130, 131]. Analogously, the temperature thresholds needed for a response reported in this and other studies could be higher than the actual thresholds *in vivo*. Repeating the experiments from this study in a compartmentalized culture system or separate analysis of the neurites in comparison with the soma could help resolve this issue.

4.1.4 TRPV1 overexpression modifies the response of WSN

TRPV1 is classically known as a heat-sensitive channel with an activation threshold above 42 °C [85, 86]. In contrast to this, my work and previous studies, as well as the evidence from behavioral experiments suggest a role for TRPV1 in warmth detection ([31, 37] and Figure 4). However, the mechanism with which TRPV1 is activated by warm stimuli remains unknown. This study showed that an increased amount of TRPV1 in TRPV1-positive cells leads to a shift of WSN response thresholds towards cooler temperatures (Figure 5). This suggests that diverging amounts of TRPV1 expression could tune the temperature-sensitivity of DRG neurons.

Early *in situ* hybridization studies in sensory neurons showed a high variability of Trpv1-expression among the studied fibers/neurons. A distinct group of neurons express high amounts of Trpv1, but low levels of typical nociceptor marker genes [132, 133]. A closer investigation of these so-called high-expressing TRPV1 cells (HE TRPV1) revealed that they are predominantly found in caudal DRGs (L1-S2) and innervate the lower extremities, particularly the perineum [87]. Interestingly, this population is specifically activated by warm stimuli (assessed by ERK1/2 activity), reaching a maximum around 46 °C, mirroring the classic profile of innocuous warm fibers. The existence of the HE TRPV1 cell as a distinct population is supported by recent single-cell sequencing datasets that show a cluster of cells with the highest expression of Trpv1 in addition to the postulated marker combination of TrkC/Esr1 (analyzed from [114, 115], data not shown).

The existence of HE TRPV1 cells suggests a possible relationship between the absolute amounts of TRPV1 expressed in sensory neurons and their ability to respond to warmth. A closer look at electrophysiological recordings of TRPV1 in response to temperature reveals a minor but substantial

current at temperatures below its assumed threshold temperature (42 °C) [86, 134–136]. This is especially evident when TRPV1 is heterologously overexpressed but also observed in primary DRG cultures, where temperature-evoked currents in TRPV1-KO cells are reduced in the warm temperature range [27]. This evidence combined with the small volume of free nerve endings could allow for fibers with high expression of TRPV1 to cross their respective receptor potential thresholds at lower temperatures, and thereby convey warm temperature signals. Indeed, this hypothesis is supported by the data collected in this study. TRPV1-overexpression lead to an enrichment of the WSN proportions, suggesting a shift in temperature thresholds towards cooler temperatures, facilitated by higher amounts of TRPV1 (Figure 5). A way to further assess this hypothesis is to correlate the TRPV1-levels of cultured DRG neurons with their response threshold. This could be either done through pharmacological stimulation with increasing levels of capsaicin, followed by warm temperature stimuli. Or, by staining for TRPV1-protein after the calcium imaging and subsequent identification of the imaged field of view [137].

4.2 Thermal ambient temperature test

4.2.1 Novel ambient temperature preference test

Behavioral tests investigating thermal detection are numerous and vary in their application and results (see sections 1.3.1, 1.3.2, and 1.3.3 for examples). One criticism towards common approaches is that they investigate the thermal detection of specific extremities such as the paws or face, focusing on non-hairy, glaborous skin [31, 37]. However, in rodents, hairy skin covers the largest part of the body and is largely responsible for thermoregulatory behaviors, such as warm- and cold-seeking [138]. In this study, we developed a spontaneous behavioral assay termed the TCP test which probes the preference of the animal to ambient and floor temperature, therefore engaging all possible thermal sensory end organs responsible for ambient temperature detection (Figure 6).

The tested setup is capable of maintaining stable ambient and floor temperatures after temperature equilibration (Figure 7). The temperature fluctuation recorded in the base-plate of the setup is similar to the precision reported for commercial TPP test setups [35, 139]. Ambient temperature fluctuated in a range between 0.5 °C and 1 °C, depending on the target temperature of both chambers (Figure 7). To the best of our knowledge, this is the first behavioral assay that tests thermal ambient temperature preference in an acute setting. However, similar approaches investigating animal temperature preference over a long period of time exist [140, 141]. In these approaches,

housing cages are immersed in differentially heated water-baths. Then, the animals' cage occupancy over multiple days is quantified. Unfortunately, the exact variability in ambient temperature was not reported in these studies, thereby lacking a benchmark to compare our setup to.

In operant behavioral assays, mice are capable of detecting temperature differences of as little as 0.5 °C [37]. Therefore, the ambient temperature fluctuation could, in theory, affect the preference of the animals. This is particularly challenging when the two chamber temperatures are similar, thereby leading to sub-optimal thermal separation between the chambers. To avoid this issue, the experiments presented in this study were done using temperature combinations with a difference of at least 3 °C between chambers. A difference below 2 °C between chambers should be avoided with the current setup. An upgrade of the used thermometers controlling the thermostat with faster versions and a reduced peltier activation latency could improve the performance of the system and reduce temperature fluctuations, allowing for a more fine-grained temperature control.

A caveat of the setup is the relatively long equilibration time prior to the experiment (Figure 7). This entails either a 90-minute waiting time before placing an animal for recording or the usage of the same enclosure for consequent animals, the latter being the chosen approach in this study. Using the same enclosure for multiple animals could affect the behavior of the animals through odor cues carried on by the previously tested animal. This was counteracted in this study by a randomized order of different mouse genotypes on different days. In some cases, as a way to test the specificity of the observed phenotype, the temperatures of the chambers are reversed during the TPP test [89]. Floor temperature in the TPP test changes in less than 5 minutes while our setup would take 60-80 minutes for the same change in ambient temperature. Therefore, a similar approach is not applicable in the TCP test. However, applying such a chamber-switch in the TCP test coupled with close monitoring of the floor and ambient temperature in each chamber, could be used to assess the preference development over a long period of time.

4.2.2 Temperature detection *vs.* thermoregulatory behavior

Ambient temperature detection serves as an input into the homeostatic control of core body temperature. Upon input reception, thermoregulation is enforced through two distinct systems. The first is the autonomic response of effector organs such as the activation (or inactivation) of the brown adipose tissue, or, the vasoconstriction (or dilatation) of peripheral blood vessels, regulating heat exchange. The second system is the animals attempt to reduce or increase body temper-

ature through behaviors, such as a licking, change of pose, or cold/heat seeking, called behavioral thermoregulation [142].

Temperature preference tests are tests of behavioral thermoregulation in which animals seek the temperature that supports their thermoregulatory needs [143]. Therefore, it is an indirect measurement of temperature detection compared to operant behavioral assays where animals learn to report a certain acute stimulus. The thermoregulatory aspect of thermal preference choice is reflected in the relatively long time needed for animals to develop a preference in a thermal gradient test, only stabilizing after 30-60 minutes [20, 35, 39]. This is also reflected in the delayed preference development in classical TPP tests and the TCP test described in this study ([34] and Figure 9).

One marked difference between the classic TPP test and our TCP test is the ambient temperature during the experiment. In the classic TPP test, the ambient temperature is kept at 25 °C while the base-plates of the assay are set to 31 – 33 °C for the control side, and a variable testing temperature on the other side. An ambient temperature of 25 °C is considered lower than the thermoneutral temperature of laboratory mice during the day phase (30 °C), meaning that animals kept at 25 °C are actively defending their body temperature through autonomic and behavioral methods of heat production/preservation [144]. Therefore, given a 25 °C ambient temperature in the TPP test, animals would prefer temperatures that would assist their thermoregulatory goal and reduce their energy expenditure. This is in line with the observation that wildtype animals prefer temperatures between 30 °C and 40 °C. Temperatures above 40 °C are avoided due to the feeling of pain and the need to counteract the heating, and temperatures below 30 °C are avoided to save energy.

In the TCP test presented in this study, however, the ambient temperature is at a minimum of 31 °C. Specifically, the animal is transferred from room temperature (below 30 °C and thermoneutrality) into a chamber that is at or above thermoneutral temperatures. Therefore, hypothetically, the animal is challenged with a different choice than in the TPP test, which consists of choosing a chamber that keeps its energy expenditure to a minimum. An additional factor that is influenced by ambient temperature is the core body temperature [144]. Ambient temperatures above 33 °C lead to an increase of core body temperature, thereby leading to the activation of thermoregulatory behavior of heat-dissipation [145]. Combined, this suggests that in the case of the TCP test, animals should always prefer the 31 °C side as it guarantees the lowest energy expenditure.

4.2.3 Evaluation of TRPV1 and TRPM2 in ambient temperature preference

TRPV1- or TRPM2-deficient animals were not subjected to ambient temperature preference before, making this study the first to investigate the role of both channels in such a paradigm. The single deficiency of TRPM2 and the combined lack of both TRPV1 and TRPM2 had a strong effect on ambient temperature preference. Specifically, TRPM2-KO animals failed to show preference when challenged with 34 °C and to a smaller extent at 38 °C. TRPV1/M2-DKO animals showed a somewhat reversed phenotype with a lack of preference when presented with the 38 °C chamber. Surprisingly, TRPV1-KO alone did not have a marked effect on the preference compared to wildtype animals (Figure 9).

TRPM2

The temperature preference of TRPM2-KO animals was only investigated in a single study using the TPP test [89]. Tan and colleagues showed that TRPM2-KO animals failed to establish a preference when presented with 33 °C (control) and 38 °C (test), suggesting a defect in detecting a plate temperature of 38 °C. While this is in a similar range with my observation, it is shifted towards higher temperatures as TRPM2-KO animals in the TCP test had their strongest phenotype at 34 °C, with a milder effect at 38 °C.

One explanation is the behavioral paradigm used. In the Tan et al. study, only the plates of the preference chambers were heated while the ambient temperature was left unchanged (room temperature). Therefore, it is possible that the animal received different temperature signals from the extremities in contact with the plate, and the rest of the body. In humans, thermal sensitivity differs depending on the stimulated body part [146, 147]. Additionally, spatial summation of thermal stimuli allows a faster and more precise detection of the thermal stimulus [37, 148, 149]. Therefore, stimulation of the body parts in contact with the base-plate alone could lead to a weaker behavioral phenotype than a stimulation of the whole body, as done in this study with the TPC test.

The TRPM2-KO phenotype in the TCP test recapitulates the calcium imaging data, where cells from TRPM2-KO animals showed a reduction in the proportion of WSN, starting at temperatures as low as 30 °C (Figure 4). The observed phenotype also argues that the reduction in WSN proportions achieved by TRPM2-KO is sufficient to render the animals insensitive to 34 °C. This

suggests that not only the type but also the number of cells conveying a certain stimulus is of importance for the detection of the stimulus. This observation agrees with the hypothesis that warm-detection is encoded in a graded population response with an increase in the numbers of responders with increased temperature [31, 80]. Therefore, a substantial loss of cells responding to temperatures between 30 – 35 °C, as is evident in TRPM2-KO cultures, would have a strong effect on the behavior in this range.

Taken together, my work supports a role of TRPM2 in warm-temperature detection, based on behavioral experiments and cellular data.

TRPV1

For TRPV1, the *in vitro* calcium imaging experiments would suggest a similar phenotype *in vivo* as for TRPM2-KO. Intriguingly, this was not the case. TRPV1-KO animals did not show any difference in temperature preference compared to wildtype animals (Figure 9). One possible explanation is the differences observed in the remaining WSNs in cultures of TRPV1- and TRPM2-KO mice. While TRPM2-KO lead to the loss of WSN across all recorded temperature change rate thresholds, TRPV1-KO cultures showed an enrichment of fast temperature change rate threshold (>1.5 °C/s) responders compared to TRPM2-KO cells. As discussed above, fast temperature change rates reduce the latency and increase the probability of stimulus detection. The movement of animals from one chamber to the other represents a fast and immediate stimulus. Therefore, it is possible that the residual population of fast temperature change rate responders in TRPV1-KO animals is sufficient for a good performance in the TCP test. To investigate the differential importance of fast and slow temperature change rate responders, animals could be trained in an operant behavioral assay to detect temperature stimuli with a fixed target temperature and varying temperature change rates. Then, the performance of wildtype, TRPV1-KO, and TRPM2-KO animals in the assay could be compared.

Another possibility is that the warmth detection by TRPV1 is not relevant in the recorded form of behavioral thermoregulation. TRPV1-KO animals show a reduced number of body licks, and a delayed vasodilation of the tail vain when challenged with warm temperature stimuli above 30 °C, compared to wildtype animals [150, 151]. This results in an overshoot in body temperature of 1 – 2 °C under these experimental conditions, strongly suggesting a role for TRPV1 in thermoregulation. Further evidence for TRPV1-involvement comes from calcium imaging recordings of spinal cord neurons. TRPV1-KO animals show a 60 % reduction in the proportion of WSN in

the spinal cord compared to wildtype animals, confirming the observations from *in vivo* calcium imaging of TG neurons, and further suggesting defects in temperature detection [152, 153].

In summary, the evidence from my *in vitro* data and data from others suggest that TRPV1 plays a role in temperature detection and thermoregulation. However, this was not reflected in the TCP test of TRPV1-deficient animals. This suggests that TRPV1 might play a context-dependent role in warm-temperature detection.

TRPV1 and TRPM2

Loss of both TRPV1 and TRPM2 in sensory neurons lead to an additive reduction in the proportion of WSN detected by calcium imaging (Figure 4). Similarly, TRPV1/M2-DKO animals showed a lack of preference when presented with 38 °C in the TCP test, exceeding the phenotype observed in TRPM2-KO animals alone (Figure 9). This is in line with the hypothesis that cells with fast temperature change rate thresholds are necessary for the performance in this behavioral paradigm (discussed above) since TRPV1/M2-DKO cultures showed a particularly strong reduction in WSN with high temperature change rate thresholds (>1.5 °C/s) (Figure 4). Surprisingly though, when presented with the 34 °C chamber, TRPV1/M2-DKO animals avoided the warmer temperature and did not recapitulate the observed lack of preference in TRPM2-KO animals. This again could be due to a compensatory mechanism that leads to increased numbers of WSN observed in TRPV1/M2-DKO cultures at temperature below 37 °C, in comparison to cultures from TRPM2-KO animals (Figure 4). Furthermore, the observation of an additive effect in TRPV1/M2-DKO animals at 38 °C also supports a role of TRPV1 in warmth detection, which was masked by TRPM2 in animals lacking TRPV1 alone.

In summary, this data supports the hypothesis that both TRPV1 and TRPM2 are important for warm temperature detection.

TRPV1-overxpression

As a way to further assess the influence of TRPV1 on temperature detection, TRPV1-overexpression in Trpv1-positive cells (TRPV1-OX) was studied. Cultures from TRPV1-OX animals showed a strong increase in the proportion of WSN compared to cultures from wildtype animals (Figure 5). Presented with either 34 °C or 38 °C in the TCP test showed a stronger avoidance of the 34 °C or 38 °C chamber than wildtype animals, reflected in a faster development of preference in TRPV1-

OX animals towards the control side than wildtype animals (Figure 10). This is recapitulated in the average number of crossings throughout the experiment but not in the average visit length. This suggests that the animals probe the test side for a similar amount of time than wildtype animals but come to a quicker decision of the preferred side.

A way to explain the behavior is to interpret the quicker preference development for 31 °C as an improved ability to detect warmth. TRPV1-OX DRG cultures show a shift in the temperature response profile towards the cooler range of warmth, increasing the number of cells reporting temperatures below 32 °C (Figure 5). Additionally, the enriched population of cells also includes a larger proportion of fast temperature change rate (>1.5 °C/s) responders, which would increase their ability to detect thermal stimuli with a reduced latency. Indeed, stimulating the hind paws of TRPV1-OX animals with a radiant heat source leads to a shorter withdrawal latency compared to wildtype animals, supporting the prediction from the DRG cultures [30]. Combined, this suggests an increased ability of TRPV1-OX animals to detect lower temperatures compared to widltypes, which could explain the faster preference development.

Interestingly, a closer look at the occupation heatmaps hints that TRPV1-OX animals predominantly reside on the most lateral side of the 31 °C chamber, while wildtype animals occupy a larger portion of the chamber (Figure 10). Due to the development of a thermal gradient between and in the chambers (discussed in section 3.2.1), it is possible that TRPV1-OX animals even show a differing preference inside the 31 °C chamber, an effect that cannot be resolved with the current experimental setup. However, an elongated version of the current setup or the usage of a classical thermal gradient could shed light on this question.

Taken together, the observed phenotype supports the hypothesis that both TRPV1 and TRPM2 play important roles in warm-temperature detection and the associated thermoregulatory behavior.

4.3 Possible caveats and future considerations

4.3.1 Alternative avenues of temperature detection

While this study is focused on the peripheral thermal sensation and its representation in DRG neurons, other cells besides DRG and TG cells are capable of detecting temperature. Vagal ganglia such as the nodose and the jugular ganglia are postulated to convey temperature stimuli to the

CNS [142]. Recent single-cell profiling shows expression of temperature sensitive channels such as TRPV1 and TRPM2 in vagal ganglia. Additionally, jugular ganglia show close transcriptional identity to previously identified DRG and TG cells, suggesting a similar functional profile which has not been characterized [154].

Besides the peripheral/visceral and possible vagal thermosensation, compelling evidence supports direct temperature detection in the CNS, termed central thermosensation. Specifically, the preoptic area of the hypothalamus (POA), a central hub for thermoregulation, is able to locally sense temperature changes and subsequent activation of effector organs [142]. Interestingly, a study by our lab showed that TRPM2 is also expressed in the POA. Calcium imaging in acute slices of the POA showed a marked reduction in the responses of temperature sensitive cells in TRPM2-KO animals. Furthermore, chemogenetic activation of TRPM2-positive cells lead to a strong reduction in body temperature, suggesting an importance of TRPM2 and TRPM2-expressing cells in the control of temperature [127]. When factored in, the lack of TRPM2 in the POA could also have an influence on the behavior of animals in the TCP test as body temperature increases with increased ambient temperatures. While this was not addressed in this study, it could be assessed via tissue-targetted knockout of TRPM2. This can be achieved either via the use of a conditional knockout mouse, or, via differential infection of central vs. peripheral neurons with adeno-associated viruses (AAV) carrying shRNA/gRNA targeting TRPM2 [155].

4.3.2 Encoding of temperature stimuli in sensory neurons

The transfer of information from a peripheral stimulus into neuronal code which is further processed and decoded in the CNS to trigger conscious and sub-conscious behavior is a matter of high interest in the field of computational neuroscience [156]. Recent advances investigating the response of retinal ganglion cells upon stimulation with visual stimuli established the basis of neural population coding in the retina [157]. Similar approaches to understand temperature coding in primary sensory neurons exist, however, they are rare [31, 80]. The recent development of *in vivo* calcium imaging methods allows for an in-depth analysis of neuronal responses to external temperature stimuli. This approach was applied in DRG, TG, and spinal cord neurons. While the studies discussed in this work have characterized different types of temperature responders, they did not attempt to build a model that explains the temperature code behind the stimuli. A possible way to tackle this task is the use of a population decoder algorithm on responses of wildtype neurons in DRG/TG and spinal cord cells. This algorithm can then be used to assess the performance of neuronal populations from animals deficient in temperature-sensitive channels such as TRPV1 and TRPM2 and correlate that to the observed *in vivo* behavior [158]. The advantage of

such methods is that they could learn the representation of any stimulus (such as temperature) in a neuronal population. This can be used as a discovery tool, allowing the uncovering and assessment of parameters that influence the population code, including some that were not previously described.

4.3.3 Temperature dependence of biological processes

This work was focused on the roles of two temperature-sensitive channels in peripheral temperature detection. However, plenty of temperature-sensitive channels, including some outside of the TRP-channel family, have also been described (section 1.3). Ultimately, every biological process is influenced by temperature. This suggests that, while there are some channels with high temperature sensitivity that carry the majority of the molecular mechanism behind temperature detection, many channels, proteins, and other cellular compounds (such as membranes) could influence temperature detection.

The temperature-dependence of any biological system also entails an influence of temperature on all neuronal aspects, including basic properties such as action potential generation and propagation. It is therefore rather surprising that many neuronal functions are stable, even under extreme temperature conditions. Recent mathematical modeling studies investigating the effect of temperature on neuronal activity suggest that temperature-robust neuronal function does not rely on channels with low or restricted temperature sensitivity. Instead, a large array of possible channel combinations with varying temperature-sensitivity were able to convey robust neuronal function [159]. The same concept of interchangeable channel activity could be applied to temperature-detection in the peripheral nervous system. Data from this study and others suggest that multiple temperature-sensitive channels share a common range of activity. This is further reflected in the observation that, often, a combined loss of multiple temperature-sensitive channels is required for significant defects in temperature detection, demonstrating the flexibility of the system [28].

Recent advances in RNA-sequncing and proteomics allow the interrogation of the inner workings of single cells. Combined with electrophysiological recordings (e.g. Patch-Seq [160]) or activity marking using photoconvertible calcium dyes [161], these tools allow the correlation between functional activity and RNA/protein. Taking it a step further, applying mathematical modeling and machine learning tools onto the acquired datasets could lead to a more in-depth understanding of the molecular mechanisms behind neuronal processes, such as thermosensation.

Acronyms

AAV	Adeno-associated virus
AC2	Adenylate cyclase 2
ANO1	Anoctamin 1
ANOVA	Analysis of variance
BSA	Bovine serum albumin
CFA	Complte freund's adjuvant
CNS	Central nervous system
CSV	Comma-separated value
DKO	Double knockout
DMEM	Dulbcco's modified eagle medium
DMSO	Dimethyl sulfoxide
DRG	Dorsal root ganglion
EDTA	Ethylene diamine tetraacetic acid
ERK1/2	Extracellular signal-regulated kinase 1/2
FCS	Fetal calf serum
FOV	Field of view
HEPES	4-(2-hydroxyethyl)-1-piperazineethanesulfonic acid)
HSN	Heat-sensitive neuron
NGF	Nerve growth factor
PBS	Phosphate buffered saline
PCR	Polymerase chain reaction
PDL	Poly-D-Lysine
PGE2	Prostaglandin E2
PI3	Phosphoinositid-3
PKA	Protein Kinase A
PKC	Protein Kinase C
PNS	Peripheral nervous system
POA	Preoptic area of the hypothalamus
PTFE	Polytetrafluoroethylene
ROI	Region of interest

SDS	Sodium dodecyl sulfate
SNE	Sensory nerve endings
SPF	Specific-pathogen-free
TCP	Thermal chamber preference
TG	Trigeminal ganglion
TRP	Transient receptor potential
WSN	Warm-sensitive neurons

Bibliography

[1] Yngve Zotterman. Specific action potentials in the lingual nerve of cat. *Skandinavisches Archiv Für Physiologie*, 75(3):105–119, September 1936. ISSN 0370839X. doi: 10.1111/j.1748-1716.1936.tb01558.x.

[2] Bernd Fritzsch. *The Senses: A Comprehensive Reference*. 2021. ISBN 978-0-12-805409-3.

[3] William D. Willis. The somatosensory system, with emphasis on structures important for pain. *Brain Research Reviews*, 55(2):297–313, October 2007. ISSN 01650173. doi: 10.1016/j.brainresrev.2007.05.010.

[4] Hind Abdo, Laura Calvo-Enrique, Jose Martinez Lopez, Jianren Song, Ming-Dong Zhang, Dmitry Usoskin, Abdeljabbar El Manira, Igor Adameyko, Jens Hjerling-Leffler, and Patrik Ernfors. Specialized cutaneous Schwann cells initiate pain sensation. *Science*, 365(6454):695–699, August 2019. ISSN 0036-8075, 1095-9203. doi: 10.1126/science.aax6452.

[5] Ellen A. Lumpkin and Michael J. Caterina. Mechanisms of sensory transduction in the skin. *Nature*, 445(7130):858–865, February 2007. ISSN 0028-0836, 1476-4687. doi: 10.1038/nature05662.

[6] Joris Vriens, Bernd Nilius, and Thomas Voets. Peripheral thermosensation in mammals. *Nature Reviews Neuroscience*, 15(9):573–589, September 2014. ISSN 1471-0048. doi: 10.1038/nrn3784.

[7] Wilfrid Jänig. Peripheral thermoreceptors in innocuous temperature detection. In *Handbook of Clinical Neurology*, volume 156, pages 47–56. Elsevier, 2018. ISBN 978-0-444-63912-7. doi: 10.1016/B978-0-444-63912-7.00002-3.

[8] A. B. Vallbo, K. E. Hagbarth, H. E. Torebjork, and B. G. Wallin. Somatosensory, proprioceptive, and sympathetic activity in human peripheral nerves. *Physiological Reviews*, 59(4):919–957, October 1979. ISSN 0031-9333, 1522-1210. doi: 10.1152/physrev.1979.59.4.919.

[9] Kim I. Chisholm, Nikita Khovanov, Douglas M. Lopes, Federica La Russa, and Stephen B. McMahon. Large Scale In Vivo Recording of Sensory Neuron Activity with GCaMP6. *eNeuro*, 5(1), April 2018. ISSN 2373-2822. doi: 10.1523/ENEURO.0417-17.2018.

[10] William D Willis and Richard E Coggeshall. *Sensory Mechanisms of the Spinal Cord: Volume 1 Primary Afferent Neurons and the Spinal Dorsal Horn*. Springer US, Boston, 2004. ISBN 978-1-4615-0037-7.

[11] Ian Darian-Smith. Thermal Sensibility. In Ronald Terjung, editor, *Comprehensive Physiology*, page cp010319. John Wiley & Sons, Inc., Hoboken, NJ, USA, January 2011. ISBN 978-0-470-65071-4. doi: 10.1002/cphy.cp010319.

[12] H. Hensel and A. Iggo. Analysis of cutaneous warm and cold fibres in primates. *Pflügers Archiv*, 329(1):1–8, March 1971. ISSN 1432-2013. doi: 10.1007/BF00586896.

[13] Frithjof Konietzny and Herbert Hensel. Warm fiber activity in human skin nerves. *Pflügers Archiv*, 359(3):265–267, September 1975. ISSN 1432-2013. doi: 10.1007/BF00587384.

[14] F. Konietzny and H. Hensel. The dynamic response of warm units in human skin nerves. *Pflügers Archiv*, 370(1):111–114, January 1977. ISSN 1432-2013. doi: 10.1007/BF00707956.

[15] H. Hensel and D. R. Kenshalo. Warm receptors in the nasal region of cats. *The Journal of Physiology*, 204(1):99–112, September 1969. ISSN 00223751. doi: 10.1113/jphysiol.1969.sp008901.

[16] N Jancsó, A Jancsó-Gábor, and J Szolcsányi. Direct evidence for neurogenic inflammation and its prevention by denervation and by pretreatment with capsaicin. *British Journal of Pharmacology and Chemotherapy*, 31(1):138–151, September 1967. ISSN 0366-0826.

[17] Michael J. Caterina, Mark A. Schumacher, Makoto Tominaga, Tobias A. Rosen, Jon D. Levine, and David Julius. The capsaicin receptor: A heat-activated ion channel in the pain pathway. *Nature*, 389(6653):816–824, 1997.

[18] M. J. Caterina, A. Leffler, A. B. Malmberg, W. J. Martin, J. Trafton, K. R. Petersen-Zeitz, M. Koltzenburg, A. I. Basbaum, and D. Julius. Impaired Nociception and Pain Sensation in Mice Lacking the Capsaicin Receptor. *Science*, 288(5464):306–313, April 2000. ISSN 0036-8075, 1095-9203. doi: 10.1126/science.288.5464.306.

[19] Andrea M. Peier, Aziz Moqrich, Anne C. Hergarden, Alison J. Reeve, David A. Andersson, Gina M. Story, Taryn J. Earley, Ilaria Dragoni, Peter McIntyre, Stuart Bevan, and Ardem Patapoutian. A TRP Channel that Senses Cold Stimuli and Menthol. *Cell*, 108(5):705–715, March 2002. ISSN 0092-8674, 1097-4172. doi: 10.1016/S0092-8674(02)00652-9.

[20] Ajay Dhaka, Amber N. Murray, Jayanti Mathur, Taryn J. Earley, Matt J. Petrus, and Ardem Patapoutian. TRPM8 Is Required for Cold Sensation in Mice. *Neuron*, 54(3):371–378, May 2007. ISSN 0896-6273. doi: 10.1016/j.neuron.2007.02.024.

[21] Diana M. Bautista, Jan Siemens, Joshua M. Glazer, Pamela R. Tsuruda, Allan I. Basbaum, Cheryl L. Stucky, Sven-Eric Jordt, and David Julius. The menthol receptor TRPM8 is the principal detector of environmental cold. *Nature*, 448(7150):204–208, July 2007. ISSN 0028-0836, 1476-4687. doi: 10.1038/nature05910.

[22] Md Shahidul Islam, editor. *Transient Receptor Potential Channels*. Number 704 in Advances in Experimental Medicine and Biology. Springer, Dordrecht, 2011. ISBN 978-94-007-0265-3 978-94-007-0264-6.

[23] Radhika Palkar, Erika K Lippoldt, and David D McKemy. The molecular and cellular basis of thermosensation in mammals. *Current Opinion in Neurobiology*, 34:14–19, October 2015. ISSN 09594388. doi: 10.1016/j.conb.2015.01.010.

[24] Miriam García-Ávila and León D. Islas. What is new about mild temperature sensing? A review of recent findings. *Temperature*, 6(2):132–141, April 2019. ISSN 2332-8940. doi: 10.1080/23328940.2019.1607490.

[25] Rui Xiao and X.Z. Shawn Xu. Temperature Sensation: From Molecular Thermosensors to Neural Circuits and Coding Principles. *Annual Review of Physiology*, 83(1):205–230, February 2021. ISSN 0066-4278, 1545-1585. doi: 10.1146/annurev-physiol-031220-095215.

[26] GAND WOOLFE and A. D. MacDonald. The evaluation of the analgesic action of pethidine hydrochloride (Demerol). *Journal of Pharmacology and Experimental Therapeutics*, 80(3): 300–307, 1944.

[27] John B. Davis, Julie Gray, Martin J. Gunthorpe, Jonathan P. Hatcher, Phil T. Davey, Philip Overend, Mark H. Harries, Judi Latcham, Colin Clapham, Kirsty Atkinson, Stephen A. Hughes, Kim Rance, Evelyn Grau, Alex J. Harper, Perdita L. Pugh, Derek C. Rogers, Sharon Bingham, Andrew Randall, and Steven A. Sheardown. Vanilloid receptor-1 is essential for inflammatory thermal hyperalgesia. *Nature*, 405(6783):183–187, May 2000. ISSN 0028-0836. doi: 10.1038/35012076.

[28] Ine Vandewauw, Katrien De Clercq, Marie Mulier, Katharina Held, Silvia Pinto, Nele Van Ranst, Andrei Segal, Thierry Voet, Rudi Vennekens, Katharina Zimmermann, Joris Vriens, and Thomas Voets. A TRP channel trio mediates acute noxious heat sensing. *Nature*, March 2018. ISSN 0028-0836, 1476-4687. doi: 10.1038/nature26137.

[29] K. Hargreaves, R. Dubner, F. Brown, C. Flores, and J. Joris. A new and sensitive method for measuring thermal nociception in cutaneous hyperalgesia. *Pain*, 32(1):77–88, January 1988. ISSN 0304-3959.

[30] Christina Hanack, Mirko Moroni, Wanessa C. Lima, Hagen Wende, Marieluise Kirchner, Lisa Adelfinger, Katrin Schrenk-Siemens, Anke Tappe-Theodor, Christiane Wetzel, P. Henning Kuich, Martin Gassmann, Dennis Roggenkamp, Bernhard Bettler, Gary R. Lewin, Matthias Selbach, and Jan Siemens. GABA Blocks Pathological but Not Acute TRPV1 Pain Signals. *Cell*, 160(4):759–770, February 2015. ISSN 00928674. doi: 10.1016/j.cell.2015.01.022.

[31] David A. Yarmolinsky, Yueqing Peng, Leah A. Pogorzala, Michael Rutlin, Mark A. Hoon, and Charles S. Zuker. Coding and Plasticity in the Mammalian Thermosensory System. *Neuron*, December 2016. ISSN 0896-6273. doi: 10.1016/j.neuron.2016.10.021.

[32] Yuji Hara, Minoru Wakamori, Masakazu Ishii, Emi Maeno, Motohiro Nishida, Takashi Yoshida, Hisanobu Yamada, Shunichi Shimizu, Emiko Mori, Jun Kudoh, Nobuyoshi Shimizu, Hitoshi Kurose, Yasunobu Okada, Keiji Imoto, and Yasuo Mori. LTRPC2 Ca2+-Permeable Channel Activated by Changes in Redox Status Confers Susceptibility to Cell Death. *Molecular Cell*, 9(1):163–173, January 2002. ISSN 1097-2765. doi: 10.1016/S1097-2765(01)00438-5.

[33] Kazuya Togashi, Yuji Hara, Tomoko Tominaga, Tomohiro Higashi, Yasunobu Konishi, Yasuo Mori, and Makoto Tominaga. TRPM2 activation by cyclic ADP-ribose at body temperature is involved in insulin secretion. *The EMBO Journal*, 25(9):1804–1815, May 2006. ISSN 0261-4189, 1460-2075. doi: 10.1038/sj.emboj.7601083.

[34] Chun-Hsiang Tan and Peter A. McNaughton. The TRPM2 ion channel is required for sensitivity to warmth. *Nature*, 536(7617):460–463, August 2016. ISSN 0028-0836, 1476-4687. doi: 10.1038/nature19074.

[35] Aziz Moqrich, Sun Wook Hwang, Taryn J. Earley, Matt J. Petrus, Amber N. Murray, Kathryn S. R. Spencer, Mary Andahazy, Gina M. Story, and Ardem Patapoutian. Impaired Thermosensation in Mice Lacking TRPV3, a Heat and Camphor Sensor in the Skin. *Science*, 307 (5714):1468–1472, March 2005. ISSN 0036-8075, 1095-9203. doi: 10.1126/science.1108609.

[36] L. A. Pogorzala, S. K. Mishra, and M. A. Hoon. The Cellular Code for Mammalian Thermosensation. *Journal of Neuroscience*, 33(13):5533–5541, March 2013. ISSN 0270-6474, 1529-2401. doi: 10.1523/JNEUROSCI.5788-12.2013.

[37] Ricardo Paricio-Montesinos, Frederick Schwaller, Annapoorani Udhayachandran, Florian Rau, Jan Walcher, Roberta Evangelista, Joris Vriens, Thomas Voets, James F.A. Poulet, and Gary R. Lewin. The Sensory Coding of Warm Perception. *Neuron*, page S0896627320301860, March 2020. ISSN 08966273. doi: 10.1016/j.neuron.2020.02.035.

[38] Isao Shimizu, Tohko Iida, Yun Guan, Chengshui Zhao, Srinivasa N. Raja, Michael F. Jarvis, Debra A. Cockayne, and Michael J. Caterina. Enhanced thermal avoidance in mice lacking

the ATP receptor P2X3. *Pain*, 116(1):96–108, July 2005. ISSN 0304-3959. doi: 10.1016/j.pain.2005.03.030.

[39] Irène Marics, Pascale Malapert, Ana Reynders, Stéphane Gaillard, and Aziz Moqrich. Acute Heat-Evoked Temperature Sensation Is Impaired but Not Abolished in Mice Lacking TRPV1 and TRPV3 Channels. *PLOS ONE*, 9(6):e99828, June 2014. ISSN 1932-6203. doi: 10.1371/journal.pone.0099828.

[40] Bruno Vilar, Chun-Hsiang Tan, and Peter A. McNaughton. Heat detection by the TRPM2 ion channel. *Nature*, 584(7820):E5–E12, August 2020. ISSN 1476-4687. doi: 10.1038/s41586-020-2510-7.

[41] Marie Mulier, Ine Vandewauw, Joris Vriens, and Thomas Voets. Reply to: Heat detection by the TRPM2 ion channel. *Nature*, 584(7820):E13–E15, August 2020. ISSN 1476-4687. doi: 10.1038/s41586-020-2511-6.

[42] Eric Schulte, Dan Davison, Thomas Dye, and Carsten Dominik. A Multi-Language Computing Environment for Literate Programming and Reproducible Research. *Journal of Statistical Software*, 46(1):1–24, January 2012. ISSN 1548-7660. doi: 10.18637/jss.v046.i03.

[43] Richard M Stallman. EMACS the extensible, customizable self-documenting display editor. In *Proceedings of the ACM SIGPLAN SIGOA Symposium on Text Manipulation*, pages 147–156, 1981.

[44] Denise J. Cai, Daniel Aharoni, Tristan Shuman, Justin Shobe, Jeremy Biane, Weilin Song, Brandon Wei, Michael Veshkini, Mimi La-Vu, Jerry Lou, Sergio E. Flores, Isaac Kim, Yoshitake Sano, Miou Zhou, Karsten Baumgaertel, Ayal Lavi, Masakazu Kamata, Mark Tuszynski, Mark Mayford, Peyman Golshani, and Alcino J. Silva. A shared neural ensemble links distinct contextual memories encoded close in time. *Nature*, 534(7605):115–118, June 2016. ISSN 1476-4687. doi: 10.1038/nature17955.

[45] G. van Rossum. Python tutorial. Technical Report CS-R9526, Centrum voor Wiskunde en Informatica (CWI), Amsterdam, May 1995.

[46] R Core Team. *R: A Language and Environment for Statistical Computing*. R Foundation for Statistical Computing, Vienna, Austria, 2020.

[47] Suramya Tomar. Converting video formats with FFmpeg. *Linux Journal*, 2006(146):10, 2006.

[48] Zuguang Gu, Roland Eils, and Matthias Schlesner. Complex heatmaps reveal patterns and correlations in multidimensional genomic data. *Bioinformatics (Oxford, England)*, 32(18):2847–2849, September 2016. ISSN 1367-4811. doi: 10.1093/bioinformatics/btw313.

[49] Gregoire Pau, Florian Fuchs, Oleg Sklyar, Michael Boutros, and Wolfgang Huber. EBImage—an R package for image processing with applications to cellular phenotypes. *Bioinformatics*, 26(7):979–981, 2010. doi: 10.1093/bioinformatics/btq046.

[50] Christopher R. John, David Watson, Michael R. Barnes, Costantino Pitzalis, and Myles J. Lewis. Spectrum: Fast density-aware spectral clustering for single and multi-omic data. *Bioinformatics (Oxford, England)*, 36(4):1159–1166, February 2020. ISSN 1367-4811. doi: 10.1093/bioinformatics/btz704.

[51] Kristen M. Thyng, Chad A. Greene, Robert D. Hetland, Heather M. Zimmerle, and Steven F. DiMarco. True colors of oceanography: Guidelines for effective and accurate colormap selection. *Oceanography*, 29(3), 2016. doi: 10.5670/oceanog.2016.66.

[52] Claus O. Wilke. *Cowplot: Streamlined Plot Theme and Plot Annotations for 'Ggplot2'*, 2020.

[53] Johan Larsson. *Eulerr: Area-Proportional Euler and Venn Diagrams with Ellipses*, 2021.

[54] Thomas Lin Pedersen. *Ggforce: Accelerating 'Ggplot2'*, 2021.

[55] Hadley Wickham. *Ggplot2: Elegant Graphics for Data Analysis*. Springer-Verlag New York, 2016. ISBN 978-3-319-24277-4.

[56] Alboukadel Kassambara. *Ggpubr: 'ggplot2' Based Publication Ready Plots*, 2020.

[57] Claus O. Wilke. *Ggridges: Ridgeline Plots in 'Ggplot2'*, 2021.

[58] Steffen Moritz and Thomas Bartz-Beielstein. imputeTS: Time series missing value imputation in r. *The R Journal*, 9(1):207–218, 2017. doi: 10.32614/RJ-2017-009.

[59] Henrik Bengtsson. *matrixStats: Functions That Apply to Rows and Columns of Matrices (and to Vectors)*, 2021.

[60] Kristian Hovde Liland, Trygve Almøy, and Bjørn-Helge Mevik. Optimal choice of baseline correction for multivariate calibration of spectra. *Applied Spectroscopy*, 64:1007–1016, 2010.

[61] Thomas Lin Pedersen. *Patchwork: The Composer of Plots*, 2020.

[62] Alboukadel Kassambara. *Rstatix: Pipe-Friendly Framework for Basic Statistical Tests*, 2021.

[63] Terry M Therneau. *A Package for Survival Analysis in r*, 2020.

[64] Alboukadel Kassambara, Marcin Kosinski, and Przemyslaw Biecek. *Survminer: Drawing Survival Curves Using 'Ggplot2'*, 2020.

[65] Hadley Wickham, Mara Averick, Jennifer Bryan, Winston Chang, Lucy D'Agostino McGowan, Romain François, Garrett Grolemund, Alex Hayes, Lionel Henry, Jim Hester, Max Kuhn, Thomas Lin Pedersen, Evan Miller, Stephan Milton Bache, Kirill Müller, Jeroen Ooms, David Robinson, Dana Paige Seidel, Vitalie Spinu, Kohske Takahashi, Davis Vaughan, Claus Wilke, Kara Woo, and Hiroaki Yutani. Welcome to the tidyverse. *Journal of Open Source Software*, 4(43):1686, 2019. doi: 10.21105/joss.01686.

[66] Connor Dowd. A New ECDF Two-Sample Test Statistic. *arXiv:2007.01360 [stat]*, July 2020.

[67] Marcel Ramos, Lucas Schiffer, Angela Re, Rimsha Azhar, Azfar Basunia, Carmen Rodriguez Cabrera, Tiffany Chan, Philip Chapman, Sean Davis, David Gomez-Cabrero, Aedin C. Culhane, Benjamin Haibe-Kains, Kasper Hansen, Hanish Kodali, Marie Stephie Louis, Arvind Singh Mer, Markus Reister, Martin Morgan, Vincent Carey, and Levi Waldron. Software for the integration of multi-omics experiments in bioconductor. *Cancer Research*, 77(21); e39-42, 2017.

[68] Martin Morgan, Valerie Obenchain, Jim Hester, and Hervé Pagès. *SummarizedExperiment: SummarizedExperiment Container*, 2020.

[69] Kevin Ushey, JJ Allaire, and Yuan Tang. *Reticulate: Interface to 'Python'*, 2020.

[70] Patrick Kimes. *Upbm: Tools for the Analysis of Universal Protein Binding Microarrays*, 2020.

[71] Carsen Stringer, Tim Wang, Michalis Michaelos, and Marius Pachitariu. Cellpose: A generalist algorithm for cellular segmentation. *Nature Methods*, 18(1):100–106, January 2021. ISSN 1548-7105. doi: 10.1038/s41592-020-01018-x.

[72] Alexander Mathis, Pranav Mamidanna, Kevin M. Cury, Taiga Abe, Venkatesh N. Murthy, Mackenzie Weygandt Mathis, and Matthias Bethge. DeepLabCut: Markerless pose estimation of user-defined body parts with deep learning. *Nature Neuroscience*, 21(9):1281–1289, September 2018. ISSN 1546-1726. doi: 10.1038/s41593-018-0209-y.

[73] Marius Pachitariu, Carsen Stringer, Sylvia Schröder, Mario Dipoppa, L. Federico Rossi, Matteo Carandini, and Kenneth D. Harris. Suite2p: Beyond 10,000 neurons with standard two-photon microscopy. *bioRxiv*, page 061507, June 2016. doi: 10.1101/061507.

[74] Shinichiro Yamamoto, Shunichi Shimizu, Shigeki Kiyonaka, Nobuaki Takahashi, Teruaki Wajima, Yuji Hara, Takaharu Negoro, Toshihito Hiroi, Yuji Kiuchi, Takaharu Okada, Shuji Kaneko, Ingo Lange, Andrea Fleig, Reinhold Penner, Miyuki Nishi, Hiroshi Takeshima, and Yasuo Mori. TRPM2-mediated Ca 2+ influx induces chemokine production in monocytes that aggravates inflammatory neutrophil infiltration. *Nature Medicine*, 14(7):738–747, July 2008. ISSN 1546-170X. doi: 10.1038/nm1758.

[75] Eder Ricardo de Moraes, Christopher Kushmerick, and Lígia Araujo Naves. Morphological and functional diversity of first-order somatosensory neurons. *Biophysical Reviews*, 9(5): 847–856, September 2017. ISSN 1867-2450. doi: 10.1007/s12551-017-0321-3.

[76] Ann E. Oliver, Gary A. Baker, Robert D. Fugate, Fern Tablin, and John H. Crowe. Effects of Temperature on Calcium-Sensitive Fluorescent Probes. *Biophysical Journal*, 78(4):2116–2126, April 2000. ISSN 0006-3495. doi: 10.1016/S0006-3495(00)76758-0.

[77] Torsten Hothorn, Frank Bretz, and Peter Westfall. Simultaneous inference in general parametric models. *Biometrical Journal*, 50(3):346–363, 2008.

[78] Mayumi Tada, Atsuya Takeuchi, Miki Hashizume, Kazuo Kitamura, and Masanobu Kano. A highly sensitive fluorescent indicator dye for calcium imaging of neural activity in vitro and in vivo. *European Journal of Neuroscience*, 39(11):1720–1728, June 2014. ISSN 1460-9568. doi: 10.1111/ejn.12476.

[79] Jn Wood, J Winter, If James, Hp Rang, J Yeats, and S Bevan. Capsaicin-induced ion fluxes in dorsal root ganglion cells in culture. *The Journal of Neuroscience*, 8(9):3208–3220, September 1988. ISSN 0270-6474, 1529-2401. doi: 10.1523/JNEUROSCI.08-09-03208.1988.

[80] Feng Wang, Erik Bélanger, Sylvain L. Côté, Patrick Desrosiers, Steven A. Prescott, Daniel C. Côté, and Yves De Koninck. Sensory Afferents Use Different Coding Strategies for Heat and Cold. *Cell Reports*, 23(7):2001–2013, May 2018. ISSN 22111247. doi: 10.1016/j.celrep.2018.04.065.

[81] Marcus Mahar and Valeria Cavalli. Intrinsic mechanisms of neuronal axon regeneration. *Nature Reviews Neuroscience*, 19(6):323–337, June 2018. ISSN 1471-0048. doi: 10.1038/s41583-018-0001-8.

[82] Christopher R. Donnelly, Ouyang Chen, and Ru-Rong Ji. How Do Sensory Neurons Sense Danger Signals? *Trends in Neurosciences*, 43(10):822–838, October 2020. ISSN 01662236. doi: 10.1016/j.tins.2020.07.008.

[83] Ji-Hong Zheng, Edgar T. Walters, and Xue-Jun Song. Dissociation of Dorsal Root Ganglion Neurons Induces Hyperexcitability That Is Maintained by Increased Responsiveness to cAMP and cGMP. *Journal of Neurophysiology*, 97(1):15–25, January 2007. ISSN 0022-3077, 1522-1598. doi: 10.1152/jn.00559.2006.

[84] Zhi-Jiang Huang, Hao-Chuan Li, Ashley A. Cowan, Su Liu, Yan-Kai Zhang, and Xue-Jun Song. Chronic compression or acute dissociation of dorsal root ganglion induces cAMP-dependent neuronal hyperexcitability through activation of PAR2. *PAIN*, 153(7):1426–1437, July 2012. ISSN 0304-3959. doi: 10.1016/j.pain.2012.03.025.

[85] M.J. Caterina, T.A. Rosen, M. Tominaga, A.J. Brake, and D. and Julius. A capsaicin-receptor homologue with a high threshold for noxious heat. *Nature*, 398:436–441, 1999.

[86] Makoto Tominaga, Michael J. Caterina, Annika B. Malmberg, Tobias A. Rosen, Heather Gilbert, Kate Skinner, Brigitte E. Raumann, Allan I. Basbaum, and David Julius. The cloned capsaicin receptor integrates multiple pain-producing stimuli. *Neuron*, 21(3):531–543, 1998.

[87] Zahra Kiasalari, Iman Salehi, Yu Zhong, Stephen B. MCmahon, Adina T. Michael-Titus, and Gregory J. Michael. Identification of perineal sensory neurons activated by innocuous heat. *The Journal of Comparative Neurology*, 518(2):137–162, January 2010. ISSN 00219967, 10969861. doi: 10.1002/cne.22187.

[88] Ekbert Hering, Rolf Martin, and Martin Stohrer. *Taschenbuch der Mathematik und Physik*. Springer-Verlag, Berlin Heidelberg, fifth edition, 2009. ISBN 978-3-540-78684-9. doi: 10.1007/978-3-540-78684-9.

[89] Chan Lek Tan, Elizabeth K. Cooke, David E. Leib, Yen-Chu Lin, Gwendolyn E. Daly, Christopher A. Zimmerman, and Zachary A. Knight. Warm-Sensitive Neurons that Control Body Temperature. *Cell*, September 2016. ISSN 00928674. doi: 10.1016/j.cell.2016.08.028.

[90] Sara C. M. Leijon, Amanda F. Neves, Joseph M. Breza, Sidney A. Simon, Nirupa Chaudhari, and Stephen D. Roper. Oral thermosensing by murine trigeminal neurons: Modulation by capsaicin, menthol and mustard oil. *The Journal of Physiology*, 597(7):2045–2061, April 2019. ISSN 0022-3751, 1469-7793. doi: 10.1113/JP277385.

[91] Chao Ma and Robert H. LaMotte. Multiple Sites for Generation of Ectopic Spontaneous Activity in Neurons of the Chronically Compressed Dorsal Root Ganglion. *The Journal of Neuroscience*, 27(51):14059–14068, December 2007. ISSN 0270-6474. doi: 10.1523/JNEUROSCI.3699-07.2007.

[92] Manfred Zimmermann. Pathobiology of neuropathic pain. *European Journal of Pharmacology*, 429(1-3):23–37, October 2001. ISSN 00142999. doi: 10.1016/S0014-2999(01)01303-6.

[93] Robert Y North, Yan Li, Pradipta Ray, Laurence D Rhines, Claudio Esteves Tatsui, Ganesh Rao, Caj A Johansson, Hongmei Zhang, Yeun Hee Kim, Bo Zhang, Gregory Dussor, Tae Hoon Kim, Theodore J Price, and Patrick M Dougherty. Electrophysiological and transcriptomic correlates of neuropathic pain in human dorsal root ganglion neurons. *Brain*, 142(5):1215–1226, May 2019. ISSN 0006-8950, 1460-2156. doi: 10.1093/brain/awz063.

[94] Kentaro Ono. Comparison of the electrophysiological and immunohistochemical properties of acutely dissociated and 1-day cultured rat trigeminal ganglion neurons. *Neuroscience Letters*, page 5, 2012.

[95] Hiroaki Tsujino, Eiji Kondo, Tetsuo Fukuoka, Yi Dai, Atsushi Tokunaga, Kenji Miki, Kazuo Yonenobu, Takahiro Ochi, and Koichi Noguchi. Activating Transcription Factor 3 (ATF3) Induction by Axotomy in Sensory and Motoneurons: A Novel Neuronal Marker of Nerve Injury. page 13.

[96] Gregory O. Dussor, Theodore J. Price, and Christopher M. Flores. Activating transcription factor 3 mRNA is upregulated in primary cultures of trigeminal ganglion neurons. *Molecular Brain Research*, 118(1-2):156–159, October 2003. ISSN 0169328X. doi: 10.1016/S0169-328X(03)00335-8.

[97] Andi Wangzhou, Lisa A. McIlvried, Candler Paige, Paulino Barragan-Iglesias, Stephanie Shiers, Ayesha Ahmad, Carolyn A. Guzman, Gregory Dussor, Pradipta R. Ray, Robert W. Gereau, and Theodore J. Price. Pharmacological target-focused transcriptomic analysis of native vs cultured human and mouse dorsal root ganglia. *Pain*, 161(7):1497–1517, July 2020. ISSN 0304-3959, 1872-6623. doi: 10.1097/j.pain.0000000000001866.

[98] Minh Q Nguyen, Claire E Le Pichon, and Nicholas Ryba. Stereotyped transcriptomic transformation of somatosensory neurons in response to injury. *eLife*, 8:e49679, October 2019. ISSN 2050-084X. doi: 10.7554/eLife.49679.

[99] William Renthal, Ivan Tochitsky, Lite Yang, Yung-Chih Cheng, Emmy Li, Riki Kawaguchi, Daniel H. Geschwind, and Clifford J. Woolf. Transcriptional Reprogramming of Distinct Peripheral Sensory Neuron Subtypes after Axonal Injury. *Neuron*, page S0896627320305705, August 2020. ISSN 08966273. doi: 10.1016/j.neuron.2020.07.026.

[100] Bryan J. Black, Rahul Atmaramani, Rajeshwari Kumaraju, Sarah Plagens, Mario Romero-Ortega, Gregory Dussor, Theodore J. Price, Zachary T. Campbell, and Joseph J. Pancrazio. Adult mouse sensory neurons on microelectrode arrays exhibit increased spontaneous and stimulus-evoked activity in the presence of interleukin-6. *Journal of Neurophysiology*, 120 (3):1374–1385, June 2018. ISSN 0022-3077. doi: 10.1152/jn.00158.2018.

[101] H. Hensel and T. Huopaniemi. Static and dynamic properties of warm fibres in the infraorbital nerve. *Pflügers Archiv*, 309(1):1–10, March 1969. ISSN 1432-2013. doi: 10.1007/BF00592277.

[102] F. Kemal Bayat, Betul Polat Budak, Esra Nur Yiğit, Gürkan Öztürk, Halil Özcan Gülçür, and Albert Güveniş. Adult mouse dorsal root ganglia neurons form aberrant glutamatergic connections in dissociated cultures. *PLOS ONE*, 16(3):e0246924, March 2021. ISSN 1932-6203. doi: 10.1371/journal.pone.0246924.

[103] Linnéa M. Nilsson, Miguel Castresana-Aguirre, Lena Scott, and Hjalmar Brismar. RNA-seq reveals altered gene expression levels in proximal tubular cell cultures compared to renal

cortex but not during early glucotoxicity. *Scientific Reports*, 10(1):10390, June 2020. ISSN 2045-2322. doi: 10.1038/s41598-020-67361-3.

[104] R. Duclaux and Sr. Kenshalo DR. Response characteristics of cutaneous warm receptors in the monkey. *Journal of Neurophysiology*, 43(1):1–15, January 1980. ISSN 0022-3077. doi: 10.1152/jn.1980.43.1.1.

[105] Rhyuji Sumino and Ronald Dubner. Response characteristics of specific thermoreceptive afferents innervating monkey facial skin and their relationship to human thermal sensitivity. *Brain Research Reviews*, 3(2):105–122, October 1981. ISSN 0165-0173. doi: 10.1016/0165-0173(81)90001-1.

[106] S N Davies, G E Goldsmith, R F Hellon, and D Mitchell. Facial sensitivity to rates of temperature change: Neurophysiological and psychophysical evidence from cats and humans. *The Journal of Physiology*, 344:161–175, November 1983. ISSN 0022-3751.

[107] R. E. Beitel, R. Dubner, R. Harris, and R. Sumino. Role of thermoreceptive afferents in behavioral reaction times to warming temperature shifts applied to the monkey's face. *Brain Research*, 138(2):329–346, December 1977. ISSN 0006-8993. doi: 10.1016/0006-8993(77)90750-8.

[108] Dan R. Kenshalo, Charles E. Holmes, and Paul B. Wood. Warm and cool thresholds as a function of rate of stimulus temperature change. *Perception & Psychophysics*, 3(2):81–84, March 1968. ISSN 0031-5117, 1532-5962. doi: 10.3758/BF03212769.

[109] H. H. Molinari, J. D. Greenspan, and D. R. Kenshalo. The effects of rate of temperature change and adapting temperature on thermal sensitivity. *Sensory Processes*, 1(4):354–362, December 1977. ISSN 0363-3799.

[110] David Yarnitsky and Jose L. Ochoa. Studies of heat pain sensation in man: Perception thresholds, rate of stimulus rise and reaction time. *Pain*, 40(1):85–91, January 1990. ISSN 0304-3959. doi: 10.1016/0304-3959(90)91055-N.

[111] Minh Q. Nguyen, Youmei Wu, Lauren S. Bonilla, Lars J. von Buchholtz, and Nicholas J. P. Ryba. Diversity amongst trigeminal neurons revealed by high throughput single cell sequencing. *PLOS ONE*, 12(9):e0185543, September 2017. ISSN 1932-6203. doi: 10.1371/journal.pone.0185543.

[112] Santosh K Mishra, Sarah M Tisel, Peihan Orestes, Sonia K Bhangoo, and Mark A Hoon. TRPV1-lineage neurons are required for thermal sensation. *The EMBO Journal*, 30(3):582–593, February 2011. ISSN 0261-4189. doi: 10.1038/emboj.2010.325.

[113] Ine Vandewauw, Grzegorz Owsianik, and Thomas Voets. Systematic and quantitative mRNA expression analysis of TRP channel genes at the single trigeminal and dorsal root ganglion level in mouse. *BMC Neuroscience*, 14:21, February 2013. ISSN 1471-2202. doi: 10.1186/1471-2202-14-21.

[114] Nikhil Sharma, Kali Flaherty, Karina Lezgiyeva, Daniel E. Wagner, Allon M. Klein, and David D. Ginty. The emergence of transcriptional identity in somatosensory neurons. *Nature*, January 2020. ISSN 0028-0836, 1476-4687. doi: 10.1038/s41586-019-1900-1.

[115] Amit Zeisel, Hannah Hochgerner, Peter Lönnerberg, Anna Johnsson, Fatima Memic, Job van der Zwan, Martin Häring, Emelie Braun, Lars E. Borm, Gioele La Manno, Simone Codeluppi, Alessandro Furlan, Kawai Lee, Nathan Skene, Kenneth D. Harris, Jens Hjerling-Leffler, Ernest Arenas, Patrik Ernfors, Ulrika Marklund, and Sten Linnarsson. Molecular Architecture of the Mouse Nervous System. *Cell*, 174(4):999–1014.e22, August 2018. ISSN 00928674. doi: 10.1016/j.cell.2018.06.021.

[116] Daniel J. Cavanaugh, Alexander T. Chesler, Alexander C. Jackson, Yaron M. Sigal, Hiroki Yamanaka, Rebecca Grant, Dajan O'Donnell, Roger A. Nicoll, Nirao M. Shah, David Julius, and Allan I. Basbaum. Trpv1 reporter mice reveal highly restricted brain distribution and functional expression in arteriolar smooth muscle cells. *The Journal of Neuroscience: The Official Journal of the Society for Neuroscience*, 31(13):5067–5077, March 2011. ISSN 1529-2401. doi: 10.1523/JNEUROSCI.6451-10.2011.

[117] Louis Faure, Yiqiao Wang, Maria Eleni Kastriti, Paula Fontanet, Kylie K. Y. Cheung, Charles Petitpré, Haohao Wu, Lynn Linyu Sun, Karen Runge, Laura Croci, Mark A. Landy, Helen C. Lai, Gian Giacomo Consalez, Antoine de Chevigny, François Lallemend, Igor Adameyko, and Saida Hadjab. Single cell RNA sequencing identifies early diversity of sensory neurons forming via bi-potential intermediates. *Nature Communications*, 11(1):4175, August 2020. ISSN 2041-1723. doi: 10.1038/s41467-020-17929-4.

[118] Yanxin Li and Jianwei Jiao. Deficiency of TRPM2 leads to embryonic neurogenesis defects in hyperthermia. *Science Advances*, 6(1):eaay6350, January 2020. ISSN 2375-2548. doi: 10.1126/sciadv.aay6350.

[119] A. Garami, Y. P. Shimansky, E. Pakai, D. L. Oliveira, N. R. Gavva, and A. A. Romanovsky. Contributions of Different Modes of TRPV1 Activation to TRPV1 Antagonist-Induced Hyperthermia. *Journal of Neuroscience*, 30(4):1435–1440, January 2010. ISSN 0270-6474, 1529-2401. doi: 10.1523/JNEUROSCI.5150-09.2010.

[120] Hong-Zhen Hu, Qihai Gu, Chunbo Wang, Craig K. Colton, Jisen Tang, Mariko Kinoshita-Kawada, Lu-Yuan Lee, Jackie D. Wood, and Michael X. Zhu. 2-Aminoethoxydiphenyl Bo-

rate Is a Common Activator of TRPV1, TRPV2, and TRPV3. *Journal of Biological Chemistry*, 279(34):35741–35748, August 2004. ISSN 0021-9258, 1083-351X. doi: 10.1074/jbc.M404164200.

[121] Diana M. Bautista, Pouya Movahed, Andrew Hinman, Helena E. Axelsson, Olov Sterner, Edward D. Högestätt, David Julius, Sven-Eric Jordt, and Peter M. Zygmunt. Pungent products from garlic activate the sensory ion channel TRPA1. *Proceedings of the National Academy of Sciences*, 102(34):12248–12252, August 2005. ISSN 0027-8424, 1091-6490. doi: 10.1073/pnas.0505356102.

[122] K. Kobayashi, T. Fukuoka, K. Obata, H. Yamanaka, Y. Dai, A. Tokunaga, and K. and Noguchi. Distinct expression of TRPM8, TRPA1, and TRPV1 mRNAs in rat primary afferent neurons with aδ/c-fibers and colocalization with trk receptors. *J. Comp. Neurol*, 493: 596–606, 2005.

[123] Sacha Malin, Derek Molliver, Julie A. Christianson, Erica S. Schwartz, Pam Cornuet, Kathryn M. Albers, and Brian M. Davis. TRPV1 and TRPA1 Function and Modulation Are Target Tissue Dependent. *Journal of Neuroscience*, 31(29):10516–10528, July 2011. ISSN 0270-6474, 1529-2401. doi: 10.1523/JNEUROSCI.2992-10.2011.

[124] Takashi Miyamoto, Matt J. Petrus, Adrienne E. Dubin, and Ardem Patapoutian. TRPV3 regulates nitric oxide synthase-independent nitric oxide synthesis in the skin. *Nature Communications*, 2:369, June 2011. ISSN 2041-1723. doi: 10.1038/ncomms1371.

[125] Viktor Sinica, Lucie Zimova, Kristyna Barvikova, Lucie Macikova, Ivan Barvik, and Viktorie Vlachova. Human and Mouse TRPA1 Are Heat and Cold Sensors Differentially Tuned by Voltage. *Cells*, 9(1):57, December 2019. ISSN 2073-4409. doi: 10.3390/cells9010057.

[126] Junjie Luo, Wei L. Shen, and Craig Montell. TRPA1 mediates sensation of the rate of temperature change in *Drosophila* larvae. *Nature Neuroscience*, 20(1):34–41, January 2017. ISSN 1546-1726. doi: 10.1038/nn.4416.

[127] K. Song, H. Wang, G. B. Kamm, J. Pohle, F. d. C. Reis, P. Heppenstall, H. Wende, and J. Siemens. The TRPM2 channel is a hypothalamic heat sensor that limits fever and can drive hypothermia. *Science*, 353(6306):1393–1398, September 2016. ISSN 0036-8075, 1095-9203. doi: 10.1126/science.aaf7537.

[128] Yingrou Tan, Wei Jie Ng, Sean Zhuo Xuan Lee, Bernett Teck Kwong Lee, Leigh A. Nattkemper, Gil Yosipovitch, Lai Guan Ng, and Hong Liang Tey. 3-Dimensional Optical Clearing and Imaging of Pruritic Atopic Dermatitis and Psoriasis Skin Reveals Downregulation of Epidermal Innervation. *Journal of Investigative Dermatology*, 139(5):1201–1204, May 2019. ISSN 0022202X. doi: 10.1016/j.jid.2018.11.006.

[129] Alex J. Clark, Guillermo Menendez, Mona AlQatari, Niral Patel, Erik Arstad, Giampietro Schiavo, and Martin Koltzenburg. Functional imaging in microfluidic chambers reveals sensory neuron sensitivity is differentially regulated between neuronal regions. *Pain*, 159(7): 1413–1425, July 2018. ISSN 0304-3959, 1872-6623. doi: 10.1097/j.pain.0000000000001145.

[130] Friedrich W. Johenning, Michal Zochowski, Stuart J. Conway, Andrew B. Holmes, Peter Koulen, and Barbara E. Ehrlich. Distinct Intracellular Calcium Transients in Neurites and Somata Integrate Neuronal Signals. *The Journal of Neuroscience*, 22(13):5344–5353, July 2002. ISSN 0270-6474. doi: 10.1523/JNEUROSCI.22-13-05344.2002.

[131] Junxuan Ma, Despina Stefanoska, Sibylle Grad, Mauro Alini, and Marianna Peroglio. Direct and Intervertebral DiscMediated Sensitization of Dorsal Root Ganglion Neurons by Hypoxia and Low pH. *Neurospine*, 17(1):42–59, March 2020. ISSN 2586-6583. doi: 10.14245/ns.2040052.026.

[132] Gregory J. Michael and John V. Priestley. Differential Expression of the mRNA for the Vanilloid Receptor Subtype 1 in Cells of the Adult Rat Dorsal Root and Nodose Ganglia and Its Downregulation by Axotomy. *The Journal of Neuroscience*, 19(5):1844–1854, March 1999. ISSN 0270-6474, 1529-2401. doi: 10.1523/JNEUROSCI.19-05-01844.1999.

[133] J V Priestley, G J Michael, S Averill, M Liu, and N Willmott. Regulation of nociceptive neurons by nerve growth factor and glial cell line derived neurotrophic factor. *Canadian Journal of Physiology and Pharmacology*, 80(5):495–505, May 2002. ISSN 0008-4212, 1205-7541. doi: 10.1139/y02-034.

[134] Viktorie Vlachová, Jan Teisinger, Klára Sušánková, Alla Lyfenko, Rüdiger Ettrich, and Ladislav Vyklický. Functional Role of C-Terminal Cytoplasmic Tail of Rat Vanilloid Receptor 1. *Journal of Neuroscience*, 23(4):1340–1350, February 2003. ISSN 0270-6474, 1529-2401. doi: 10.1523/JNEUROSCI.23-04-01340.2003.

[135] Thomas Voets. Quantifying and Modeling the Temperature-Dependent Gating of TRP Channels. In Bernd Nilius, Susan G. Amara, Thomas Gudermann, Reinhard Jahn, Roland Lill, Stefan Offermanns, and Ole H. Petersen, editors, *Reviews of Physiology, Biochemistry and Pharmacology 162*, pages 91–119. Springer Berlin Heidelberg, Berlin, Heidelberg, 2012. ISBN 978-3-642-29255-2 978-3-642-29256-9. doi: 10.1007/112_2011_5.

[136] Ana Sánchez-Moreno, Eduardo Guevara-Hernández, Ricardo Contreras-Cervera, Gisela Rangel-Yescas, Ernesto Ladrón-de-Guevara, Tamara Rosenbaum, and León D Islas. Irreversible temperature gating in trpv1 sheds light on channel activation. *eLife*, 7:e36372, June 2018. ISSN 2050-084X. doi: 10.7554/eLife.36372.

[137] Changyang Linghu, Shannon L. Johnson, Pablo A. Valdes, Or A. Shemesh, Won Min Park, Demian Park, Kiryl D. Piatkevich, Asmamaw T. Wassie, Yixi Liu, Bobae An, Stephanie A. Barnes, Orhan T. Celiker, Chun-Chen Yao, Chih-Chieh (Jay) Yu, Ru Wang, Katarzyna P. Adamala, Mark F. Bear, Amy E. Keating, and Edward S. Boyden. Spatial Multiplexing of Fluorescent Reporters for Imaging Signaling Network Dynamics. *Cell*, 183(6):1682–1698.e24, December 2020. ISSN 0092-8674. doi: 10.1016/j.cell.2020.10.035.

[138] A. A. Romanovsky. Skin temperature: Its role in thermoregulation. *Acta Physiologica*, 210 (3):498–507, 2014. ISSN 1748-1716. doi: 10.1111/apha.12231.

[139] Jacques Noël, Katharina Zimmermann, Jérome Busserolles, Emanuel Deval, Abdelkrim Alloui, Sylvie Diochot, Nicolas Guy, Marc Borsotto, Peter Reeh, Alain Eschalier, and Michel Lazdunski. The mechano-activated K+ channels TRAAK and TREK-1 control both warm and cold perception. *The EMBO Journal*, 28(9):1308–1318, May 2009. ISSN 0261-4189. doi: 10.1038/emboj.2009.57.

[140] Brianna N. Gaskill, Stephanie A. Rohr, Edmond A. Pajor, Jeffrey R. Lucas, and Joseph P. Garner. Working with what you've got: Changes in thermal preference and behavior in mice with or without nesting material. *Journal of Thermal Biology*, 36(3):193–199, April 2011. ISSN 03064565. doi: 10.1016/j.jtherbio.2011.02.004.

[141] Brianna N. Gaskill, Christopher J. Gordon, Edmond A. Pajor, Jeffrey R. Lucas, Jerry K. Davis, and Joseph P. Garner. Heat or Insulation: Behavioral Titration of Mouse Preference for Warmth or Access to a Nest. *PLOS ONE*, 7(3):e32799, March 2012. ISSN 1932-6203. doi: 10.1371/journal.pone.0032799.

[142] Chan Lek Tan and Zachary A. Knight. Regulation of Body Temperature by the Nervous System. *Neuron*, 98(1):31–48, April 2018. ISSN 0896-6273. doi: 10.1016/j.neuron.2018.02.022.

[143] Takaki Yahiro, Naoya Kataoka, Yoshiko Nakamura, and Kazuhiro Nakamura. The lateral parabrachial nucleus, but not the thalamus, mediates thermosensory pathways for behavioural thermoregulation. *Scientific Reports*, 7(1):5031, July 2017. ISSN 2045-2322. doi: 10.1038/s41598-017-05327-8.

[144] Vojtěch Škop, Juen Guo, Naili Liu, Cuiying Xiao, Kevin D. Hall, Oksana Gavrilova, and Marc L. Reitman. Mouse Thermoregulation: Introducing the Concept of the Thermoneutral Point. *Cell Reports*, 31(2):107501, April 2020. ISSN 22111247. doi: 10.1016/j.celrep.2020.03.065.

[145] Park Yonghak, Seiji Miyata, and Erkin Kurganov. TRPV1 is crucial for thermal homeostasis in the mouse by heat loss behaviors under warm ambient temperature. *Scientific Reports*, 10 (1):8799, December 2020. ISSN 2045-2322. doi: 10.1038/s41598-020-65703-9.

[146] Maohui Luo, Zhe Wang, Hui Zhang, Edward Arens, Davide Filingeri, Ling Jin, Ali Ghahramani, Wenhua Chen, Yingdong He, and Binghui Si. High-density thermal sensitivity maps of the human body. *Building and Environment*, 167:106435, January 2020. ISSN 03601323. doi: 10.1016/j.buildenv.2019.106435.

[147] Nicola Gerrett, Yacine Ouzzahra, and George Havenith. Distribution of Skin Thermal Sensitivity. In Philippe Humbert, Howard Maibach, Ferial Fanian, and Pierre Agache, editors, *Measuring the Skin*, pages 1–17. Springer International Publishing, Cham, 2015. ISBN 978-3-319-26594-0. doi: 10.1007/978-3-319-26594-0_72-1.

[148] Joel D. Greenspan and Dan R. Kenshalo. The Primate as a Model for the Human Temperature-Sensing System: 2. Area of Skin Receiving Thermal Stimulation (Spatial Summation). *Somatosensory Research*, 2(4):315–324, January 1985. ISSN 0736-7244. doi: 10.3109/07367228509144571.

[149] Davide Filingeri. Neurophysiology of Skin Thermal Sensations. In Ronald Terjung, editor, *Comprehensive Physiology*, pages 1429–1491. John Wiley & Sons, Inc., Hoboken, NJ, USA, June 2016. ISBN 978-0-470-65071-4. doi: 10.1002/cphy.c150040.

[150] Park Yonghak, Seiji Miyata, and Erkin Kurganov. TRPV1 is crucial for thermal homeostasis in the mouse by heat loss behaviors under warm ambient temperature. *Scientific Reports*, 10 (1):8799, May 2020. ISSN 2045-2322. doi: 10.1038/s41598-020-65703-9.

[151] A. Garami, E. Pakai, D. L. Oliveira, A. A. Steiner, S. P. Wanner, M. C. Almeida, V. A. Lesnikov, N. R. Gavva, and A. A. Romanovsky. Thermoregulatory Phenotype of the Trpv1 Knockout Mouse: Thermoeffector Dysbalance with Hyperkinesis. *Journal of Neuroscience*, 31(5):1721–1733, February 2011. ISSN 0270-6474, 1529-2401. doi: 10.1523/JNEUROSCI.4671-10.2011.

[152] Chen Ran, Mark A. Hoon, and Xiaoke Chen. The coding of cutaneous temperature in the spinal cord. *Nature Neuroscience*, 19(9):1201–1209, September 2016. ISSN 1546-1726. doi: 10.1038/nn.4350.

[153] Chen Ran and Xiaoke Chen. Probing the coding logic of thermosensation using spinal cord calcium imaging. *Experimental Neurology*, 318:42–49, August 2019. ISSN 00144886. doi: 10.1016/j.expneurol.2019.04.009.

[154] Jussi Kupari, Martin Häring, Eneritz Agirre, Gonçalo Castelo-Branco, and Patrik Ernfors. An Atlas of Vagal Sensory Neurons and Their Molecular Specialization. *Cell Reports*, 27(8): 2508–2523.e4, May 2019. ISSN 22111247. doi: 10.1016/j.celrep.2019.04.096.

[155] Rosemary C. Challis, Sripriya Ravindra Kumar, Ken Y. Chan, Collin Challis, Keith Beadle, Min J. Jang, Hyun Min Kim, Pradeep S. Rajendran, John D. Tompkins, Kalyanam Shivkumar, Benjamin E. Deverman, and Viviana Gradinaru. Systemic AAV vectors for widespread and targeted gene delivery in rodents. *Nature Protocols*, 14(2):379–414, February 2019. ISSN 1754-2189, 1750-2799. doi: 10.1038/s41596-018-0097-3.

[156] Rodrigo Quian Quiroga and Stefano Panzeri. Extracting information from neuronal populations: Information theory and decoding approaches. *Nature Reviews Neuroscience*, 10(3): 173–185, March 2009. ISSN 1471-003X, 1471-0048. doi: 10.1038/nrn2578.

[157] Minjoo Kim, Nicholas J. Sisco, Jacob K. Hilton, Camila M. Montano, Manuel A. Castro, Brian R. Cherry, Marcia Levitus, and Wade D. Van Horn. Evidence that the TRPV1 S1-S4 membrane domain contributes to thermosensing. *Nature Communications*, 11(1):4169, August 2020. ISSN 2041-1723. doi: 10.1038/s41467-020-18026-2.

[158] Joshua I. Glaser, Ari S. Benjamin, Raeed H. Chowdhury, Matthew G. Perich, Lee E. Miller, and Konrad P. Kording. Machine learning for neural decoding. *arXiv:1708.00909 [cs, q-bio, stat]*, July 2020.

[159] Margaret L. DeMaegd and Wolfgang Stein. Temperature-robust activity patterns arise from coordinated axonal Sodium channel properties. *PLOS Computational Biology*, 16(7): e1008057, July 2020. ISSN 1553-7358. doi: 10.1371/journal.pcbi.1008057.

[160] Marcela Lipovsek, Cedric Bardy, Cathryn R. Cadwell, Kristen Hadley, Dmitry Kobak, and Shreejoy J. Tripathy. Patch-seq: Past, Present, and Future. *The Journal of Neuroscience: The Official Journal of the Society for Neuroscience*, 41(5):937–946, February 2021. ISSN 1529-2401. doi: 10.1523/JNEUROSCI.1653-20.2020.

[161] Benjamien Moeyaert, Graham Holt, Rajtarun Madangopal, Alberto Perez-Alvarez, Brenna C. Fearey, Nicholas F. Trojanowski, Julia Ledderose, Timothy A. Zolnik, Aniruddha Das, Davina Patel, Timothy A. Brown, Robert N. S. Sachdev, Britta J. Eickholt, Matthew E. Larkum, Gina G. Turrigiano, Hod Dana, Christine E. Gee, Thomas G. Oertner, Bruce T. Hope, and Eric R. Schreiter. Improved methods for marking active neuron populations. *Nature Communications*, 9(1):4440, October 2018. ISSN 2041-1723. doi: 10.1038/s41467-018-06935-2.

Appendix

Table 1 | List of all animals used for calcium imaging results presented in this study.

TeirBase ID	Experiment #	Sex	Genotype	Age (weeks)	Animal Line	Date of birth	Date of experiment
1311632	139	M	Wildtype	10	C57BL/6N	2018-05-29	2018-08-10
1311631	141	M	Wildtype	10	C57BL/6N	2018-05-29	2018-08-06
1311633	143	M	Wildtype	13	C57BL/6N	2018-05-29	2018-08-26
1325794	143	M	Wildtype	9	C57BL/6N	2018-07-15	2018-09-14
1320191	143	M	TRPV1-KO	9	TRPV1	2018-06-21	2018-08-26
1323693	143	M	TRPV1-KO	9	TRPV1	2018-07-13	2018-09-14
1325807	143	M	TRPV1-KO	10	TRPV1	2018-07-17	2018-09-22
1331188	143	M	Wildtype	7	TRPV1/DTA	2018-08-01	2018-09-22
1355330	155	M	Wildtype	13	TRPM2ko	2018-10-15	2019-01-12
1355336	155	M	TRPM2-KO	13	TRPM2ko	2018-10-15	2019-01-12
1355332	157	F	TRPM2-KO	15	TRPM2ko	2018-10-15	2019-01-30
1355329	157	F	Wildtype	15	TRPM2ko	2018-10-15	2019-01-30
1366191	159	M	Wildtype	10	C57BL/6N	2018-11-26	2019-02-01
1370753	159	M	TRPV1-KO	8	TRPV1	2018-12-05	2019-02-01
1377162	163	M	Wildtype	11	C57BL/6N	2018-12-27	2019-03-15
1370754	163	M	TRPV1-KO	14	TRPV1	2018-12-05	2019-03-15
1388894	167	F	TRPM2-KO	10	TRPM2ko	2019-02-06	2019-04-15
1388898	167	M	Wildtype	10	TRPM2ko	2019-02-06	2019-04-15
1415318	174	M	TRPV1-OX	11	Tag-V1$_{5917ko}$	2019-04-21	2019-07-07
1437582	178	M	Wildtype	14	C57BL/6N	2019-07-07	2019-10-15
1450849	178	M	TRPV1-OX	9	Tag-V1$_{5917ko}$	2019-08-12	2019-10-15
1462242	179	M	Wildtype	10	C57BL/6N	2019-09-20	2019-11-30
1459959	179	M	Wildtype	11	C57BL/6N	2019-09-13	2019-12-01
1459248	179	M	TRPV1M2-DKO	11	TRPM3/M3/V1-ko	2019-09-11	2019-11-30
1459247	179	M	TRPV1M2-DKO	12	TRPM3/M3/V1-ko	2019-09-11	2019-12-01
1517125	191	M	Wildtype	10	TRPV1/DTA	2020-02-24	2020-05-04
1525677	195	M	Wildtype	13	C57BL/6N	2020-03-29	2020-07-01
1527691	195	M	TRPV1M2-DKO	13	TRPM3/M3/V1-ko	2020-04-04	2020-07-01
1527590	195	M	TRPV1-OX	12	Tag-V1$_{5917ko}$	2020-04-06	2020-07-01
1525678	196	M	Wildtype	14	C57BL/6N	2020-03-29	2020-07-06
1527579	196	M	TRPV1-OX	13	Tag-V1$_{5917ko}$	2020-04-05	2020-07-06
1525680	197	M	Wildtype	16	C57BL/6N	2020-03-29	2020-07-20
1527716	197	M	Wildtype	15	vGat-flpo.LepR-cre	2020-04-06	2020-07-20

Table 2 | List of all animals used for behavioral data presented in this study.

TeirBase ID	Cohort	Sex	Genotype	Age (weeks)	Animal Line	Date of birth	Date of experiment
1420083	1	M	TRPM2-KO	22	TRPM2-KO	2019-05-13	2019-10-17
1422414	1	M	TRPM2-KO	22	TRPM2-KO	2019-05-14	2019-10-17
1420084	1	M	TRPM2-KO	22	TRPM2-KO	2019-05-13	2019-10-17
1420085	1	M	TRPM2-KO	22	TRPM2-KO	2019-05-13	2019-10-17
1419638	1	M	TRPV1-KO	23	TRPV1	2019-05-09	2019-10-17
1419639	1	M	TRPV1-KO	23	TRPV1	2019-05-09	2019-10-17
1419642	1	M	TRPV1-KO	23	TRPV1	2019-05-09	2019-10-17
1419641	1	M	TRPV1-KO	23	TRPV1	2019-05-09	2019-10-17
1419640	1	M	TRPV1-KO	23	TRPV1	2019-05-09	2019-10-17
1422474	1	M	TRPV1M2-DKO	21	TRPM2/M3/V1-ko	2019-05-20	2019-10-17
1423767	1	M	TRPV1M2-DKO	21	TRPM2/M3/V1-ko	2019-05-23	2019-10-17
1423765	1	M	TRPV1M2-DKO	21	TRPM2/M3/V1-ko	2019-05-23	2019-10-17
1436273	1	M	Wildtype	22	C57BL/6N	2019-05-14	2019-10-17
1436277	1	M	Wildtype	22	C57BL/6N	2019-05-14	2019-10-17
1436276	1	M	Wildtype	22	C57BL/6N	2019-05-14	2019-10-17
1436274	1	M	Wildtype	22	C57BL/6N	2019-05-14	2019-10-17
1436275	1	M	Wildtype	22	C57BL/6N	2019-05-14	2019-10-17
1484199	2	M	TRPV1-KO	8	TRPV1	2019-11-21	2020-01-15
1484200	2	M	TRPV1-KO	8	TRPV1	2019-11-21	2020-01-15
1484201	2	M	TRPV1-KO	8	TRPV1	2019-11-21	2020-01-15
1484202	2	M	TRPV1-KO	8	TRPV1	2019-11-21	2020-01-15
1489081	2	M	TRPV1M2-DKO	6	TRPM2/M3/V1-ko	2019-12-03	2020-01-15
1489082	2	M	TRPV1M2-DKO	6	TRPM2/M3/V1-ko	2019-12-03	2020-01-15
1489083	2	M	TRPV1M2-DKO	6	TRPM2/M3/V1-ko	2019-12-03	2020-01-15
1489084	2	M	TRPV1M2-DKO	6	TRPM2/M3/V1-ko	2019-12-03	2020-01-15
janvier20200107-09	2	M	Wildtype	7	C57BL/6NRj	2019-11-26	2020-01-15
janvier20200107-10	2	M	Wildtype	7	C57BL/6NRj	2019-11-26	2020-01-15
janvier20200107-11	2	M	Wildtype	7	C57BL/6NRj	2019-11-26	2020-01-15
janvier20200107-12	2	M	Wildtype	7	C57BL/6NRj	2019-11-26	2020-01-15
1507803	3	M	TRPM2-KO	7	TRPM2ko	2020-02-10	2020-03-28
1507804	3	M	TRPM2-KO	7	TRPM2ko	2020-02-10	2020-03-28
1507998	3	M	TRPM2-KO	6	TRPM2ko	2020-02-13	2020-03-28
1507999	3	M	TRPM2-KO	6	TRPM2ko	2020-02-13	2020-03-28
1507756	3	M	TRPV1-KO	7	TRPV1	2020-02-07	2020-03-28
1507757	3	M	TRPV1-KO	7	TRPV1	2020-02-07	2020-03-28
1507758	3	M	TRPV1-KO	7	TRPV1	2020-02-07	2020-03-28
1507759	3	M	TRPV1-KO	7	TRPV1	2020-02-07	2020-03-28
1507993	3	M	Wildtype	7	C57BL/6N	2020-02-10	2020-03-28
1507994	3	M	Wildtype	7	C57BL/6N	2020-02-10	2020-03-28
1513517	3	M	Wildtype	6	C57BL/6N	2020-02-18	2020-03-28

Continued on next page

Continued from previous page

TeirBase ID	Cohort	Sex	Genotype	Age (weeks)	Animal Line	Date of birth	Date of experiment
1513518	3	M	Wildtype	6	C57BL/6N	2020-02-18	2020-03-28
1520432	4	M	TRPM2-KO	11	TRPM2ko	2020-03-10	2020-05-25
1520436	4	M	TRPM2-KO	11	TRPM2ko	2020-03-10	2020-05-25
1520437	4	M	TRPM2-KO	11	TRPM2ko	2020-03-10	2020-05-25
1520426	4	M	TRPM2-KO	11	TRPM2ko	2020-03-10	2020-05-25
bl6-j202005-1	4	M	Wildtype	11	C57BL/6NRj	2020-03-10	2020-05-25
bl6-j202005-2	4	M	Wildtype	11	C57BL/6NRj	2020-03-10	2020-05-25
bl6-j202005-3	4	M	Wildtype	11	C57BL/6NRj	2020-03-10	2020-05-25
bl6-j202005-4	4	M	Wildtype	11	C57BL/6NRj	2020-03-10	2020-05-25
1527556	5	M	TRPV1-OX	9	Tag-V1$_{5917ko}$	2020-04-04	2020-06-08
1527557	5	M	TRPV1-OX	9	Tag-V1$_{5917ko}$	2020-04-04	2020-06-08
1527570	5	M	TRPV1-OX	9	Tag-V1$_{5917ko}$	2020-04-04	2020-06-08
1527571	5	M	TRPV1-OX	9	Tag-V1$_{5917ko}$	2020-04-04	2020-06-08
1527661	5	M	TRPV1M2-DKO	9	TRPM2/M3/V1-ko	2020-04-03	2020-06-08
1527662	5	M	TRPV1M2-DKO	9	TRPM2/M3/V1-ko	2020-04-03	2020-06-08
1527663	5	M	TRPV1M2-DKO	9	TRPM2/M3/V1-ko	2020-04-03	2020-06-08
1527664	5	M	TRPV1M2-DKO	9	TRPM2/M3/V1-ko	2020-04-03	2020-06-08
2866191	6	M	TRPM2-KO	6	V1-DTA-M2KO	2020-05-11	2020-06-24
2866194	6	M	TRPM2-KO	6	V1-DTA-M2KO	2020-05-11	2020-06-24
2866196	6	M	Wildtype	45	V1-DTA-M2KO	2019-08-17	2020-06-24
2866197	6	M	Wildtype	45	V1-DTA-M2KO	2019-08-17	2020-06-24
2866202	6	M	Wildtype	37	V1-DTA-M2KO	2019-10-10	2020-06-24
2866236	6	M	Wildtype	6	V1-DTA-M2KO	2020-05-15	2020-06-24
2866239	6	M	Wildtype	6	V1-DTA-M2KO	2020-05-15	2020-06-24
1537080	7	M	TRPV1-OX	10	Tag-V1$_{5917ko}$	2020-05-23	2020-08-03
1538839	7	M	TRPV1-OX	9	Tag-V1$_{5917ko}$	2020-05-31	2020-08-03
1539792	7	M	TRPV1-OX	9	Tag-V1$_{5917ko}$	2020-06-03	2020-08-03
1539793	7	M	TRPV1-OX	9	Tag-V1$_{5917ko}$	2020-06-03	2020-08-03
1536859	7	M	TRPV1-OX	11	Tag-V1$_{5917ko}$	2020-05-20	2020-08-03
j20200708-01	7	M	Wildtype	9	C57BL/6NRj	2020-06-02	2020-08-03
j20200708-02	7	M	Wildtype	9	C57BL/6NRj	2020-06-02	2020-08-03
j20200708-03	7	M	Wildtype	9	C57BL/6NRj	2020-06-02	2020-08-03
j20200708-04	7	M	Wildtype	9	C57BL/6NRj	2020-06-02	2020-08-03
j-20200805-01	8	M	Wildtype	10	C57BL/6NRj	2020-06-25	2020-08-31
j-20200805-02	8	M	Wildtype	10	C57BL/6NRj	2020-06-25	2020-08-31
j-20200805-03	8	M	Wildtype	10	C57BL/6NRj	2020-06-25	2020-08-31
j-20200805-04	8	M	Wildtype	10	C57BL/6NRj	2020-06-25	2020-08-31
1562092	9	M	TRPV1-KO	6	TRPV1	2020-08-16	2020-09-29
1562093	9	M	TRPV1-KO	6	TRPV1	2020-08-16	2020-09-29
1562094	9	M	TRPV1-KO	6	TRPV1	2020-08-16	2020-09-29
1562095	9	M	TRPV1-KO	6	TRPV1	2020-08-16	2020-09-29
1559595	10	M	TRPM2-KO	10	TRPM2ko	2020-08-05	2020-10-12
1559596	10	M	TRPM2-KO	10	TRPM2ko	2020-08-05	2020-10-12
1558198	10	M	TRPM2-KO	10	TRPM2ko	2020-08-02	2020-10-12
1557882	10	M	TRPM2-KO	11	TRPM2ko	2020-07-29	2020-10-12

Code Snippet .1 | Suite2p parameters used to perform rigid motion correction and signal extraction from raw .tiff files produced by metafluor.

```
ops = {
    # file paths
        'look_one_level_down': False, # whether to look in all subfolders when
         ↪  searching for tiffs
    'fast_disk': [], # used to store temporary binary file, defaults to
     ↪  save_path0
    'delete_bin': False, # whether to delete binary file after processing
    'mesoscan': False, # for reading in scanimage mesoscope files
    'h5py': [], # take h5py as input (deactivates data_path)
    'h5py_key': 'data', #key in h5py where data array is stored
    'save_path0': [], # stores results, defaults to first item in data_path
    'subfolders': [],
    # main settings
        'nplanes' : 1, # each tiff has these many planes in sequence
    'nchannels' : 1, # each tiff has these many channels per plane
    'functional_chan' : 1, # this channel is used to extract functional ROIs
     ↪  (1-based)
    'tau':  0.7, # this is the main parameter for deconvolution
    'fs': 4.,  # sampling rate (PER PLANE - e.g. if you have 12 planes then
     ↪  this should be around 2.5)
    'force_sktiff': False, # whether or not to use scikit-image for tiff
     ↪  reading
    'frames_include' : -1,
    # output settings
        'preclassify': 0.0, # apply classifier before signal extraction with
    # probability 0.5 (turn off with value 0)
    'save_mat': False, # whether to save output as matlab files
    'combined': True, # combine multiple planes into a single result /single
     ↪  canvas for GUI
    'aspect': 1.0, # um/pixels in X / um/pixels in Y (for correct aspect ratio
     ↪  in GUI)
    # bidirectional phase offset
        'do_bidiphase': False,
    'bidiphase': 0,
    # registration settings
        'do_registration': 2, # whether to register data (2 forces
         ↪  re-registration)
    'keep_movie_raw': False,
    'nimg_init': 300, # subsampled frames for finding reference image
    'batch_size': 500, # number of frames per batch
    'maxregshift': 0.1, # max allowed registration shift, as a fraction of
     ↪  frame max(width and height)
    'align_by_chan' : 1, # when multi-channel, you can align by non-functional
     ↪  channel (1-based)
    'reg_tif': False, # whether to save registered tiffs
    'reg_tif_chan2': False, # whether to save channel 2 registered tiffs
    'subpixel' : 10, # precision of subpixel registration (1/subpixel steps)
    'smooth_sigma': 1.15, # ~1 good for 2P recordings, recommend >5 for 1P
     ↪  recordings
    'th_badframes': 1.0, # this parameter determines which
    # frames to exclude when determining cropping - set it smaller to exclude
     ↪  more frames
        'pad_fft': False,
    # non rigid registration settings
        'nonrigid': False, # whether to use nonrigid registration
```

```
    'block_size': [128, 128], # block size to register (** keep this a multiple
     ↪  of 2 **)
    'snr_thresh': 1.2, # if any nonrigid block is below this threshold,
    # it gets smoothed until above this threshold. 1.0 results in no smoothing
        'maxregshiftNR': 5, # maximum pixel shift allowed for nonrigid,
         ↪  relative to rigid
    # 1P settings
        '1Preg': False, # whether to perform high-pass filtering and tapering
    'spatial_hp': 50, # window for spatial high-pass filtering before
     ↪  registration
    'pre_smooth': 0, # whether to smooth before high-pass filtering before
     ↪  registration
    'spatial_taper': 50, # how much to ignore on edges
    # (important for vignetted windows, for FFT padding do not set BELOW
     ↪  3*ops['smooth_sigma'])
    # cell detection settings
        'roidetect': True, # whether or not to run ROI extraction
    'sparse_mode': True,
    'spatial_scale': 0, # 0: multi-scale; 1: 6 pixels, 2: 12 pixels, 3: 24
     ↪  pixels, 4: 48 pixels
    'connected': True, # whether or not to keep ROIs fully connected (set to 0
     ↪  for dendrites)
    'navg_frames_svd': 5000, # max number of binned frames for the SVD
    'nsvd_for_roi': 5000, # max number of SVD components to keep for ROI
     ↪  detection
    'max_iterations': 20, # maximum number of iterations to do cell detection
    'threshold_scaling': 5., # adjust the automatically determined threshold by
     ↪  this scalar multiplier
    'max_overlap': 1.0, # cells with more overlap than this get removed during
     ↪  triage, before refinement
    'high_pass': 10, # running mean subtraction with window of size 'high_pass'
     ↪  (use low values for 1P)
    # ROI extraction parameters
        'inner_neuropil_radius': 2, # number of pixels to keep between ROI and
         ↪  neuropil donut
    'min_neuropil_pixels': 350, # minimum number of pixels in the neuropil
    'allow_overlap': False, # pixels that are overlapping are thrown out
    #(False) or added to both ROIs (True)
    # channel 2 detection settings (stat[n]['chan2'], stat[n]['not_chan2'])
        'chan2_thres': 0.65, # minimum for detection of brightness on channel 2
    # deconvolution settings
        'baseline': 'maximin', # baselining mode (can also choose 'prctile')
    'win_baseline': 60., # window for maximin
    'sig_baseline': 10., # smoothing constant for gaussian filter
    'prctile_baseline': 8.,# optional (whether to use a percentile baseline)
    'neucoeff': .7,  # neuropil coefficient
    'anatomical_only': 2 # sets th ROI detection into anatomical mode
}
```